NOTICE

The quality of this microform is heavily dependent upon the quality of the original thesis submitted for microfilming. Every effort has been made to ensure the highest quality of reproduction possible.

If pages are missing, contact the university which granted the degree.

Some pages may have indistinct print especially if the original pages were typed with a poor typewriter ribbon or if the university sent us an inferior photocopy.

Reproduction in full or in part of this microform is governed by the Canadian Copyright Act, R.S.C. 1970, c. C-30, and subsequent amendments.

AVIS

La qualité de cette microforme dépend grandement de la qualité de la thèse soumise au microfilmage. Nous avons tout fait pour assurer une qualité supérieure de reproduction.

S'il manque des pages, veuillez communiquer avec l'université qui a conféré le grade.

La qualité d'impression de certaines pages peut laisser à désirer, surtout si les pages originales ont été dactylographiées à l'aide d'un ruban usé ou si l'université nous a fait parvenir une photocopie de qualité inférieure.

La reproduction, même partielle, de cette microforme est soumise à la Loi canadienne sur le droit d'auteur, SRC 1970, c. C-30, et ses amendements subséquents.

FINLINE DISCONTINUITY ANALYSIS USING VECTORIAL FINITE ELEMENTS

By

Senglee Foo, B.A.Sc., M.A.Sc.

A thesis submitted to the

Faculty of Graduate Studies and Research

in partial fulfillment of the requirements

for the degree of

Doctor of Philosophy

Department of Electrical Engineering

McGill University

February, 1992

ISBN 0-315-74648-3

Canada

Abstract

In this thesis, a numerically efficient three-dimensional finite element scheme is used to analyze arbitrarily-shaped discontinuities in inhomogeneous-dielectric-loaded waveguides. Special emphasis is placed on discontinuity problems in finlines and related structures. A simple but accurate recursive algorithm, the boundary-marching method, for modeling uniform waveguides of arbitrarily-shaped cross-section is developed for the analysis. This algorithm is used to generate the matrix representations of various waveguides, including the unilateral finlines. It is shown that, by using the substructure formulation and the matrix representation of the uniform guide, the finite element mesh of the discontinuity problem can be truncated to a proximity very close to the discontinuity without compromising with the result accuracy. Finally, characteristics of inductive strips in unilateral finline are evaluated using the finite element scheme. The scattering parameters of the inductive strips obtained with the finite element method agree with published measurements and other numerical solutions to within a few percent with a relatively small number of elements. Various effects of the manufacturing process, such as the effect of mounting grooves, finite metalization thickness and deflection of dielectric substrate, on the discontinuity parameters are studied in detail using the finite element scheme.

RÉSUMÉS

Dans cette thèse, la méthode numérique tridimensionnelle des éléments finis est utilisée pour analyser les discontinuités de formes arbitraires dans des guides d'ondes chargés en diélectriques hétérogènes. Une attention particulière a été accordée aux problèmes de discontinuité rencontrés dans des structures en ailettes et autres structures du même type. Un algorithme récursif simple mais précis, la méthode des limites mobiles, modélisant des guides d'ondes de sections transversales de formes arbitraires, a été développé pour la présente analyse. Cet algorithme est utilisé pour produire la représentation matricielle de divers guides d'ondes, parmi lesquels les structures unidirectionnelles en ailettes. Il est démontré que, par l'utilisation de la formulation de base et de la représentation matricielle du guide uniforme, le maillage d'éléments finis du problème de discontinuité peut etre tronquée à une limite très proche de la discontinuité sans mettre en cause la précision des résultats. Enfin, les caractéristiques des bandes inductives dans les structures unidirectionnelles en ailettes sont évaluées par application de la méthode des éléments finis. Les paramètres de diffraction des bandes inductives obtenus avec la méthode des éléments finis s'accordent avec les mesures publiées et autres solutions numériques à quelques pourcents près, avec un nombre d'éléments relativement limité. Les effets divers - rayures d'assemblage, épaisseur de métalisation finie, déflection de la couche diélectrique inférieure - que les procédés de fabrication des matériaux utilisés peuvent avoir sur les paramètres de discontinuité sont étudiés en détails en utilisant la méthode des éléments finis.

ACKNOWLEDGEMENTS

I must express my deepest gratitude to my supervisor, Dr. P.P.Silvester. This thesis would not have been possible without his encouragement, support, help and guidance throughout the work. During the entire period of my study at McGill, he has been always available to discuss any problem, big or small, related or unrelated to the research. I have benefited from his experience in many aspects.

I would like to thank Dr. A. Pinchuk for introducing me to McGill, and Mr. V. Kanellopoulous for many useful discussions, his company and his help on translating the Abstract. I gratefully acknowledge the generous assistance and support given by the staff of the Department of Electrical Engineering, McGill University. I am also very grateful for the assistance and facilities provided by the McGill University Computing Centre.

I wish to thank Environment Canada, Montreal, Quebec, for permitting me accessing the Cray computer. Special thank must also go to Dr. Nicholas Chepurnyi of the Environment Canada, and Mr. Phil Garnatz of Cray Research, Minneapolis, Minnesota, for their extensive and generous assistance in adapting my PC-based Ada programs to the Cray computer. Nicholas is always willing and able to help me with any problem that I have with the Cray computer. Phil has done a tremendous job in vectorizing my "Static Condensation" package and compiling my Ada programs.

Funding provided by the Natural Sciences and Engineering Research Council of Canada and Centre de Recherche Informatique de Montreal are gratefully acknowledged.

Personally, I would like to thank my wife Yinlan, and daughter Shanny for their understanding, patience and support during the study.

CLAIM TO ORIGINAL CONTRIBUTION

The major contributions of this thesis are:

(i) the development of a general recursive method, the boundary-marching algorithm, for discontinuity analysis involving inhomogeneous dielectric-loaded guides, using finite element method, where it permits truncation of the finite element mesh at a proximity very close to the discontinuity without compromising result accuracy;

(ii) the characterization of discontinuities in unilateral finlines including effects of finite metalization of the fin, the influence of the mounting groove, and the effect of substrate bending.

Summary

This thesis describes the development of a numerically efficient three-dimensional finite element scheme for analysing the transmission/reflection characteristics of discontinuities embedded in inhomogeneous waveguides. The method is then applied directly to characterize three-dimensional discontinuities in E-plane circuits.

The purpose of this study, general scope of the thesis and the basic features of E-plane circuits are briefly described in Chapter 1. In this Chapter, various analysis methods developed for E-plane circuits analysis, such as the homogeneous waveguide approximation method, the transverse resonance technique, the spectral domain method, the transmission line method, and the finite difference method are also briefly described.

Chapter 2 lays the foundation for the three-dimensional finite element analysis. Potential difficulties associated with the application of the vectorial finite element formulation to the finline discontinuity analysis are discussed. Mathematical formulation and the associated boundary conditions of the vectorial finite element scheme are presented.

In Chapter 3, the concept of the boundary-marching algorithm for modeling waveguide structures is introduced. Mathematical formulation of the algorithm and its applicability are described.

Chapter 4 describes the actual implementation of the numerical schemes used in the analysis. Special emphasis is placed on the static condensation package, a numerical procedure used in the boundary-marching process.

In Chapter 5, the algorithm of the analysis is examined by using known solutions. First, the auxiliary matrix generated by the ballooning algorithm is used to simulate the eigenmodes in a rectangular guide. Then, the field distribution in an dielectric-loaded guide is calculated and compared to the known solution. The S-parameters of capacitive windows are then evaluated by using the proposed algorithm. Results are found to agree with the approximate analytical solution to within a few percent.

Chapter 6 illustrates finline discontinuity analysis using the three-dimensional finite element method. It begins with evaluation of electric field distributions in unilateral finlines. The field distribution are generated using the boundary-marching algorithm. Characteristics of inductive strips in unilateral finlines are evaluated using the proposed algorithm. The S-parameters of a typical inductive strip in the unilateral finline are computed and compared to the measured results and the results calculated with other numerical techniques. The effects of manufacturing processes, including the mounting grooves, metalization thickness and the substrate bending are studied in detail.

Chapter 7 summarizes the thesis. The detailed derivations of the mixed-order vectorial finite element scheme are given in Appendix I. Gauss-Legendre quadrature used in the derivations of the local matrices of the vectorial finite elements is briefly described in Appendix II. Finally, Appendix III illustrates the extraction of the admittance matrix of a discontinuity from the finite element solution. The details of conversion of the scattering parameters from the admittance parameters are also given.

TABLE OF CONTENTS

Chapter 1

General Introduction

1.1 Analysis of E-Plane Integrated Circuit

E-plane circuits, including finline, shielded microstrip and suspended stripline, belongs to a class of microwave transmission media called quasi-planar transmission line. Figure 1-1 shows some typical E-plane structures. Among these structures, finlines will be the main interest of this study. A finline can be viewed as a ridged waveguide with a thin metallic fin backed by a dielectric substrate. For applications at higher frequencies, especially at millimeter wavelengths, they are considered a better alternative than their microwave counterparts, such as microstrip line and stripline. The quasi-planar structure of E-plane circuits allows one to integrate the entire circuit pattern on the planar surface of a dielectric substrate with the conventional MIC (Microwave Integrated Circuit) technologies; yet, it reduces the radiation losses and tolerance requirements on the waveguide housing. In practice, the design of the finline circuit takes into account the effect of the metallic housing. The circuit is printed on a thin dielectric substrate. The substrate, including the circuit pattern, is then inserted into a precisely milled slit in a rectangular waveguide as shown in Figure 1-2.

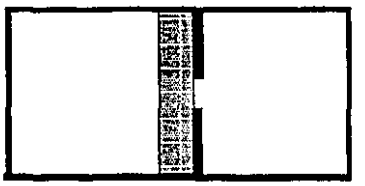

Unilateral
finline

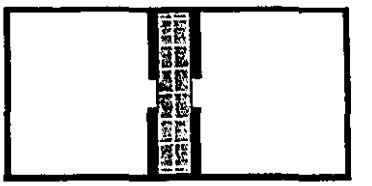

Bilateral
finline

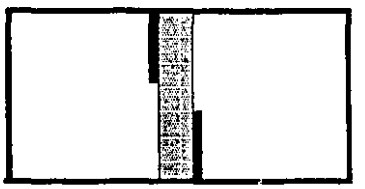

Antipodal
finline

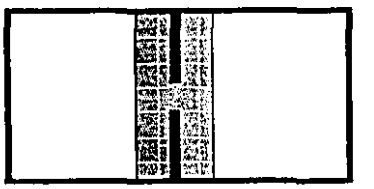

Insulated
finline

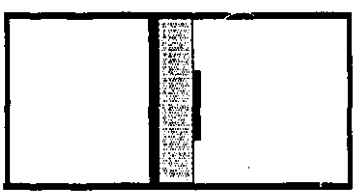

Shielded
Microstrip

Suspended
Stripline

Figure 1-1
Typical E-plane transmission lines
(Cross-sectional views)

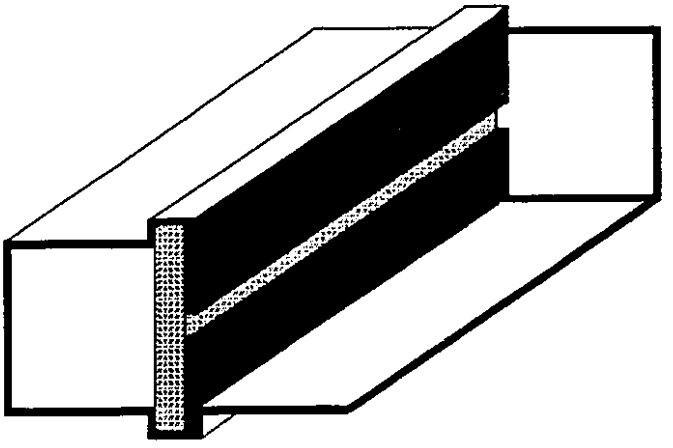

Isometric view

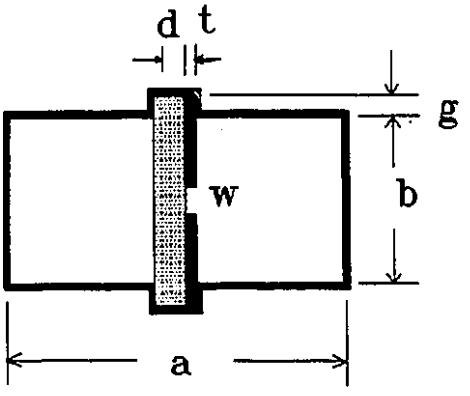

Cross-sectional view

t — Metalization thickness
s — Strip width
g — Depth of mounting groove
w — Slot width
d — Substrate thickness

Figure 1-2
A practical unilateral finline

The insertion of the dielectric substrate makes the E-plane transmission lines inhomogeneous in nature. The electromagnetic waves propagating in the finline structures are, therefore, hybrid waves because they are neither transverse electric (TE) nor transverse magnetic (TM) types, as in the case of empty waveguides or waveguides with uniform dielectric filling. The propagating modes in such structures must be a combination of TE and TM waves which are coupled via the boundary and interface conditions. This is because, in general, the inhomogeneous boundary conditions cannot be satisfied by pure TE or pure TM fields alone. It can be shown that only a combination of both field types, a hybrid field, can satisfy all the boundary conditions at once. By convention, the hybrid fields are denoted as either HE_{mn}, or EH_{mn} modes. The HE-mode designates the hybrid fields with a dominating TE mode (or H wave), while EH-mode designates the hybrid fields with a dominating TM mode (or E wave). The single-mode bandwidth in a finline is greater than the bandwidth of the corresponding hollow waveguide.

The process of E-plane circuit design requires design information such as the guide wavelength and the characteristic impedance of the transmission line in use, the characteristics of various discontinuities in the given transmission line, and the properties of the higher order modes. In finline design, understanding of the influence of finite metalization thickness, effect of mounting grooves and substrate bending aids in the accurate design of circuits and assists in prediction of their performances. Several analytical and numerical techniques have been developed for studying E-plane circuits and their discontinuities. The presence of the sharp-edged metallic fin and the dielectric loading make the E-plane circuit analysis a relatively difficult task. The

sharp edge of the metalization leads to difficulties in the accurate modeling of the edge field and the surface currents on the thin fin. The dielectric loading causes the wave propagation in the E-plane circuit to be hybrid in nature. The analysis technique, therefore, very often involves rigorous full-wave analysis or some constrained approximation methods. The approximation methods used for the analysis include Cohn's method [55], ridged waveguide model [42,43,54], empirical expressions [56]. Cohn's method can be used to analyze E-plane circuits with certain types of symmetry in cross-sectional geometry and it yields accurate results for finline of narrow slot width. Based on the fact that finlines are essentially ridged waveguides with a dielectric backing, Meier [42] introduced the fictitious ridged waveguide model, uniformly filled with an equivalent dielectric constant. The equivalent dielectric constant for a given finline configuration is determined experimentally or by other numerical methods such as the transverse resonance method. The method works well for relatively thin substrates with small dielectric constant.

For more accurate results, full-wave approaches such as the spectral domain technique (SDM), mode matching method, method of lines (MOL), transmission line method (TLM), transverse resonance method (TRM), finite difference method (FDM), and finite element method (FEM) are employed. The spectral domain method was first proposed by Itoh and Mittra [57] for the evaluation of the dispersion characteristics of shielded microstrip lines. In this method, all field components are subject to a Fourier transformation with respect to the direction perpendicular to the surface containing the circuit pattern (the surface is sometimes referred to as the frequency selective surface, or FSS). The analysis is then performed by studying the behavior of the resulting spatial spectrum. SDM is considered one of the most popular methods in

finline analysis for the idealized finline model with zero metalization thickness, zero mounting groove depth [28,48,49,51,52]. It is very accurate and efficient for finline analysis. However, it is also very restricted on the geometry of the problem. The transverse resonance is another important tool in E-plane circuit analysis. It was one of the well known procedures for analyzing dielectric-loaded waveguide in the 1950s and 1960s and has been extended to finline discontinuity analysis by Sorrentino and Itoh [46]. The transverse resonance method was found well suited and computationally efficient in providing either the propagation characteristics or the discontinuity parameters of E-plane circuits. It has been applied to various discontinuity analyses [29,46]. The transverse resonance method basically involves forming a resonant cavity containing the discontinuity by placing electric or magnetic walls some distance away from the discontinuity. The cavity is then modeled as a two-port network. The propagation parameters or the discontinuity parameters of interest are then obtained by computing the resonant frequencies of the cavity. The primary limitation of the TRM is that it cannot include the higher order mode interactions between the waveguide walls and the discontinuity. The modal analysis technique described by Wexler [58] for solving waveguide discontinuities was first applied to finline discontinuity analysis by Hennaway and Schunemann [44]. The mode-matching technique is one of the most rigorous and powerful methods for E-plane discontinuity analysis and it is applicable to a broad class of abrupt junction type of finline discontinuities, such as abrupt transition between two finlines, impedance transformer and inductive strip [44,47]. Transmission line method (TLM) is another often used method in evaluating E-plane circuits. The method is founded on the modeling of the spatial electromagnetic field in terms of a distributed transmission-line network. Electric and magnetic fields are made equivalent to voltage and current in the

network. The impulse response of the equivalent two-dimensional or three-dimensional network of transmission line is then evaluated, in a discrete time interval, by exciting voltage or current pulses. The spectral response of the structure is found by performing a Fourier transform on the impulse response. It has been used to characterize various finline structures [40]. Numerous other numerical schemes, such as the method of lines and finite difference method, have also been adopted for finline analysis. However, all the above-mentioned methods are primarily restricted to problems of certain geometry, such as rectangular shape.

Finite element method (FEM) has been adopted for solving a great variety of boundary value problems of arbitrarily-shaped geometry. Its flexibility in physical geometry of problems makes it an invaluable tool in solving many practical engineering problems. However, it has not been applied in E-plane circuit analysis until very recently [30,40,59]. Eswarappa, Costache, Hoefer [30,40] showed that two-dimensional finite element method can be used to accurately derive the dispersion characteristics of finline structures of arbitrarily-shaped cross sections, covering the metalization thickness, substrate mounting grooves and bending of the substrate. Picon, Hanna, Citerne [59] showed that three-dimensional finite element method using conventional tetrahedron can be used to find the scattering parameters of a general discontinuity problem. The major reason that finite element method remains unpopular in this area can be attributed to the following facts.

1. Finite element method requires relatively large memory and computer time. This is especially true for E-plane circuit analysis since a large number of elements are required to model the sharp edges of the fin. For three-

dimensional discontinuity problems, the resultant matrix size is tremendously large due to the fact that many more elements are needed to model the two uniform waveguide sections attached to the discontinuity.

2. The existence of so called spurious modes in finite element solution makes it an unreliable method for solving waveguide problems that requires vector formulation.

3. Various numerical schemes can be used to reduce three-dimensional E-plane circuit problems to equivalent two-dimensional problems. It is, therefore, more efficient to apply other such numerical schemes, if an idealized model (with zero fin thickness, zero mounting groove) is under consideration.

1.2 Dissertation Objectives

The primary purpose of this study is twofold:

1. to develop a finite element scheme for three-dimensional discontinuity analysis in inhomogeneously dielectric-loaded waveguides of arbitrary cross-section,

2. to apply the three-dimensional finite element method to characterize finline discontinuities, and to provide an accurate estimate of effects, such as mounting grooves, metalization thickness and substrate bending, on the parameters of finline discontinuities.

To make the three-dimensional finite element method attractive and practical for waveguide discontinuity analysis, it is necessary to limit the overall size of the resultant system matrix, that is, to reduce the required number of elements in the finite element mesh. For most discontinuity problems, a large proportion of the elements are used not to approximate the discontinuity, but to interpolate between the discontinuity and the excitation planes in two uniform waveguide sections. This is because the distance between the excitation planes and the discontinuity must be far enough to allow the evanescent modes to decay significantly at the excitation planes. Evidently, if one can find a means to terminate the mesh at the very close proximity to the discontinuity and yet model the waveguide correctly, the goal of reducing the resultant matrix size is achieved. For discontinuity problems involving waveguides of regular cross-sectional shape, such as rectangular or circular geometry, an equivalent boundary condition based on the expansion of normal modes of the guide can be found. However, when the discontinuity is embedded in an inhomogeneous guide of irregular cross-section, which is exactly the case here, the equivalent boundary condition for the waveguide cannot be found since there is no analytic solution for the waveguide. It is the primary objective of this study to develop a numerical scheme for this purpose.

It has been observed that parameters of manufacturing process, such as finite metalization thickness of the fin and holding grooves to fix the inset, considerably influence circuit behavior. The influence of these parameters on the propagation parameters and dispersive characteristics of finline have been studied by several authors [36,37,38]. A two dimensional finite element method using the longitudinal field components, H_z and E_z, has also been applied in the study of these phenomena [30].

However, how these parameters affect a three-dimensional finline discontinuity has not yet been reported. It is the objective of this study to perform a full investigation of these manufacturing effects, including the mounting grooves, finite metalization thickness of the fin, and the substrate bending on the finline discontinuities. To achieve this goal, it is necessary to use a three-dimensional numerical tool. The three-dimensional finite element technique is considered one of the best candidates for the task.

Chapter 2

Three-dimensional vectorial finite elements

2.1 Vectorial Finite Element

The finite element method, a numerical method based on the calculus of variations, has become a very popular numerical procedure for solving physical and mathematical problems governed by differential equations. In electromagnetic and microwave engineering, it is particularly useful in solving boundary value problems involving arbitrarily-shaped boundaries, and anisotropic or inhomogeneous materials. For three-dimensional wave propagation problems, however, the well-developed finite element methods in terms of scalar formulations are inadequate. The finite element based on a variational expression in terms of the full electric field vector E or the full magnetic field vector H must be used. The most serious difficulty in applying the vectorial finite element method to three-dimensional inhomogeneous dielectric waveguide problems is the appearance of undesirable nonphysical solutions, the so-called spurious modes. As indicated in several papers [9,10,11,12,13,15] that the spurious solutions are a direct result of the fact that the constraint of $\nabla \cdot D=0$ or $\nabla \cdot H=0$ is not satisfied. Extensive research efforts have been expended on finding a solution to suppress or eliminate such spurious solutions. Recently, an orthospectral finite element obtained by using mixed-order interpolation functions on hexahedra [3,6,7] has been

shown to produce solutions free of spurious modes. The method is applicable to variational formulations in terms of the full electric field vector E or the full magnetic field vector H. Since the hexahedral mixed-order element is well suited for E-plane transmission line problems, it is adopted for this application here.

The fundamental operations and procedures associated with the finite element method are quite simple and similar to other numerical approximation processes. However, the method also possesses two distinct and unique characteristics. They are the utilization of the integral formulation technique to generate a system of algebraic equations and the use of continuous piecewise-smooth functions to approximate the unknown quantity. The finite element procedure can be summarized by the following discrete steps:

1. discretising the problem domain into smaller subregions (finite elements),
2. interpolating the unknown quantity of interest with piecewise defined polynomial functions in terms of some unknown scalar quantities (nodal values),
3. minimizing the corresponding functional of the governing differential equation for all elements,
4. obtaining the system of equations of the problem by performing a global assembly,
5. solving the resultant system of simultaneous equations.

2.2 Variational Formulation

The variational principle states that if there exists a functional $\mathcal{F}$ in a domain Ω with boundary Γ such that

$$\mathcal{F}(\mathbf{E}) = \int_{\Omega} \mathrm{G}(\mathbf{E})\, d\Omega \;+\; \int_{\Gamma} \mathrm{g}(\mathbf{E})\; d\Gamma \tag{2-1}$$

where G(**E**) is a valid differential equation in domain Ω, g(**E**) is the given boundary conditions on S, and **E** is the unknown function of interest, then the function **E** is the solution of the differential equation G(**E**), if **E** is chosen such that it extremizes the functional $\mathcal{F}(\mathbf{E})$. If this is the case, then, the differential equation G(**E**) is also said to be the Euler equation of the functional $\mathcal{F}$. Webb [8] shown that the following functional

$$\mathcal{F}(\mathbf{E}) = \frac{1}{2}\int_{\Omega}\Big\{-\frac{1}{\mu_r}(\nabla\times\mathbf{E})\cdot(\nabla\times\mathbf{E}) + k_0^2\epsilon_r\mathbf{E}\cdot\mathbf{E}\Big\}d\Omega \;+\; \int_{\Gamma}\mathbf{E}\times(\nabla\times\mathbf{E})\cdot d\Gamma \tag{2-2}$$

has the vector Helmolz equation,

$$\frac{1}{\mu_r}\nabla\times\nabla\times\mathbf{E} - k_0^2\epsilon_r\mathbf{E} = 0, \tag{2-3}$$

as its Euler equation, subject to the following boundary conditions:

$$(\nabla\times\mathbf{E})\times\mathbf{1}_n = 0 \qquad \text{(homogeneous Neumann on magnetic wall)}, \tag{2-4}$$

$$\mathbf{E}\times\mathbf{1}_n = 0 \qquad \text{(homogeneous Dirichlet on perfect electric conductors)}, \tag{2-5}$$

$$\mathbf{E}\times\mathbf{1}_n = \mathbf{E}_0 \qquad \text{(inhomogeneous Dirichlet on excitation planes)}. \tag{2-6}$$

Here **E** is the electric field, μ_r is the relative permeability of the medium, ϵ_r is the relative permitivity of the medium and $k_0 = \omega^2\,(\epsilon_o\mu_o)$ is the free-space wave constant. The surface integral in eqn. (2-2) vanishes because of homogeneous boundary condition described by eqn. (2-4). The eqn. (2-4) is therefore said to be a "natural boundary

condition" to the functional $\mathcal{F}$ and need not be enforced in the finite element process. However, the two boundary conditions described by eqns. (2-5) and (2-6) must be imposed, whenever required. Finally, the functional $\mathcal{F}$ for the lossless problem is

$$\mathcal{F}(\mathbf{E}) = \frac{1}{2}\int_{\Omega}\left\{-\frac{1}{\mu_r}(\nabla\times\mathbf{E})\cdot(\nabla\times\mathbf{E}) + k_0^2\epsilon_r\mathbf{E}\cdot\mathbf{E}\right\}\, d\Omega \tag{2-7}$$

In this study, only the lossless case will be considered. That is, all the materials, including the dielectric substrates and the metallic enclosure and fin, are lossless. The functional $\mathcal{F}$ given by eqn. (2-2) is the basis of formulation of this study.

2.3 Finite Element Discretization

The first step of the finite element process is to subdivide the entire problem domain into smaller subdomains. In order to avoid the appearance of spurious modes, orthospectral (mixed-order hexahedral) finite elements cast in terms of the projection components [6] are utilized. That is, within each element, the electric field vector $\mathbf{E}$ is written

$$\mathbf{E} = 1^{\xi}E_{\xi} + 1^{\eta}E_{\eta} + 1^{\nu}E_{\nu}, \tag{2-8}$$

where 1^{ξ}, 1^{η}, 1^{ν} are the reciprocal unitary vectors to the local coordinates, and E_{ξ}, E_{η}, E_{ν} are the covariant projection components of $\mathbf{E}$. Each component of the electric field $\mathbf{E}$ in each element is approximated by element functions $\alpha_m^{\xi}(\xi,\eta,\nu)$, $\alpha_m^{\eta}(\xi,\eta,\nu)$, $\alpha_m^{\nu}(\xi,\eta,\nu)$:

$$E_\xi = \sum_{m=1}^{18} E_m^\xi \alpha_m^\xi(\xi,\eta,\nu), \tag{2-9}$$

$$E_\eta = \sum_{m=19}^{36} E_m^\eta \alpha_m^\eta(\xi,\eta,\nu), \tag{2-10}$$

$$E_\nu = \sum_{m=37}^{54} E_m^\nu \alpha_m^\nu(\xi,\eta,\nu). \tag{2-11}$$

Here E_m^ξ, E_m^η, E_m^ν are the nodal electric field values to be determined, $\alpha_m^\xi(\xi,\eta,\nu)$ is the interpolation function for the ξ-component of **E** at local node m, linear in ξ and quadratic in η and ν; $\alpha_m^\eta(\xi,\eta,\nu)$ is the interpolation function for the η-component of **E** at local node m, linear in η and quadratic in ξ and ν; $\alpha_m^\nu(\xi,\eta,\nu)$ is the interpolation function for the ν-component of **E** at local node m, linear in ν, and quadratic in ξ and ν. The numbering scheme of the first/second-order hexahedral element is shown in Figure 2-1 and Figure 2-2. Detail of these functions are given in Appendix I. Substituting eqn. (2-8) to eqn. (2-11) into eqn. (2-7), and applying the standard finite element minimization procedure to the functional [8,61] gives the following system of equations:

$$\{ -\tfrac{1}{\mu_r}[S] + k_0^2 \epsilon_r [T] \}\ [\mathrm{E}] = [0]. \tag{2-12}$$

Here $[E]$ is a column matrix representing the nodal electric fields, $[S]$ is the square matrix that results from the curl-curl term in the functional, and $[T]$ corresponds to the dot-product term in the functional. Derivations of the [S] and [T] matrices are also given in Appendix I.

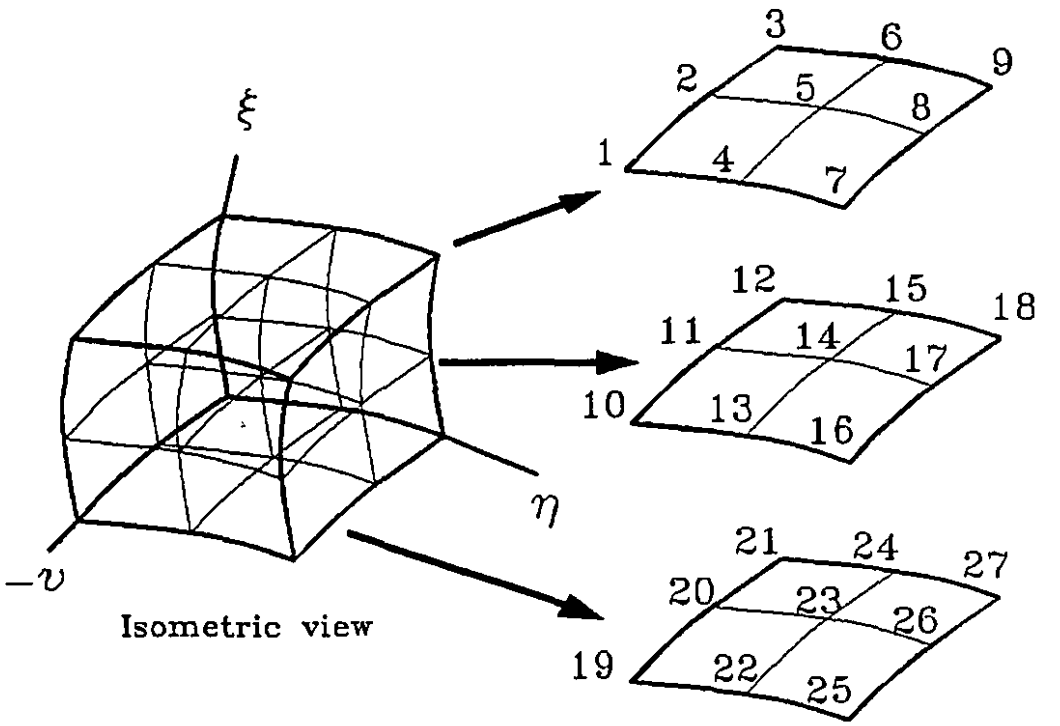

Figure 2–1
Numbering system of the geometric nodes of the mixed–order hexahedral element

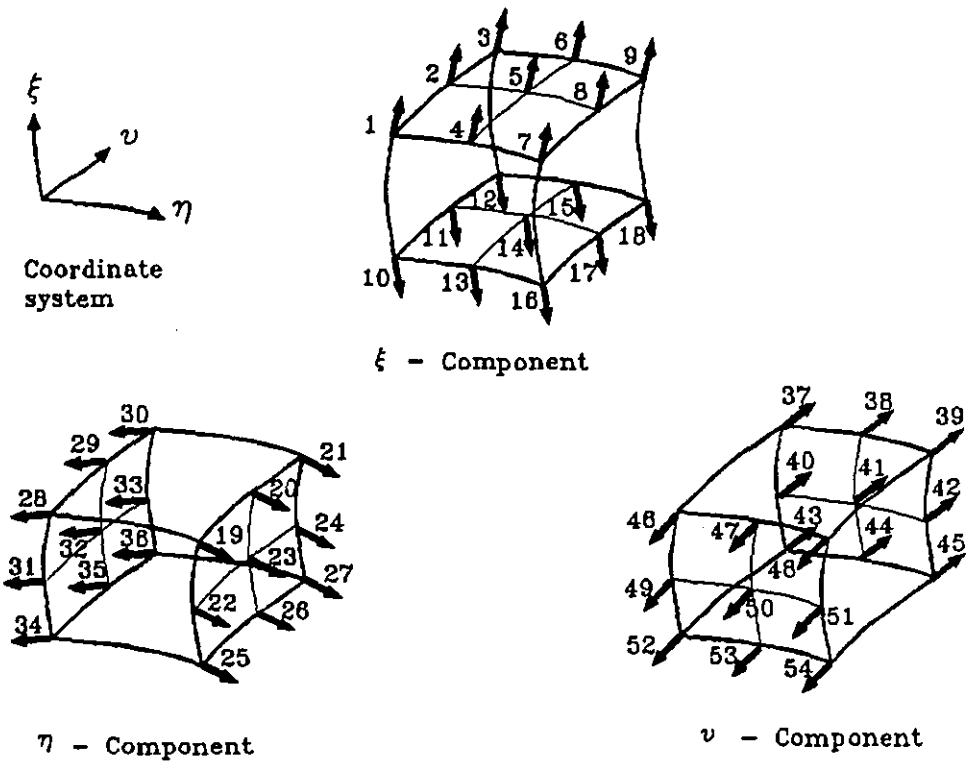

Figure 2-2
Numbering system of local field nodes of the mixed-order hexahedral element

2.4 System matrix of equations

As shown in Fig. 2-2, there are 54 local field nodes in each first/second-order orthospectral element. Therefore, each element can be represented by a 54×54 local matrix, obtained by eqn. (2-11). The system matrix of the problem can be obtained by summing the effects from all elements, and enforcing the proper boundary conditions. The essential boundary conditions that must be enforced are:

$\mathbf{E} \times 1_n = 0$ (homogeneous Dirichlet on perfect electric conductors),

$\mathbf{E} \times 1_n = \mathbf{E}_0$ (inhomogeneous Dirichlet on excitation planes),

$(\mathbf{E} \times 1_n)_i = (\mathbf{E} \times 1_n)_j$ (continuity of tangential field components between any two adjacent element i and element j).

The entry of each global field node is formed by adding the contributions from the related local field nodes of each element. All nodes subjected to Dirichlet boundary conditions contribute to the right-hand-side of the system matrix. For deterministic problems, the assembled global matrix represents the system of equations of the problem in the form $\underline{\mathbf{A}}\mathbf{x}=\underline{\mathbf{B}}$.

Chapter 3

Boundary-marching method

3.1 Introduction

Finite elements formulated in terms of vector field components have been widely used in characterizing arbitrarily shaped waveguides. Recently, the finite element method has also been successfully applied in analyzing some subclasses of waveguide discontinuity problems which are essentially two-dimensional, such as E-plane and H-plane discontinuities. However, a general waveguide discontinuity is three-dimensional. It joins two or more waveguides, possibly dissimilar; it has an arbitrary shape in all directions, and may contain inhomogeneous materials. In such cases, a full three-dimensional analysis is required. When using the finite element method, one also needs to model the two infinite waveguides directly attached to the discontinuity section. The most common way of dealing with such infinite guides is to truncate the guides at a distance sufficiently far from the discontinuity, with a large number of mesh nodes. Proper boundary conditions are then applied at the truncated surfaces, assuming that the field decays significantly before reaching the truncations. This approach results in an undesirably large mesh and therefore is not practical in many three-dimensional problems. For some special cases, where the waveguide geometry is rectangular, circular

or elliptical, an equivalent boundary condition, derived from analytically known guided modes, may be used to truncate the mesh at a smaller distance from the discontinuity. However, if the geometry of the waveguide structure is more general, there is no analytic solution for the waveguide and an equivalent boundary condition for the infinite guide section cannot be found easily. This is especially true in the case of inhomogeneously dielectric-loaded waveguides.

This Chapter presents a very general finite element scheme which can be used to model an arbitrarily-shaped guide that may be inhomogeneous in the transverse direction. The algorithm uses a simple recursive method to generate a submatrix which relates the field characteristics on the near-field surface to the field conditions on the far-field surface. As a result, it can be used to truncate the finite element mesh at a distance very close to the discontinuity without losing any generality, for any arbitrarily-shaped guide. This procedure resembles the "roof-raising" process used in static and diffusion fields by Kisak, Silvester and Telford [1], and the related but more general two-dimensional "ballooning" algorithm applied to electrostatics problems by Silvester, Lowther, Carpenter and Wyatt [2].

Waveguide analysis with the finite element method has long been troubled by the appearance of spurious modes. Although these are commonly encountered in eigenvalue problems, it has been shown that spurious modes can affect solutions to deterministic problems also [3,4]. The orthospectral ("spectrally correct") elements obtained by using mixed-order approximating functions on hexahedra [3,6] have been shown to produce solutions free of spurious modes. The boundary-marching algorithm developed here is based on elements of this type and, as would be expected, no spurious-mode corruption of solutions has been encountered.

3.2 Variational formulation

The general configuration of the class of discontinuity problems considered here is illustrated in Fig. 3-1. The waveguide discontinuity or junction region is viewed as being composed of three subregions: *(i)* a uniform guide Ω_1, *(ii)* the discontinuity region proper, Ω_d, and *(iii)* the second uniform guide Ω_2, not necessarily similar to Ω_1. All medium nonuniformities are confined to the discontinuity region. The cross-sections of the uniform guides are not restricted. They may be inhomogeneous and arbitrary in geometry. In the uniform guides and in the discontinuity region Ω_d the electric field must everywhere satisfy the vector Helmholtz equation

$$\frac{1}{\mu_r}\nabla\times\nabla\times\mathbf{E}-k_0^2\epsilon_r\mathbf{E}=0, \tag{3-1}$$

subject to boundary conditions of the following types:

$$(\nabla\times\mathbf{E})\times\mathbf{1}_n=0 \qquad \text{(homogeneous Neumann on magnetic wall)}, \tag{3-2}$$

$$\mathbf{E}\times\mathbf{1}_n=0 \qquad \text{(homogeneous Dirichlet on perfect electric conductors)}, \tag{3-3}$$

$$\mathbf{E}\times\mathbf{1}_n=\mathbf{E}_0 \qquad \text{(inhomogeneous Dirichlet on excitation planes)}. \tag{3-4}$$

As is well known [8], solving the Helmholtz equation for the electric field vector in the lossless case is equivalent to extremizing the variational functional

$$\mathfrak{F}(\mathbf{E})=\frac{1}{2}\int_{\Omega}\Big\{-\frac{1}{\mu_r}(\nabla\times\mathbf{E})\cdot(\nabla\times\mathbf{E})+k_0^2\epsilon_r\mathbf{E}\cdot\mathbf{E}\Big\}d\Omega. \tag{3-5}$$

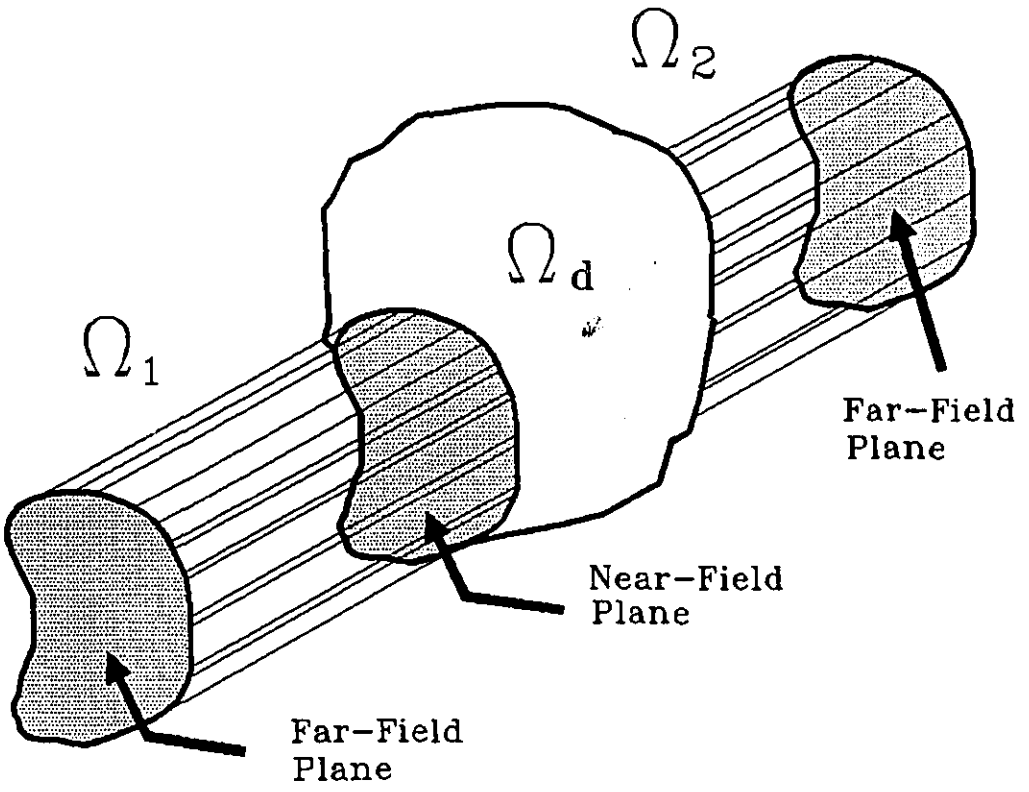

Figure 3–1

Discontinuity problem of a general waveguide
of arbitrarily–shaped cross–section

The finite element methods contemplated here rely on this formulation. Discretizing the entire region into finite elements and applying the standard finite element minimization procedure to the functional, as described in chapter 2, gives the following system of equations:

$$\{ -\frac{1}{\mu_r}[S] + k_0^2 \epsilon_r [T] \} \ [\mathrm{E}] = [0]. \tag{3-6}$$

Here $[E]$ is a column matrix representing the nodal electric fields, $[S]$ is the square matrix that results from the curl-curl term in the functional, and $[T]$ corresponds to the dot-product term in the functional. For convenience in the subsequent developments of the boundary-marching algorithm, eqn. (3-6) is simplified to the following expression:

$$[\mathrm{W}][\mathrm{E}] = [0] \tag{3-7}$$

where $[\mathrm{W}] = -\frac{1}{\mu_r}[S] + k_0^2 \epsilon_r [T]$.

3.3 Boundary-Marching Algorithm

The main interest here is placed on the modeling of the two uniform waveguide sections. The primary objective is to generate matrix representations of the uniform guides which can be used to interrelate the nodal field on a near-field plane to the nodal field values on the far-field planes where the field distributions are known a priori. The boundary-marching algorithm is proposed for this purpose. Four steps of the boundary-marching process are illustrated in Fig. 3-2. As indicated, the far-field and near-field planes are initially placed at the same location; then the far-field plane is moved away step by step, with the distance at each step growing larger as the far-field plane recedes. To develop the computational algorithm, let Ω^0 be the volume of the initial segment of a uniform guide; let Γ_1 and Γ_2 be the two surfaces enclosing this segment of the guide. Because the guide is uniform, Γ_1 and Γ_2 are congruent. The guide segment is discretized into finite elements, with the following restriction on the manner of subdivision: the placement of finite element nodes and edges must leave Γ_1 and Γ_2 congruent, i.e., the element and node placement on Γ_1 must correspond exactly to that on Γ_2. On discretizing the segment into a number of finite elements and minimizing the corresponding electric-field functional, the following set of simultaneous equations is obtained:

$$\begin{bmatrix} [W]_{11} & [W]_{1i} & [W]_{12} \\ [W]_{i1} & [W]_{ii} & [W]_{i2} \\ [W]_{21} & [W]_{2i} & [W]_{22} \end{bmatrix} \begin{bmatrix} [E]_1 \\ [E]_i^0 \\ [E]_2 \end{bmatrix} = 0. \tag{3-8}$$

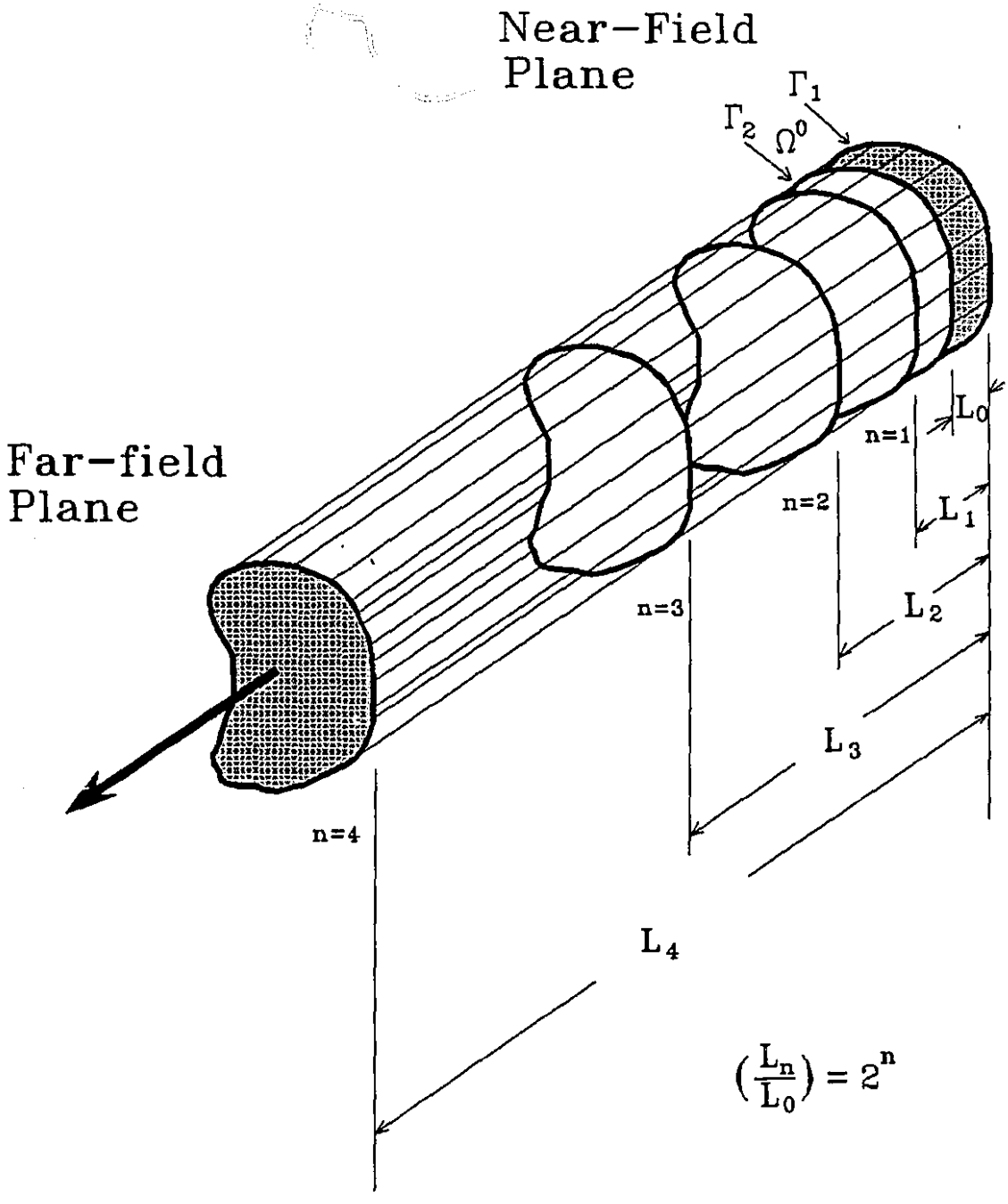

Figure 3–2
Boundary–marching process

This matrix equation has been partitioned so that the submatrices identified by subscript 1 correspond to finite element nodes located on plane 1 (the near-field plane), those identified by subscript 2 correspond to finite element nodes located on plane 2, and those identified by i are in the interior of the guide segment. (The superscripts are of no significance for the moment; they are introduced only for notational consistency with further development.) Thus $[E]_1$ represents the nodal electric fields on boundary surface 1, $[E]_2$ the nodal electric fields on boundary plane 2, and $[E]_i^0$ is the set of all nodal electric fields inside the region. Since any two transverse planes in the guide are sufficient to describe the uniform guide, all additional nodes between the two planes, the internal field nodes $[E]_i^0$, are not of interest and are eliminated by a static condensation scheme [61,62]. The system of equations for waveguide segment Ω^0 is thereby reduced to the more compact form

$$\begin{bmatrix} [S]_{11}^0 & [S]_{12}^0 \\ [S]_{21}^0 & [S]_{22}^0 \end{bmatrix} \begin{bmatrix} [E]_1^0 \\ [E]_2^0 \end{bmatrix} = 0, \tag{3-9}$$

where the number of matrix rows and columns equals the number of nodal variables on the bounding surfaces Γ_1 and Γ_2 only; the subscript i has disappeared altogether. The new submatrices $[S]_{mn}^0$ are obtained from the nine submatrices $[W]_{mn}$ of the finite element functional by

$$[S]^0_{11} = [W]_{11} - [W]_{1i}([W]_{ii})^{-1}[W]_{i1} \tag{3-10}$$

$$[S]^0_{12} = [W]_{12} - [W]_{1i}([W]_{ii})^{-1}[W]_{i2} \tag{3-11}$$

$$[S]^0_{21} = [W]_{21} - [W]_{2i}([W]_{ii})^{-1}[W]_{i1} \tag{3-12}$$

$$[S]^0_{22} = [W]_{22} - [W]_{2i}([W]_{ii})^{-1}[W]_{i2}. \tag{3-13}$$

The notation follows that for the full matrix representation: submatrix $[S]^0_{mn}$ interrelates field components associated with nodes on surface Γ_m of the condensed element with those on surface Γ_n.

Now the coefficient matrix of eqn. (3-9) describes the interrelationship of electric field components at the two ends of a fixed length of uniform guide, with no assumptions as to the length (it need not be smaller than a wavelength). A section of guide twice that length can therefore be modeled without loss of accuracy by cascading two such matrices. The description of a double-length segment of guide is thus obtained by combining two identical segments as described by eqn. (3-9) and enforcing field continuity on their common boundary:

$$\begin{bmatrix} [S]^0_{11} & [S]^0_{12} & 0 \\ [S]^0_{21} & [S]^0_{11} + [S]^0_{22} & [S]^0_{12} \\ 0 & [S]^0_{21} & [S]^0_{22} \end{bmatrix} \begin{bmatrix} [E]^0_1 \\ [E]^0_i \\ [E]^0_2 \end{bmatrix} = 0. \tag{3-14}$$

As before, the electric field at the internal nodes is of no interest. It can be eliminated from further consideration, removing $[E]^0_i$ by the same process of static condensation as previously. What results is a description of a "super-element" twice as long as the original one:

$$\begin{bmatrix} [S]^1_{11} & [S]^1_{12} \\ [S]^1_{21} & [S]^1_{22} \end{bmatrix} \begin{bmatrix} [E]^1_1 \\ [E]^1_i \end{bmatrix} = 0, \tag{3-15}$$

where the superscript 1 indicates that one doubling of the guide length has taken place. The four new submatrices are obtained much as before:

$$[S]^1_{11} = [S]^0_{11} - [S]^0_{1i}\left([S]^0_{ii}\right)^{-1}[S]^0_{i1}, \tag{3-16}$$

$$[S]^1_{12} = - [S]^0_{1i}\left([S]^0_{ii}\right)^{-1}[S]^0_{i2}, \tag{3-17}$$

$$[S]^1_{21} = - [S]^0_{2i}\left([S]^0_{ii}\right)^{-1}[S]^0_{i1}, \tag{3-18}$$

$$[S]^1_{22} = [S]^0_{22} - [S]^0_{2i}\left([S]^0_{ii}\right)^{-1}[S]^0_{i2}. \tag{3-19}$$

The new super-element representing the guide section is twice as long, and therefore has twice the volume of the original section: $\Omega^1 = 2\Omega^0$.

Further lengthening of the guide segment is achieved by applying the same procedure recursively. After each of n recursions, the matrix relating the excitation field on boundary surface 1 to the field distribution on the far-field plane can be expressed in terms of the submatrices of the previous recursion as follows:

$$[S]^{k+1}_{11} = [S]^k_{11} - [S]^k_{1i}\left([S]^k_{ii}\right)^{-1}[S]^k_{i1} \tag{3-20}$$

$$[S]^{k+1}_{12} = - [S]^k_{1i}\left([S]^k_{ii}\right)^{-1}[S]^k_{i2} \tag{3-21}$$

$$[S]^{k+1}_{21} = - [S]^k_{2i}\left([S]^k_{ii}\right)^{-1}[S]^k_{i1} \tag{3-22}$$

$$[S]^{k+1}_{22} = [S]^k_{22} - [S]^k_{2i}\left([S]^k_{ii}\right)^{-1}[S]^k_{i2}. \tag{3-23}$$

At each recursion step, the length of the super-element (i.e., of the guide segment) is augmented by a factor of 2. Consequently, in the course of N recursions, the length of the uniform guide in the propagation direction grows by a factor of 2^N. In effect the procedure is equivalent to marching out the boundary of the uniform guide from the excitation plane to the far-field plane, sufficiently far for all evanescent modes to decay to a negligible level. The method therefore provides a simple way for simulation and investigation of wave propagation in any arbitrarily-shaped guide. The advantage of the algorithm becomes even more pronounced in the case of inhomogeneously dielectric-loaded guide, where any competitive method currently available (e.g., any integral equation method) becomes too complicated, if not impossible.

To summarize the full computational algorithm: The finite element matrix for a finite, generally quite short, length of guide is constructed using standard techniques. It is partitioned into submatrices according to whether the node numbers refer to bounding plane 1 (the near-field plane), plane 2 (the farther plane), or the interior i. The nine submatrices are then manipulated in an N-step recursion as follows.

Step 1: initialize.

$$[S]^0_{11} = [W]_{11} - [W]_{1i}([W]_{ii})^{-1}[W]_{i1}$$
$$[S]^0_{12} = [W]_{12} - [W]_{1i}([W]_{ii})^{-1}[W]_{i2}$$
$$[S]^0_{21} = [W]_{21} - [W]_{2i}([W]_{ii})^{-1}[W]_{i1}$$
$$[S]^0_{22} = [W]_{22} - [W]_{2i}([W]_{ii})^{-1}[W]_{i2}.$$

Step 2: march out, for $k = 0, \ldots, N-1$.

$$
\begin{aligned}
[S]_{11}^{k+1} &= [S]_{11}^{k} - [S]_{1i}^{k}\left([S]_{ii}^{k}\right)^{-1}[S]_{i1}^{k} \\
[S]_{12}^{k+1} &= - [S]_{1i}^{k}\left([S]_{ii}^{k}\right)^{-1}[S]_{i2}^{k} \\
[S]_{21}^{k+1} &= - [S]_{2i}^{k}\left([S]_{ii}^{k}\right)^{-1}[S]_{i1}^{k} \\
[S]_{22}^{k+1} &= [S]_{22}^{k} - [S]_{2i}^{k}\left([S]_{ii}^{k}\right)^{-1}[S]_{i2}^{k}.
\end{aligned}
$$

Step 3: record result.

$$
\begin{bmatrix} [S]_{11}^{N} & [S]_{12}^{N} \\ [S]_{21}^{N} & [S]_{22}^{N} \end{bmatrix} \begin{bmatrix} [E]_{1}^{N} \\ [E]_{i}^{N} \end{bmatrix} = 0.
$$

The guide length grows as 2^N, so only 20 recursion steps will turn an initial explicit guide model millimeters long into the same number of kilometers.

3.4 Conclusions

A general recursive method has been proposed and validated for creating finite element models of very great lengths (thousands of free-space wavelengths) of arbitrarily-shaped waveguide. The method is valid for any guide, so long as a technique is available for constructing a finite element model of a finite length of the guide. It is particularly useful for analysis of waveguide components and discontinuity regions, where it permits truncation of the finite element mesh very close to the discontinuity region without compromising result accuracy. It does not introduce any error beyond

the discretization error inherited from the finite element meshing; it is unconditionally stable, except possibly at frequencies very close to the cut-off frequency of the lowest eigenmode, where the ratio of free-space wavelength to guided wavelength approaches the floating-point precision available. This algorithm appears to be particularly useful for discontinuity analyses involving inhomogeneous dielectric-loaded guides, such as finline and shielded microstrips, but further verifying work is needed to establish what limits there may be to its use.

Chapter 4

Software Implementation

4.1 Programming Language

All necessary software for the computations in this thesis are written in Ada. Ada is a modern software engineering language designed to be used for large software systems. It encompasses all the basic principles associated with modern software engineering: structuring, modularity, data abstraction, information hiding, strong typing and error handling [66, 67, 68, 69, 70, 71]. It makes modular program development a reality. The primary advantage of Ada is that it allows construction of small, functionally cohesive modules with clearly defined interfaces, and enables the programming to piece them together into large, cohesive systems. Implementing with Ada results in a design identical to the actual system itself. The software can therefore be maintained the same way as maintaining the system itself. Furthermore, Ada emphasizes program readability, and therefore eases program maintenance.

4.2 Program Structure

The programs of this thesis are divided into six main modules:

Mesh Generator

Generates the 3-D finite element mesh, for a given waveguide structure. It is also used to generate the finite element mesh for discontinuities.

Matrix Condenser

Assembles the global matrix of the waveguide structure, based on the information given by the mesh generator, and condenses out all unwanted field nodes.

Boundary Expander

Performs the boundary-marching algorithm using the global matrix generated by the Matrix Condenser, for a given number of recursions.

Substructure connector

Connects any two waveguide sections, and condenses out all the unwanted field nodes. This program is also used to connect the two uniform waveguides to the discontinuity section.

Admittance calculator

Computes the admittance of a discontinuity.

Eigenvector solver

Generates the eigenvector of a waveguide structure.

The most time-consuming part of all the computations here is to perform the static condensation in the Matrix Condenser, Boundary Expander, and the Substructure Connector modules. The static condensation is performed by a small Ada package. Therefore, the speed of computations is dependent on the efficiency of the static condensation package. An efficient node-by-node condensation scheme is being used in this study.

4.3 Static Condensation Scheme

To condense a matrix, the static condensation processes make use of the following recursive formula:

$$
\begin{aligned}
[S]_{11}^{k+1} &= [S]_{11}^{k} - [S]_{1i}^{k}\left([S]_{ii}^{k}\right)^{-1}[S]_{i1}^{k} \\
[S]_{12}^{k+1} &= - [S]_{1i}^{k}\left([S]_{ii}^{k}\right)^{-1}[S]_{i2}^{k} \\
[S]_{21}^{k+1} &= - [S]_{2i}^{k}\left([S]_{ii}^{k}\right)^{-1}[S]_{i1}^{k} \\
[S]_{22}^{k+1} &= [S]_{22}^{k} - [S]_{2i}^{k}\left([S]_{ii}^{k}\right)^{-1}[S]_{i2}^{k}.
\end{aligned}
$$

Implementing the static condensation scheme in the matrix format requires large computer memory and storage. To improve the efficiency of computations, and to reduce the memory and storage requirements, the static condensation procedure is implemented in a node-by-node condensation approach. The node-by-node static condensation removes one field node at a time. Fig. 4-1 shows the node-by-node static condensation scheme for a $N \times N$ matrix. To remove node i from the matrix, we need to perform the following steps:

1. Compute new values for all row $k \neq i$, and all columns $j \neq i$ using,

$$a'_{kj} = a_{kj} - a_{ki} * a_{ii}^{-1} * a_{ij} .$$

The efficiency of computations can be improved by checking the values of a_{ki} and a_{ij}. The entry a_{kj} needs to be updated only when neither a_{ki} nor a_{ij} is zero. Furthermore, for a symmetric matrix, only the upper part of the matrix needs to be computed.

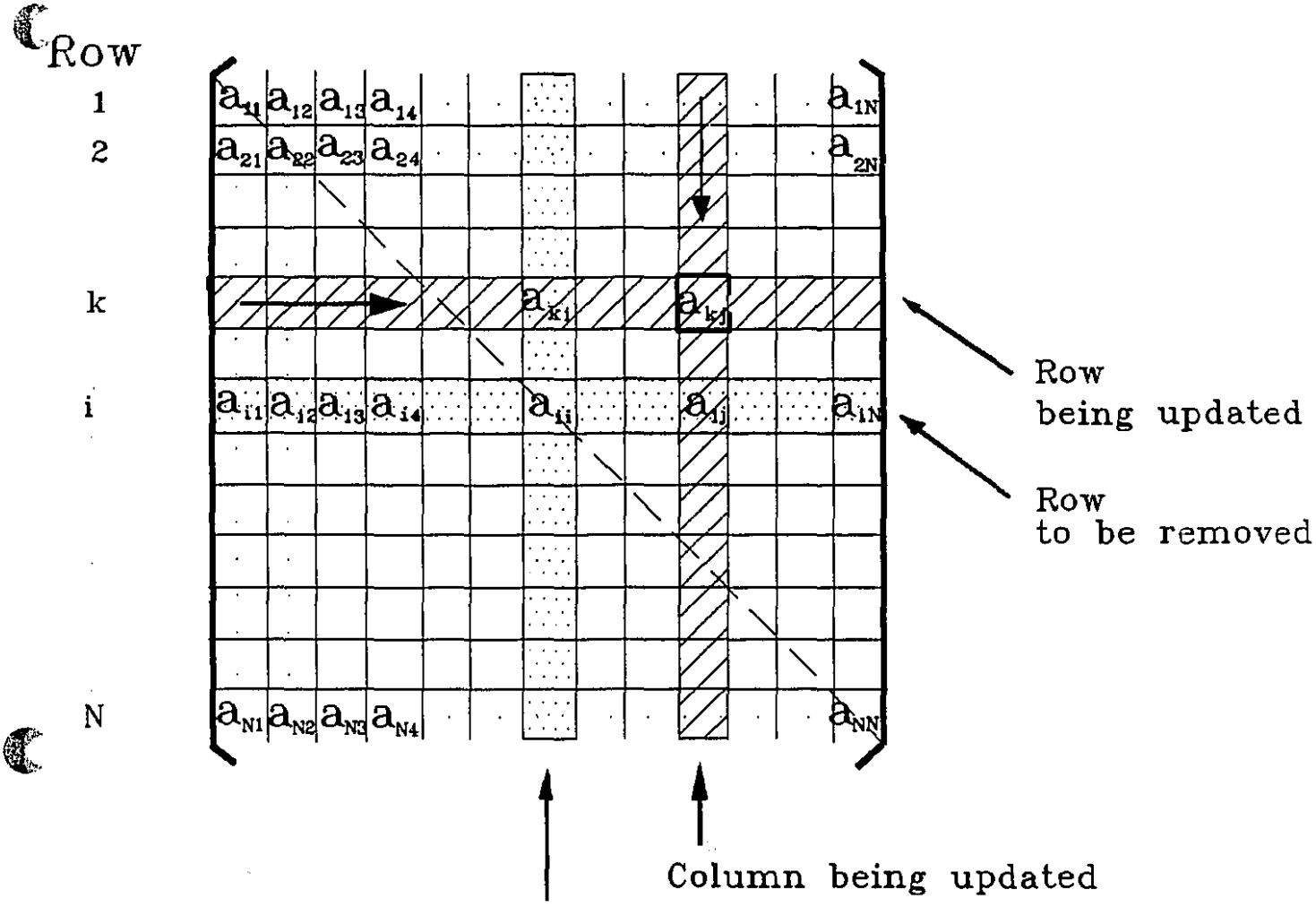

$$a'_{kj} = a_{kj} - a_{ki} * a_{ii}^{-1} * a_{ij} \quad \forall \quad k \neq i \ , \ j \neq i$$

Figure 4-1
Node-by-Node Static Condensation Scheme

2. Remove column i and row i from the matrix by rearranging the entries as follow:

$$\begin{aligned}
a'(k,j) &= a(k,j), && \text{for all row } k<i, \text{ column } j<i,\\
a'(k,j) &= a(k+1,j), && \text{for all row } k>i, \text{ column } j<i,\\
a'(k,j) &= a(k,J+1), && \text{for all row } k<i, \text{ column } j>i,\\
a'(k,j) &= a(k+1,J+1), && \text{for all row } k>i, \text{ column } j>i.
\end{aligned}$$

The final matrix will be an (N-1) order matrix. Therefore, for the worst case situation, assuming that the original $N \times N$ matrix is a full, symmetric matrix, the number of operations required to condense it into an (N-1) order matrix is,

$$\frac{(N-1)^2}{2} \quad \text{subtractions,}$$

$$(N-1)^2 \quad \text{multiplications/divisions.}$$

To reduce an $N \times N$ matrix into an $M \times M$ matrix, the procedure must be repeated by (N-M) times. In each step, the matrix is one order smaller than the previous matrix. Therefore, a maximum of

$$\left(\frac{(N-1)!}{2(M-1)!}\right)^2 \quad \text{subtractions,}$$

$$\left(\frac{(N-1)!}{(M-1)!}\right)^2 \quad \text{multiplications/divisions,}$$

will be required to condense the matrix. In practice, the matrix to be condensed is not full 100%. This is especially true when the condensation scheme is first applied to the

global matrix which is relatively sparse. On the average, one would be able to improve the number of computations by another $20\% - 40\%$ by checking the values of the entries a_{ki} and a_{ij}.

4.4 Gauss-Legendre Quadrature

Evaluations of the [S] and [T] local matrices for each finite element involve volumetric numerical integrations. To obtain good computational efficiency and integration accuracy, Gauss-Legendre quadrature is used to evaluate such integral. Appendix II gives the detail of the integration scheme.

4.5 Gaussian Elimination

Solving discontinuity problem with finite element method results in a set of linear algebraic equations, $\underline{A}x=\underline{B}$. Since the proposed finite element scheme results in a relatively small (in the order of a few thousands unknowns) but dense matrix, the Gaussian elimination procedure is used here to solve the resultant system equations. The matrix is first converted into a triangular upper matrix by using pivoting and eliminating processes. The solution is then found by performing the back substitution procedure.

Chapter 5

Waveguide analysis by boundary-marching algorithm

5.1 Introduction

Chapter 3 showed how an accurate matrix representation for an infinitely long waveguide can be generated by using the boundary-marching algorithm. This Chapter is intended to show how the matrix can be used for simulating wave propagations and discontinuity analysis in waveguide of arbitrary cross-sectional shape. The boundary-marching technique has been extensively tested on guides of several different cross-sectional shapes. All test programs used Crowley-type orthospectral elements [6] and were written in the Ada language. Two computers were used: an 80386-based (MS-DOS) machine for program development and debugging, followed by a Cray X-MP supercomputer for subsequent production runs.

5.2 Wave propagation in Rectangular Waveguides

The boundary-marching algorithm is first tested here against the well-known characteristics of the rectangular waveguide. The matrix representation of a rectangular waveguide of width a=20.32mm and height of b=10.16mm is generated by using the boundary-marching algorithm with 7 recursions. The operating frequency of the simulation is chosen such that at least the first four transverse electric eigenmodes, TE_{10}, TE_{01}, TE_{21}, TE_{11} are non-evanescent. A total of 25 elements are used to approximate the cross-section of the waveguide. Applying homogeneous Neumann conditions on the far-field plane, various propagation modes in the rectangular waveguide can be simulated by exciting the guide with proper excitation field on the near-field plane. First, the TE_{10} is simulated by using an x-polarized point source located in the middle of the cross-section of the near-field plane. Figure 5-1 shows the comparison of the calculated TE_{10} mode field distributions with the idealized case, Sin(y) distribution. With single-precision arithmetic, the maximum field strength error is less than 0.05%. Next, the TE_{01} propagation is simulated with a y-polarized point source located in the middle of the cross-section of the near-field plane. In this case, one gets a Sin(x) field distribution with a maximum field strength error of less than 0.1%.

The problem becomes more interesting when a dielectric slab is loaded into the rectangular waveguide. The characteristics and approximate expressions of the dielectric-slab-loaded waveguides have been well documented and can be found in [60,65]. The basic modes of propagation in such waveguides are longitudinal-section electric (LSE) modes which can be represented by a single magnetic-type Hertzian potential:

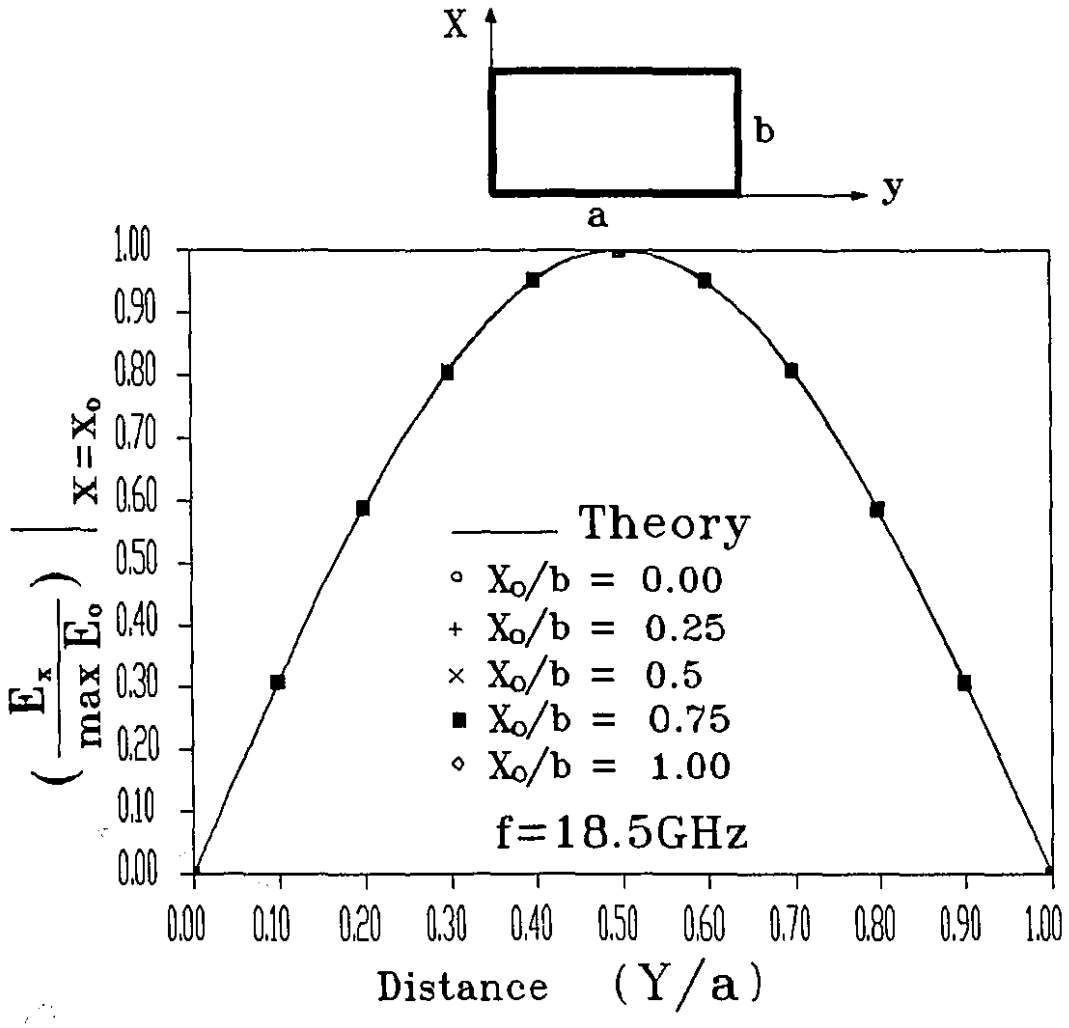

Note: The six curves overlap to within 0.05% accuracy.

Figure 5-1

Field strength distribution in a rectangular waveguide

$$\Pi_h = \mathbf{a}_x \Phi_h e^{-\gamma z} . \tag{5-1}$$

And the electric field is given by

$$\mathbf{E} = -j\omega\mu_o \nabla \times \Pi_h . \tag{5-2}$$

The scalar function Φ_h must satisfy the following relation:

$$\nabla_t^2 \Phi_h + [\gamma^2 + \epsilon(x)\, k_o^2]\, \Phi_h = 0, \tag{5-3}$$

where $\epsilon(x)=1$ in the air-filled portion of the guide ($y<d$), and $\epsilon(x)=\epsilon_r$ in the dielectric-filled portion of the guide ($d<y<a$). A solution for Φ_h which satisfies the boundary conditions at both the dielectric interface and on the perfectly conducting walls is

$$\Phi_h = \begin{cases} A \sin(k_{x1} y) \cos(\frac{m\pi x}{b}) , & 0 \le y \le d, \\ B \sin(k_{x2}[a-y]) \cos(\frac{m\pi x}{b}) , & d \le y \le a, \end{cases} \tag{5-4}$$

subject to the following relations:

$$\begin{aligned} k_{x1} \tan(k_{x2}[a-d]) &= -k_{x2} \tan(k_{x1} d), \\ k_{x2}^2 &= k_{x1}^2 + (\epsilon_r - 1) k_0^2 \end{aligned} \tag{5-5}$$

where A and B are amplitude constants, k_{x1} and k_{x2} are the wave numbers in the air and in the substrate, respectively. There are infinite number of solutions for the wave numbers k_{x1} and k_{x2} that satisfy the conditions. For the purpose of this investigation, the special case of m=0 is used. In this case, both $\mathbf{E}_z$ and $\mathbf{H}_x$ vanish and the only non-vanishing electric component is $\mathbf{E}_x$. This is also called the H_{no} modes. In this case, the electric field becomes,

$$\mathbf{E} = -j\omega\mu_o\gamma\ \Phi_h\ e^{-\gamma z}\ . \tag{5-6}$$

Therefore, for a given z value, the electric field can be described by,

$$E_x = \begin{cases} A \sin(k_{x1}y), & 0 \le y \le d, \\ B \sin(k_{x2}[a-y]), & d \le y \le a. \end{cases} \tag{5-7}$$

A waveguide half-filled with dielectric slab with the dielectric constant of ϵ_r=2.22 is being considered here. By solving the conditions set by eqn. (5-5), it is found that the wave numbers for the lowest mode H_{10} are:

$$\left(\frac{\gamma}{k_o}\right) = 0.32955\ ,$$
$$k_{x1} = 0.148406\ ,$$
$$k_{x2} = 0.228402\ .$$

The amplitude constants A and B are set to

$$A = 1.064022\,,$$

$$B = 1.021225\,.$$

Figure 5-2 gives the theoretical and the computed electric field distribution. The results are computed with the identical finite element scheme as that of the empty waveguide case (25 elements, 7 recursions). The maximum field strength error is less than 0.03%.

For the purpose of the discontinuity analysis, it is essential to understand how the matrix responds to higher-order mode excitations. The algorithm is therefore tested here by investigating the decay behavior of the evanescent modes, as the boundary of the far-field plane is marched out from the excitation plane. Fig. 5-3 shows how the reflected waves of the $TE_{0,1}$, $TE_{0,2}$ and $TE_{2,0}$ modes decay with guide length in a typical rectangular waveguide. The operating frequency is chosen so that the $TE_{1,0}$ mode is the only propagating mode in the waveguide. All computations were carried out in 64-bit arithmetic, so that noticeable roundoff error accumulation in the fourteenth or fifteenth digit is to be expected. In fact, the roundoff error falls substantially below that level in two of the modes. The magnitude of the forward transmission of the scattering coefficient of the propagating mode ($TE_{1,0}$ mode), as a function of the length of the waveguide is also shown in Fig. 5-3. Clearly, about 6 or 7 recursions are more than adequate in this case to make the guide "infinite" for all practical purposes. Even quite near cutoff, about 20 or 30 recursion steps suffice, yielding a waveguide length of 10^5—10^8 times guide width.

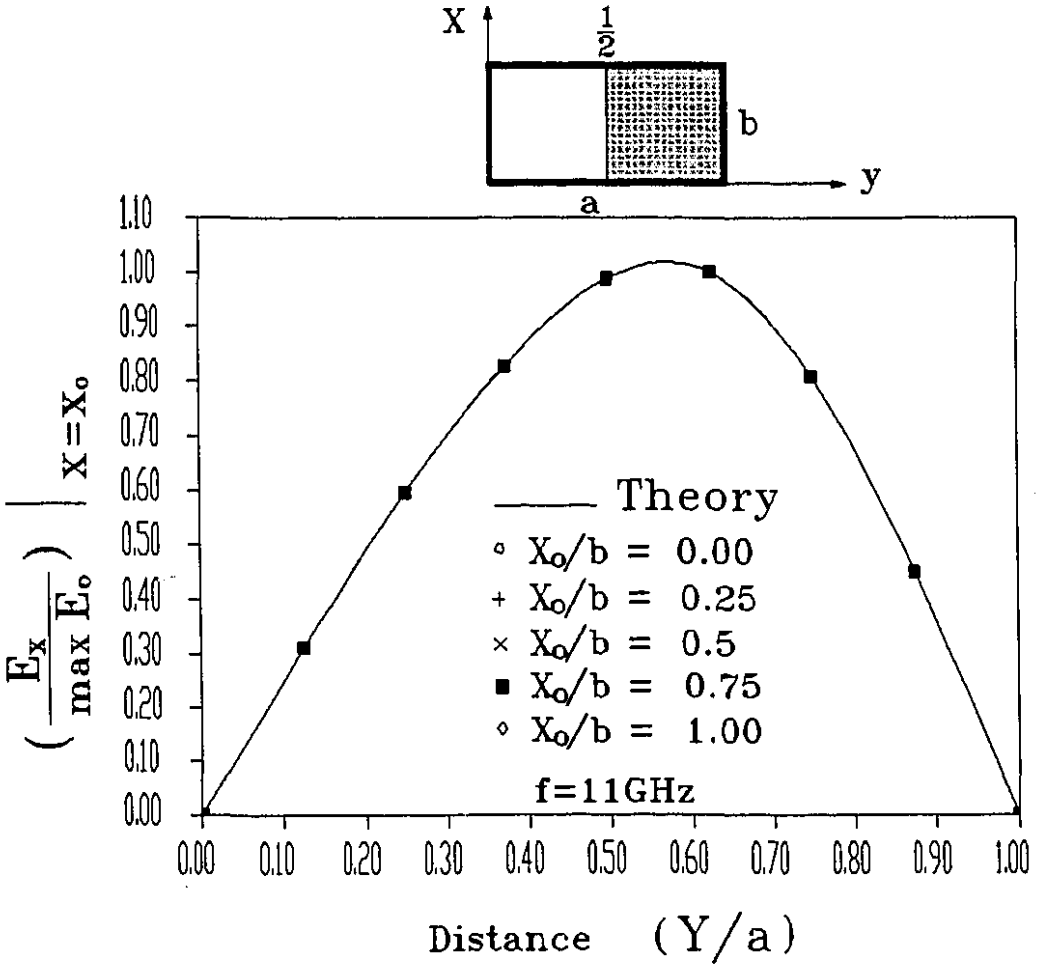

Note: The six curves overlap to within 0.03% accuracy.

Figure 5-2

Field strength distribution in a dielectric-loaded waveguide

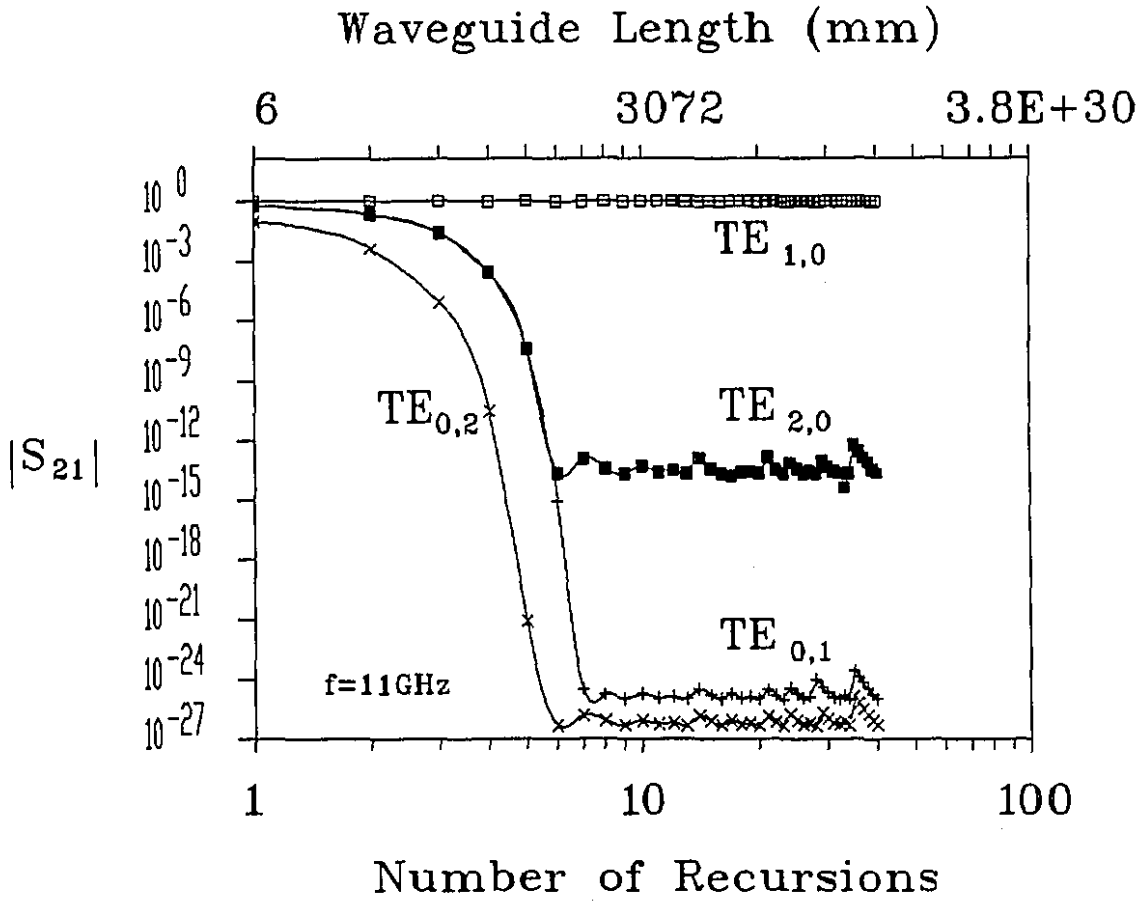

Figure 5-3
Decaying behaviour of evanescent modes
in a rectangular waveguide

5.3 Discontinuity analysis

To illustrate how the boundary-marching procedure can be incorporated into waveguide discontinuity analysis, the scattering parameters of a zero-thickness asymmetric capacitive window is evaluated here. The asymmetric capacitive window (zero-thickness) can be modeled as a shunt susceptance. An approximate expression for the normalized susceptance of the capacitive window was given by Marcurvitz [60],

$$(\frac{B}{Y_o}) = \mathrm{Log_e}\,[\,\csc\,(\mathrm{Y})\,] + \frac{Q_2\cos^4(\mathrm{Y})}{1+\,Q_2\sin^4(\mathrm{Y})} + \tfrac{1}{4}\,\mathrm{X}^2\,[\,1\,-3\sin^2\,(\mathrm{Y})\,]^2\cos^4(\mathrm{Y}), \qquad (5\text{-}8)$$

where,

$$\mathrm{X} = (\frac{b}{\lambda_g}),$$
$$\mathrm{Y} = (\frac{\pi d}{2b}),$$
$$Q_2 = \frac{1}{\sqrt{1-4X^2}} - 1,$$
$$\lambda_g = \frac{\lambda}{\sqrt{1-(\frac{\lambda}{\lambda_c})^2}}.$$

For given waveguide dimensions and operating frequency, the normalized susceptance can be computed according to eqn. (5-8). Fig. 5-4 shows the finite element scheme for the solution of the zero-thickness capacitive window. The detail of the procedure for computing S-parameters from finite element solution is described in Appendix III. First, the prescribed field conditions on the far-field planes are generated using the matrix representation for the uniform waveguide. For frequencies below the cut-off frequency of the second higher order mode, the TE_{10} field distribution is obtained for any field excitation on the near-field plane. Once the prescribed field distributions on the far-field planes are known, the reference plane of the transmission and reflection parameters can be calibrated by using a

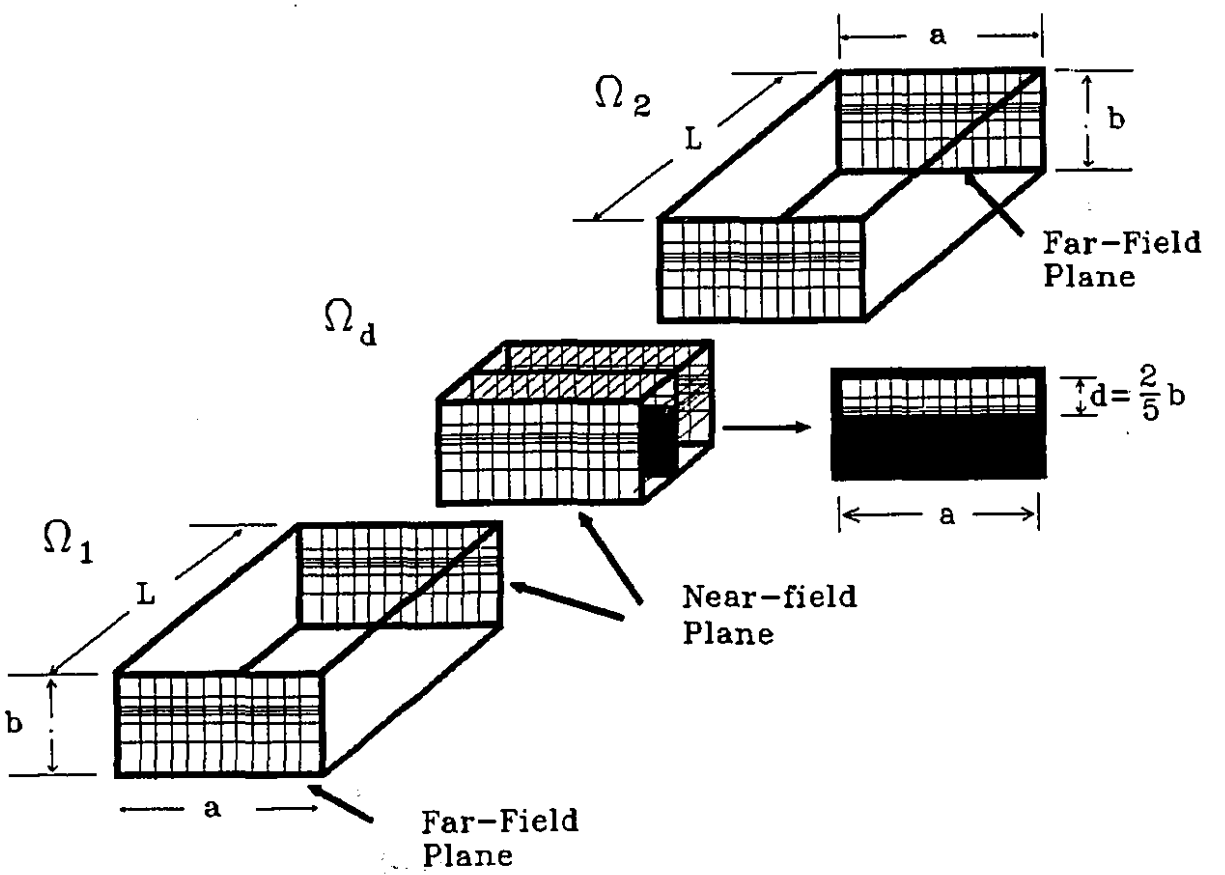

Figure 5-4

Finite element scheme of a zero-thickness capacitive window problem

matched "through" segment. The calibration also eliminates any error that may arise as a result of signal loss or phase distortions in the waveguide segments. The scattering parameters of the structure are first computed with the discontinuity section replaced by a segment of empty waveguide of known finite length. Matching the boundary conditions on the near-field planes, the scattering parameters of the structure can be extracted from the functionals, for different excitation conditions on the far-field planes. The calibration factors are determined by setting the magnitude of the forward transmission of the scattering coefficients to unity and the phase to 0 degrees. Then the scattering parameters of the structure including the discontinuity are computed by replacing the "calibration segment" with the discontinuity. Dividing the transmission and reflection parameters by the proper calibration factor, and subtracting the phase offset from the phase angles of the parameters, one obtains the final scattering parameters at the desired reference plane. By using the same segment length for the calibration segment as for the discontinuity segment, the transmission and reflection parameters are calibrated to the plane where the zero-thickness window resides. If desired, the parameters could also be calibrated to some other reference plane, by choosing different lengths for the calibration segment and the discontinuity segment.

Phase and amplitude of the forward transmission coefficient of the scattering parameters of the capacitive window are shown in Fig. 5-5, for different frequencies. The results agree with the analytical approximation given by Marcuvitz [60] to within 1-2 percent. Since the Marcuvitz solution is not exact, it cannot be used to establish firm error bounds. However, the finite element solution and Marcuvitz's approximation are thought to incur errors of roughly similar magnitude, so their agreement is held to confirm the validity of the boundary-marching technique.

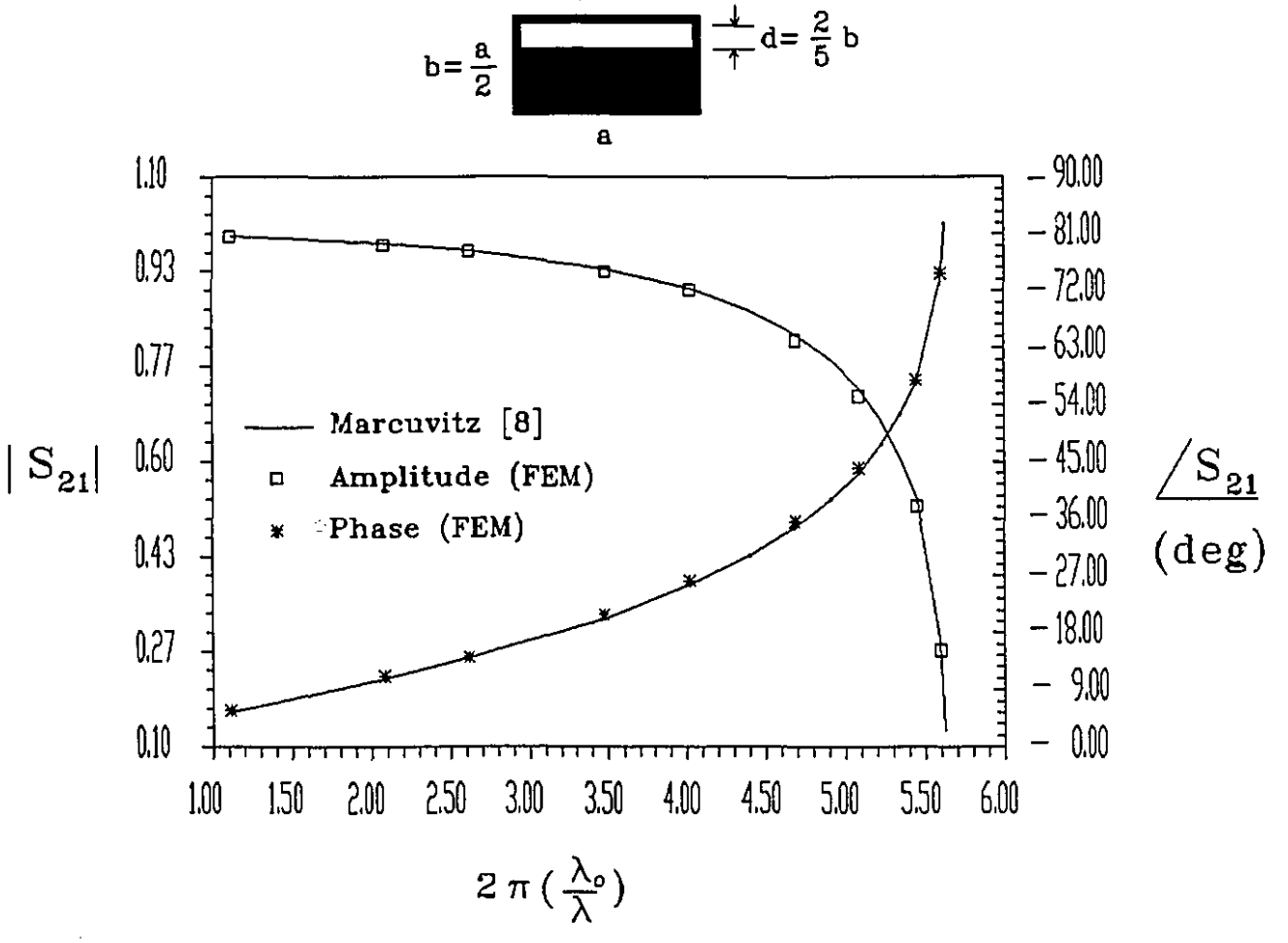

Figure 5-5

Scattering parameters of the zero-thickness capacitive window

Chapter 6

Inductive strips in unilateral finlines

6.1 Introduction

The design of millimeter-wave components in finline technologies requires the accurate characterization of various finline discontinuities. The inductive strip is one of the most essential building blocks of common bandpass filters implemented with E-plane circuit technologies. As a result, this type of discontinuity has been studied extensively by using various approximate and rigorous approaches [28,29,32]. However, all these analyses were based on the idealized finline model of zero fin thickness and negligible effect from the mounting groove. Neglecting such effects results in a shift in the desired range of operating frequencies in practical circuits. This phenomenon has been well demonstrated by the responses of multi-resonator filters [33,34,35] where the frequency responses of the theoretical results and the measured results are consistently shifted by a few percent. It has been reported that the error of neglecting such effects can go as high as 7 percent [31]. Furthermore, due to the imperfection on the mechanical fitting and thermal expansion on the metal enclosure, more errors can be contributed from the bending of the substrate and the fin. Several authors [36,37,38]

have studied the effect of finite metalization thickness and influence of the mounting grooves on the modal spectrum, propagation constants and the characteristic impedance of the finline structure. However, the real interest in the design process is how these parameters affect the parameters of a discontinuity in the finline structure. The purpose of this study is to provide a sensitivity analysis on the inductive strip for various depths of mounting grove, different thicknesses of metalization and varying degrees of bending of the substrate on the discontinuity parameters of an inductive strip in a unilateral finline. The results allow one to predict and design a finline component such as filter with a better accuracy.

Finline discontinuities are often analyzed by rigorous techniques, such as spectral-domain approaches or the transverse resonance method, which essentially reduce the three-dimensional problems into two-dimensional problems by reducing one degree of freedom in the transverse direction that is perpendicular to the substrate. These methods provide accurate results, if the metalization thickness and the effect of the mounting grooves are negligible. Recently, a two-dimensional finite element method has been applied to analyze the dispersion characteristics of finlines [30,40] of various cross-sections. However, due to demanding requirements on computer memory and storage, the three-dimensional finite element method has not yet been popular in finline discontinuity analysis. This thesis shows an efficient approach of applying the full three-dimensional finite element method in finline discontinuity analysis. The method allows one to analyze E-plane discontinuities, including various manufacturing effects such as the effect of the mounting grooves, influence of the metalization thickness and the effect of substrate bending.

6.2 Method of Analysis

Fig.6-1 delineates the problem under consideration. The substructure formulation has been incorporated into this algorithm. The problem domain is separated into three subregions: *(i)* Uniform finline one, Ω_1, *(ii)* Discontinuity region, Ω_d, *(iii)* Uniform finline two, Ω_2. The discontinuity region is subdivided into a number of mixed-order curvilinear finite elements formulated in terms of the covariant projection components as discussed in Chapter 2. The utilization of mixed-order finite elements eliminates the possibility of the appearance of any spurious mode [3,6]. To model the two infinitely-long, inhomogeneous waveguide sections, the boundary-marching algorithm is used. Utilization of the boundary-marching algorithm allows truncation of the finite element mesh in the discontinuity region at a distance very close to the discontinuity without any compromise with the result accuracy.

The trial functions of the electric field components must also satisfy the following boundary conditions at the boundary between element i and element j:

$$(\mathbf{E}\times\mathbf{1}_n)_i = (\mathbf{E}\times\mathbf{1}_n)_j \quad \text{(Continuous tangential field across elements).} \tag{6-1}$$

However, no conditions are enforced on the normal field components. Letting the normal field components free increases the number of degree of freedom and improves the field approximation at the singularities, the sharp edges of the zero thickness fin.

As indicated in [5] the uniform finline can be modeled more than adequately with just n=6 recursions. A total number of recursions of n=5 is suitable for most of the applications.

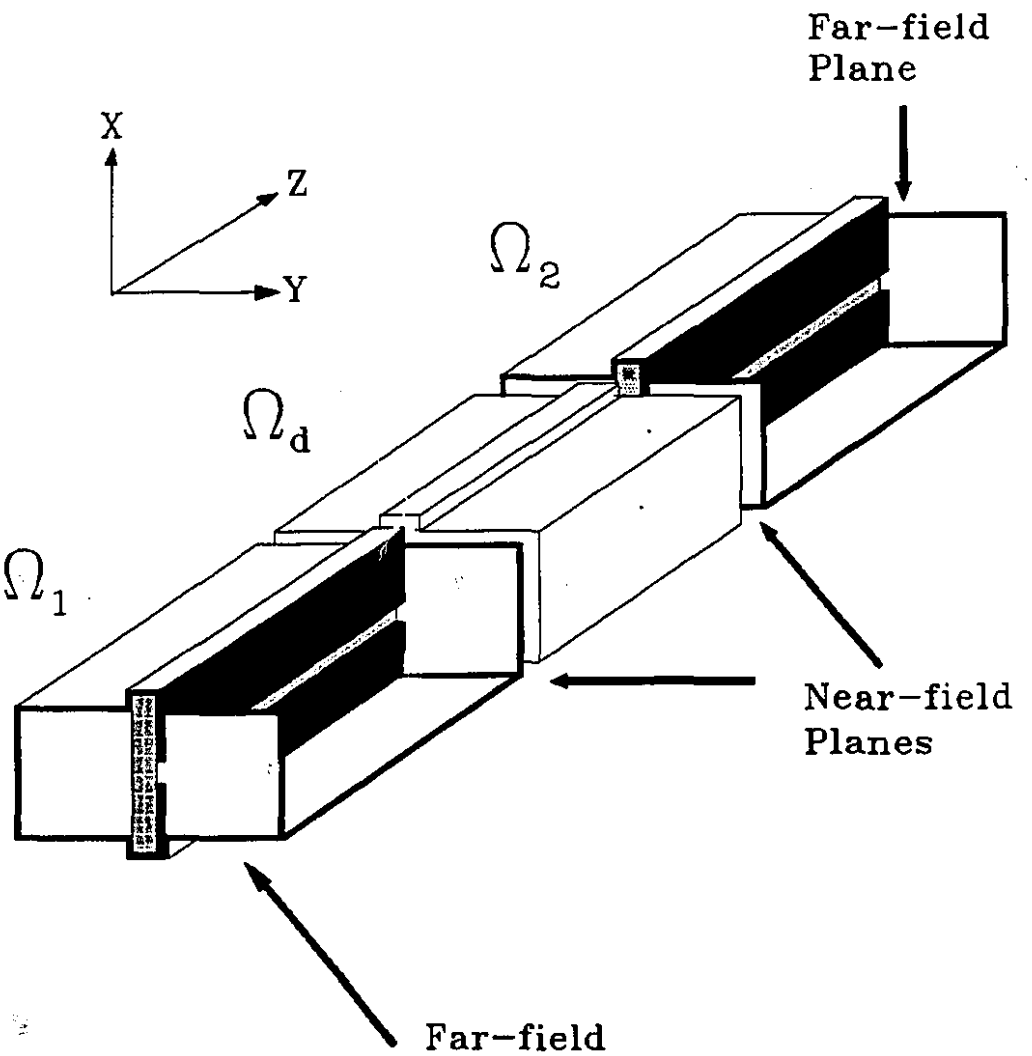

Ω_1 —— Uniform finline 1

Ω_2 —— Uniform finline 2

Ω_d —— Discontinuity region

Figure 6-1
Configuration of the problem

6.3 Scattering Parameters of Idealized Model

Computer programs based on the mixed-order finite element and the boundary-marching procedures have been developed and written in the Ada language. A Cray X-MP supercomputer was used for the computations. Fig. 6-2 shows the dimensions and the equivalent circuit of the inductive strip under consideration. The normalized susceptances of an inductive strip of idealized finline model are computed using the substructure method as shown in Fig. 6-1. 98 elements are used to approximate the field distribution in the discontinuity region, Ω_d. Before proceeding with the discontinuity analysis, the prescribed fields on the far-field planes must first be determined. The excitation field conditions on the far-field planes can be generated using the matrix representation of the uniform finline obtained by the boundary-marching algorithm. For operating frequencies lying within the single-mode bandwidth of the unilateral finline, the field distribution of the lowest eigenmode of the line is obtained by exciting the uniform finline with any non-trivial excitation on the near-field plane. Fig. 6-3 to Fig. 6-6 show an example of the transverse electric field distributions in a typical unilateral finline. These field plots are obtained by exciting the uniform guide with a few x-directed nodal fields on the near-field plane. The uniform guide was simulated with the boundary-marching algorithm with only 5 recursions. Once the excitation fields for the far-field planes are found, the scattering parameters of the structure can be extracted from the functional, by applying various arrangements of the far-field conditions on the far-field planes, and matching the boundary conditions on the near-field planes. The reference plane of the transmission and reflection parameters can be calibrated by using a matched "through" segment. The calibration procedure also eliminates any error that may arise as a result of signal loss or phase distortions in the waveguide segments.

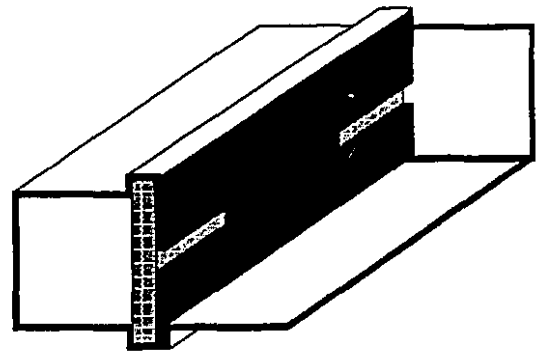

(a) 3-D View

t — Metalization thickness
s — Strip width
g — Depth of mounting groove
w — Slot width
d — Substrate thickness

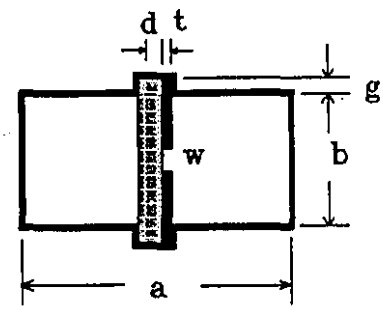

(b) Cross-Sectional View

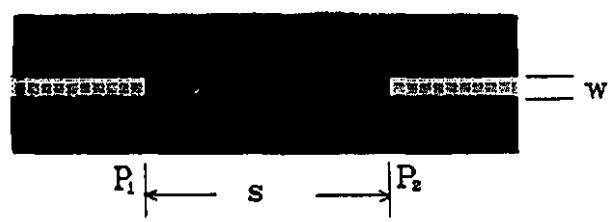

(c) Side View

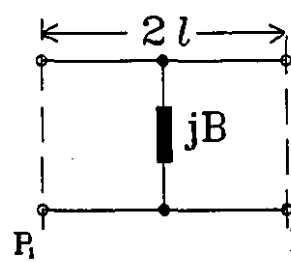

(d) Equivalent circuit

Figure 6-2
Inductive strip in unilateral finline

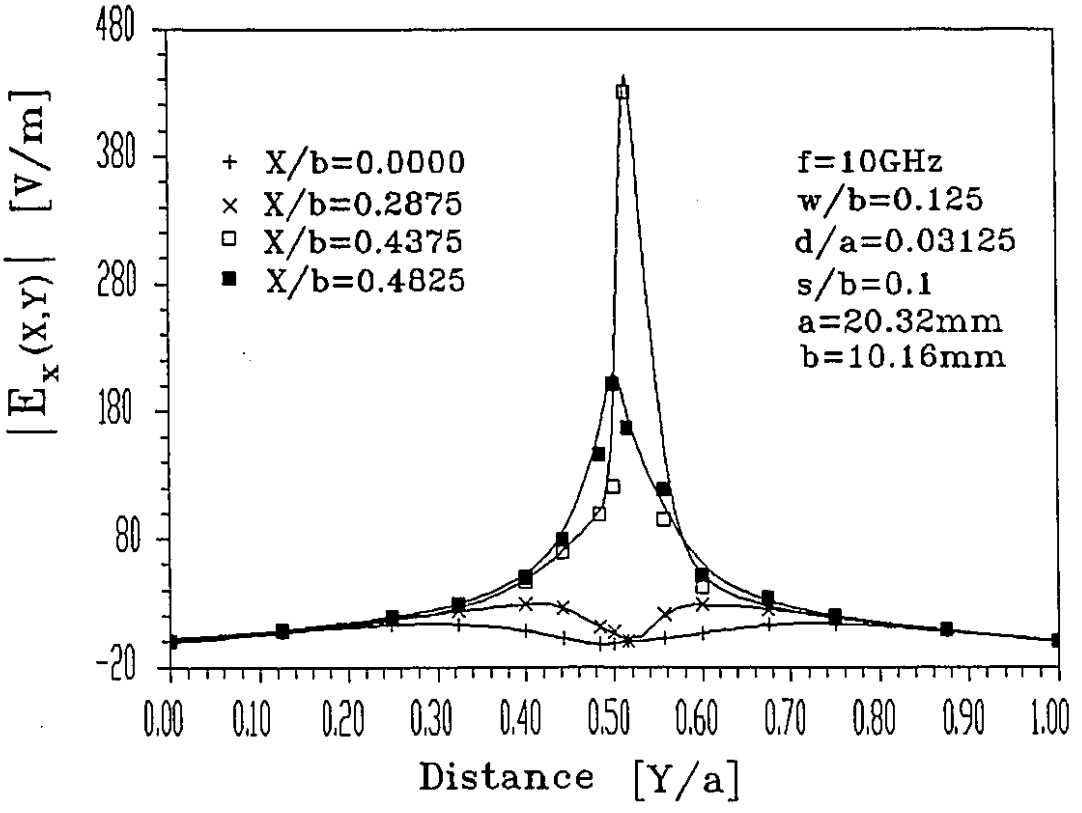

Figure 6-3

Electric field distribution in unilateral finline
(X-component versus Y)

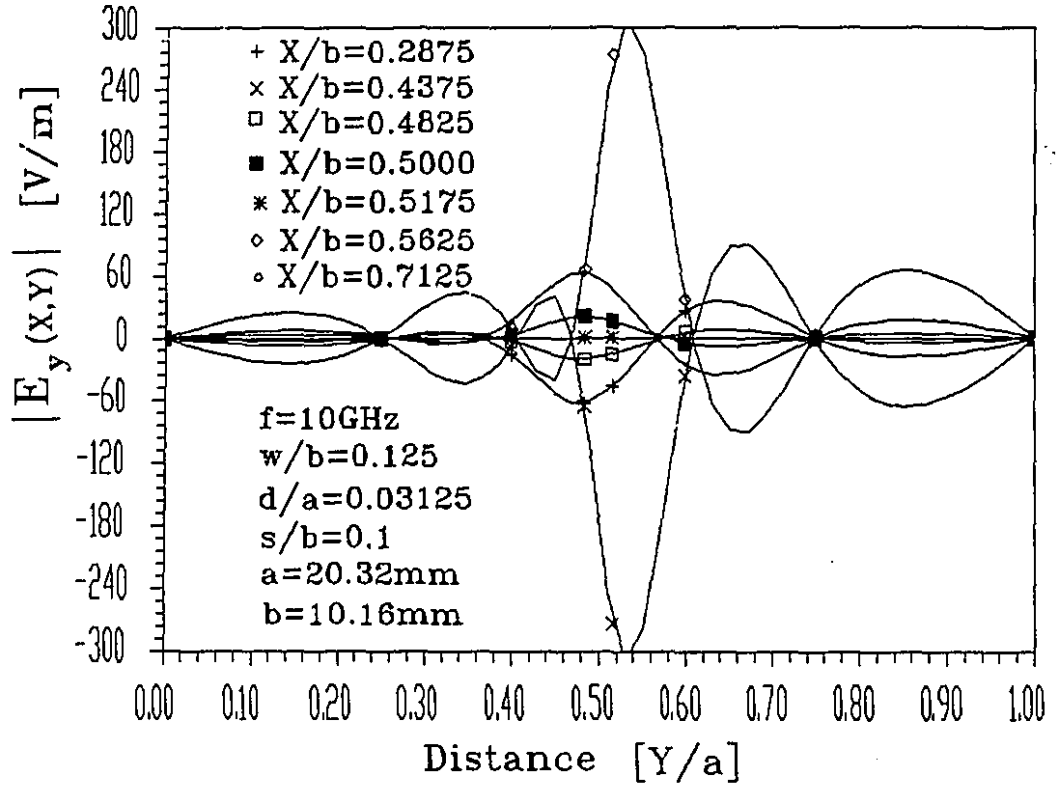

Figure 6-4

Electric field distribution in unilateral finline
(Y-component versus Y)

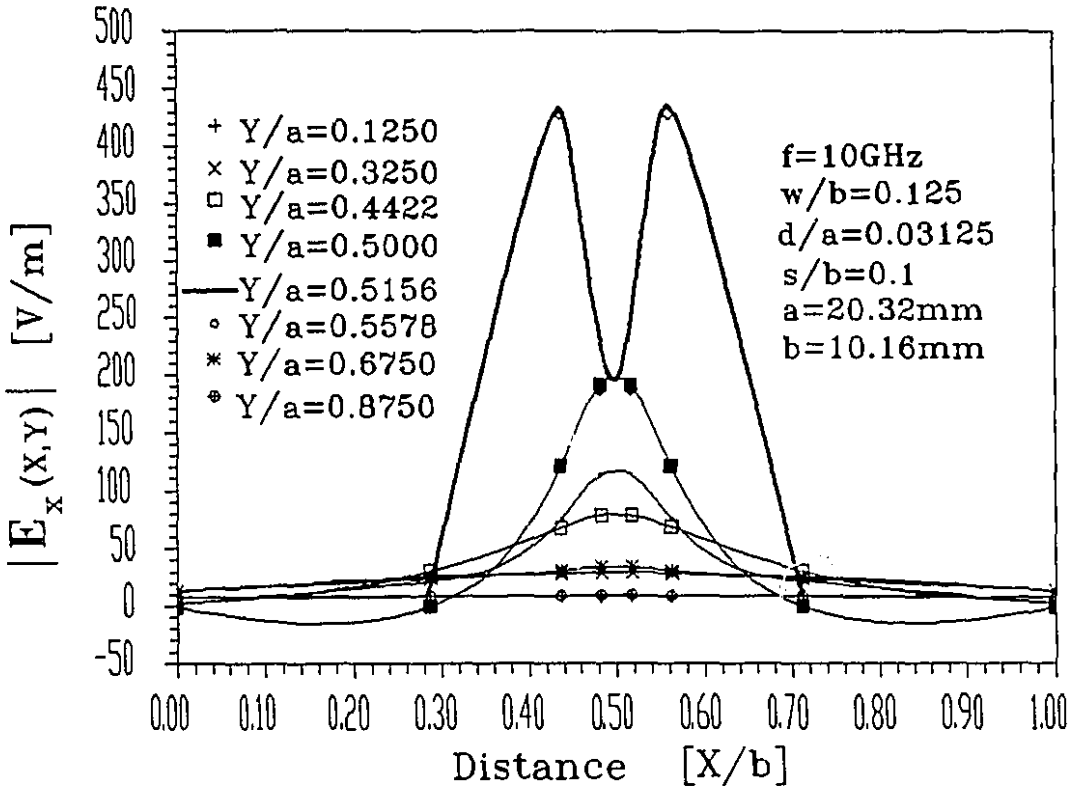

Figure 6-5

Electric field distribution in unilateral finline
(X-component versus X)

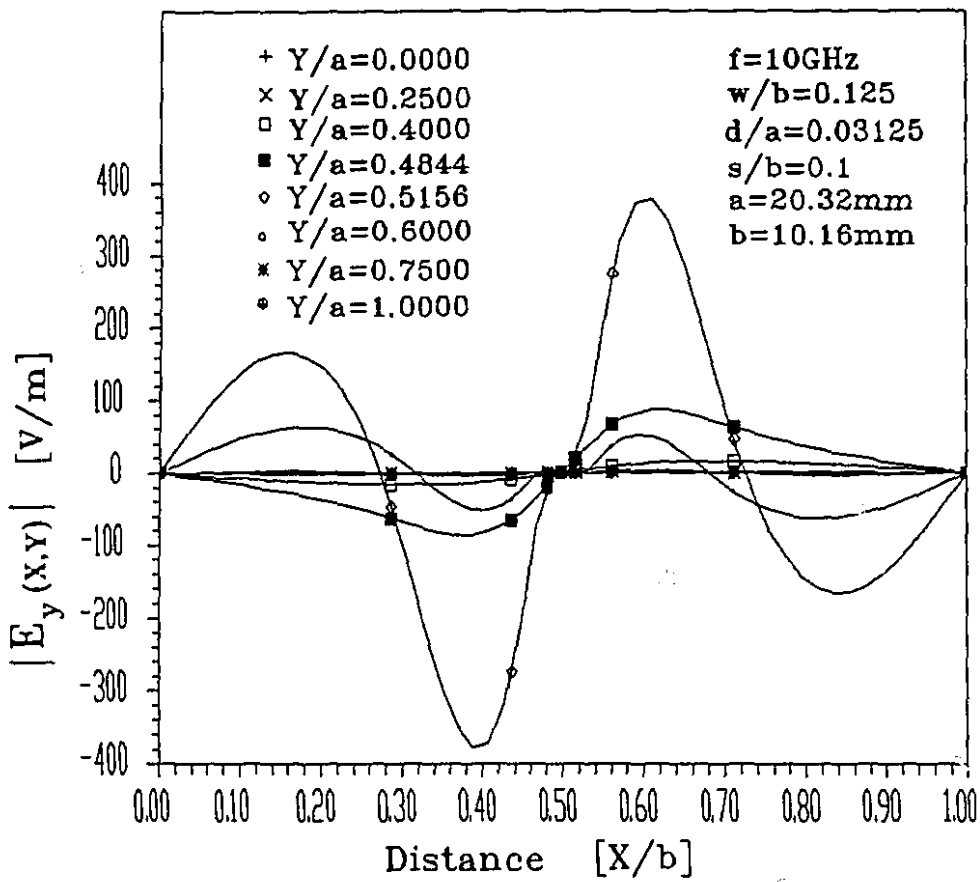

Figure 6-6

Electric field distribution in unilateral finline
(Y-component versus X)

During the calibration phase, the scattering parameters of the structure are computed with the discontinuity section replaced by a segment of the unilateral finline of the same cross-sectional geometry as the two uniform guide sections. The length of the "through" segment is determined by the location of the desired reference planes. The calibration factors are determined by setting the magnitude of the forward transmission of the scattering coefficients to unity and the phase to 0 degrees. Then the scattering parameters of the structure including the discontinuity are computed by replacing the "calibration segment" with the actual discontinuity. Subtracting the phase offset from the phase angles of the parameters, one obtains the final scattering parameters at the desired planes. By using the same segment length for the calibration segment as for the discontinuity segment, the transmission and reflection parameters are calibrated to the center plane of the discontinuity. The parameters could be calibrated to some other reference plane, by choosing different lengths for the calibration segment and the discontinuity segment. Fig. 6-7 shows the comparison between the results computed by Jansen and Koster [28] using the rigorous hybrid-mode spectral domain approach, and the results obtained by the three-dimensional finite element method. In this case, only 98 mixed-order elements are used to approximate the electric field in the discontinuity region. The lengths of the initial segments of the uniform finline sections are chosen such that the resolution of the uniform guide sections is one-tenth of the wavelength of the operating frequencies. The total number of recursions used in the boundary-marching algorithm is five. The finite element results agree with the spectral domain results to within a few percent, and better than 2% for the strip width of s/b=0.1. It is possible to further improve the accuracy by increasing the number of elements used in the discontinuity region, for higher operating

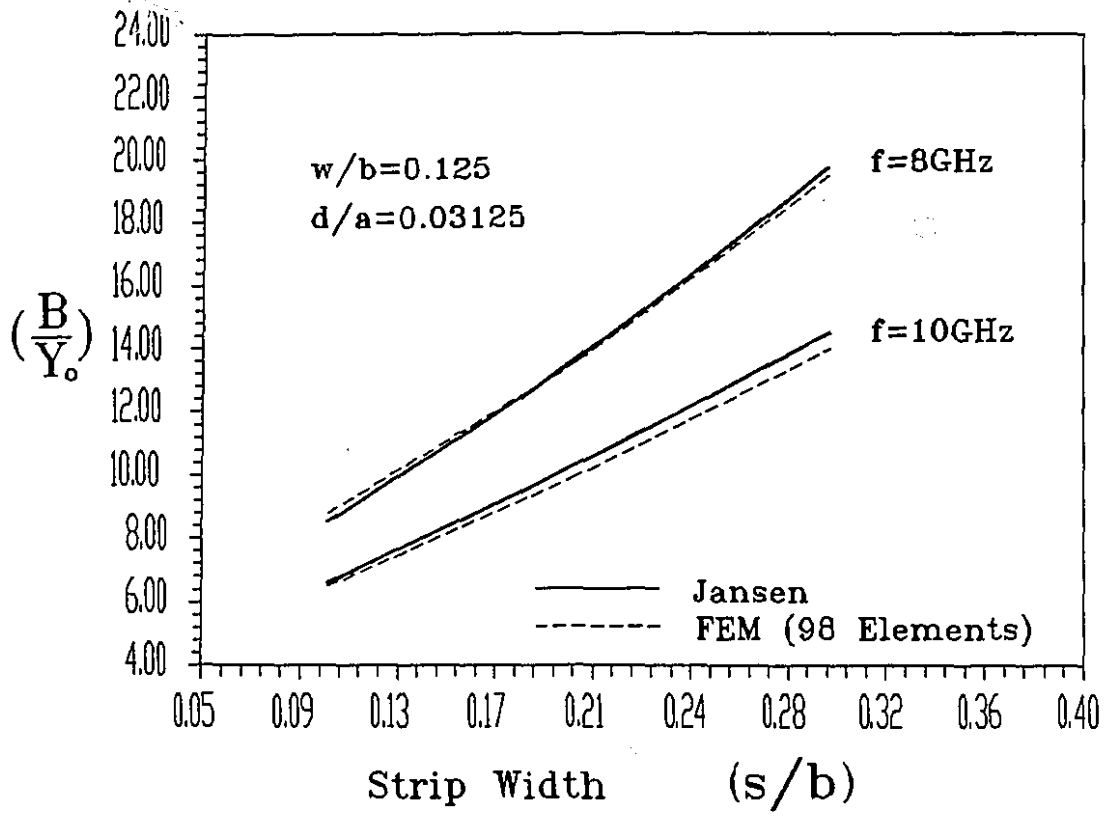

Figure 6-7

Normalized shunt susceptance of inductive strips in idealized unilateral finline

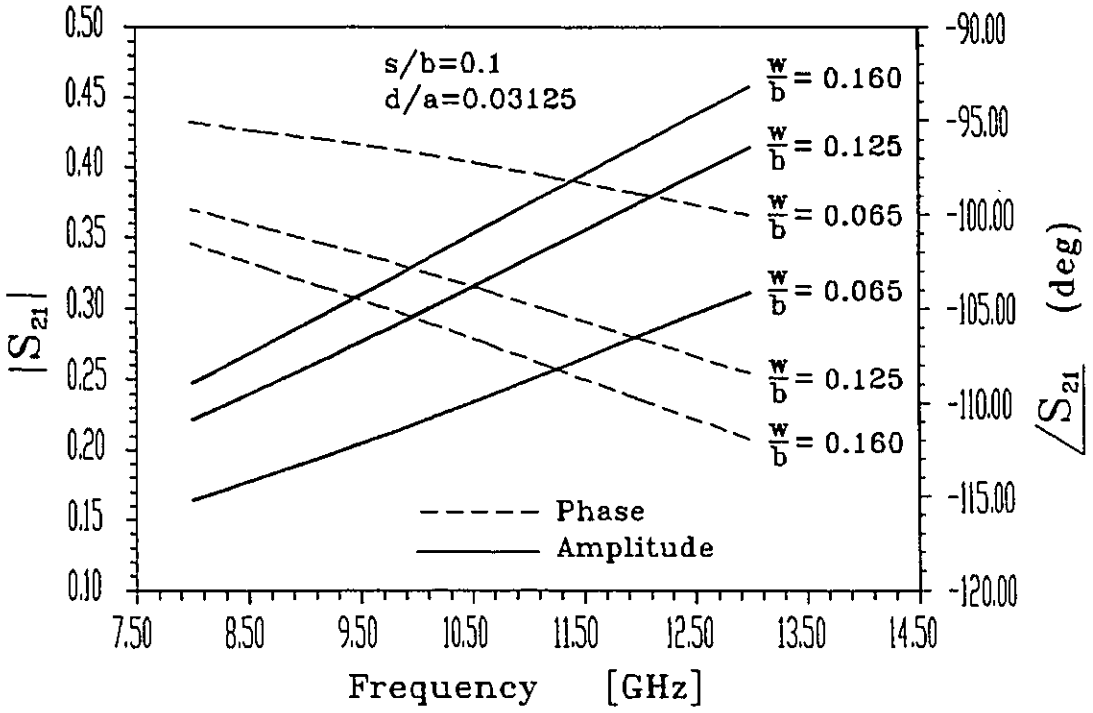

Figure 6-8

Forward transmission coefficient of scattering parameters of inductive strips in idealized unilateral finline

frequencies or larger strip width, s. Fig. 6-8 shows phase and amplitude of the forward transmission coefficient of the scattering parameters of the inductive strip of strip-width s/b=0.1, for various slot-widths and frequencies. The phases of the scattering parameters are calibrated to the center of the discontinuity by using a through segment of the same length as the discontinuity itself.

6.4 Effects of Mounting Grooves

In practice, finline construction starts by printing the circuit pattern on a piece of thin substrate using the microwave integrated circuit technologies. The substrate including the circuit pattern eventually will be inserted into a waveguide housing. To support the substrate in the waveguide housing, a slit is precisely machined in the middle, or at a location slightly offset from the middle, of the metallic enclosure. Since the design of the circuit pattern assumes a perfect rectangular waveguide housing, the slit in the guide modifies the circuit parameters and circuit performance. The effect of the mounting grooves is a function of many parameters such as the operating frequency, dielectric constant, and the substrate thickness. The influence of mounting grooves on the modal spectrum of a unilateral finline has been studied by several authors [36,37,38,40]. It was found that, for small groove depths, the dominant mode is unaffected. However, as the groove depth increases, the dominant mode interacts strongly with the next higher order mode, resulting in an increase in the dominant mode propagation constant. In general, the cut-off frequency of the higher order mode is slightly lowered, thereby resulting in lower single-mode operating bandwidth. The responses of several finline filters [33,34,35] show that the mounting grooves, in general, result in a shift in the operating frequencies. However, these effects have not

yet been quantified in terms of the discontinuity parameters of the circuits. Here, the susceptances of the inductive strips of various slot-width are computed using the finite element method, for various groove depths. Fig. 6-9 shows the error of the susceptance of the inductive strip as a function of the groove depth, for several frequencies. It is seen that the effect of the mounting groove is more severe at the higher end of the frequency spectrum. These results also confirm [38] that the groove depth lowers the single-mode operating bandwidth. Initially, the groove depth causes an increase in the susceptance of the discontinuity. As the groove depth increases, the susceptance of the discontinuity is slightly lowered as a result of the increase of interaction between the dominant mode and the higher order modes. When the groove depth approaches a value where the second order mode becomes a propagation mode, the susceptance of the discontinuity can no longer be predicted accurately. With reference to Fig. 6-9, it is evident that the groove depth of a unilateral finline must not be made greater than 1/3 of the height of the waveguide housing, in order to keep the effect of the groove below 3% for most of the usable operating frequencies. Fig. 6-10 shows the error in the susceptance of unilateral finlines of different slot widths and various substrate thicknesses. It is observed that the susceptances of the inductive strip in finlines of smaller slot width is altered slightly more by the presence of the groove. This is probably because the dispersion characteristics of finlines with smaller slot-width are affected more severely by the mounting groove. For the same reason, the deviation in the discontinuity parameter is increased as the substrate thickness increases, for the same slot width. From these results, one may conclude that the effect of the mounting groove is in general not negligible. However, the effect is less than 1%, if the groove depth is restricted to less than 0.15 of the height of the waveguide housing. In cases where the groove depth rises as high as 1/3 of the height of the housing, the error in the

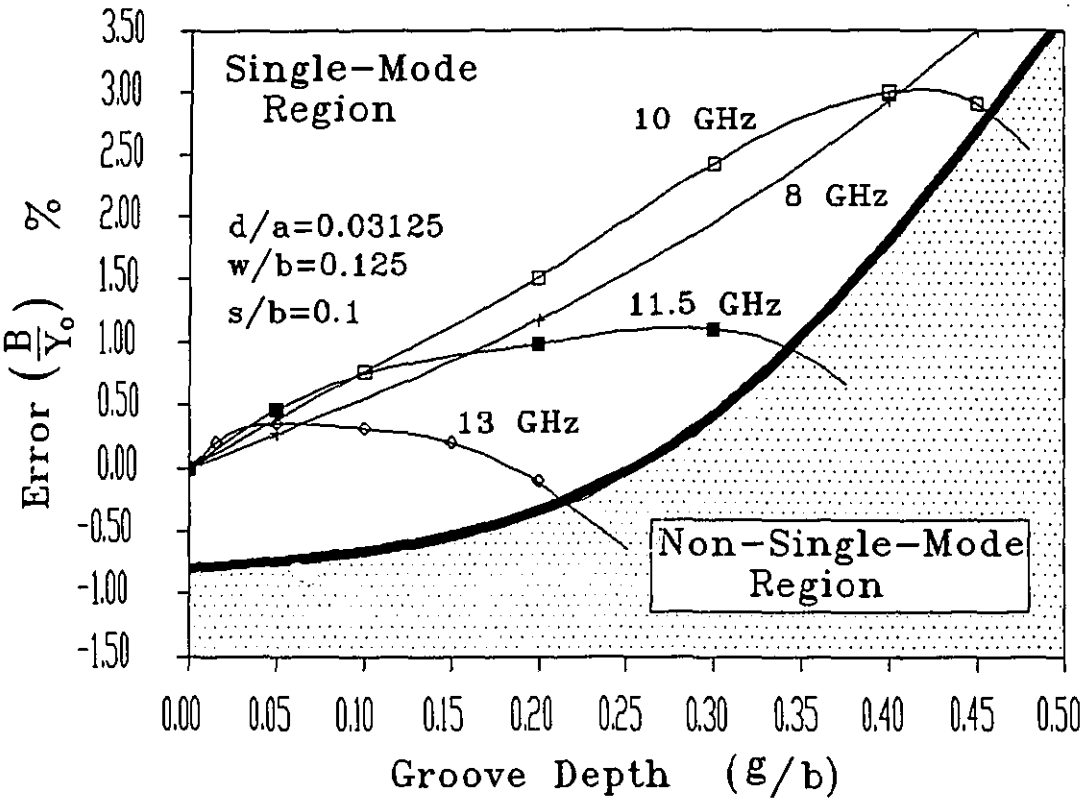

Figure 6-9

Effect of mounting grooves on the normalized susceptance of inductive strips in idealized unilateral finline

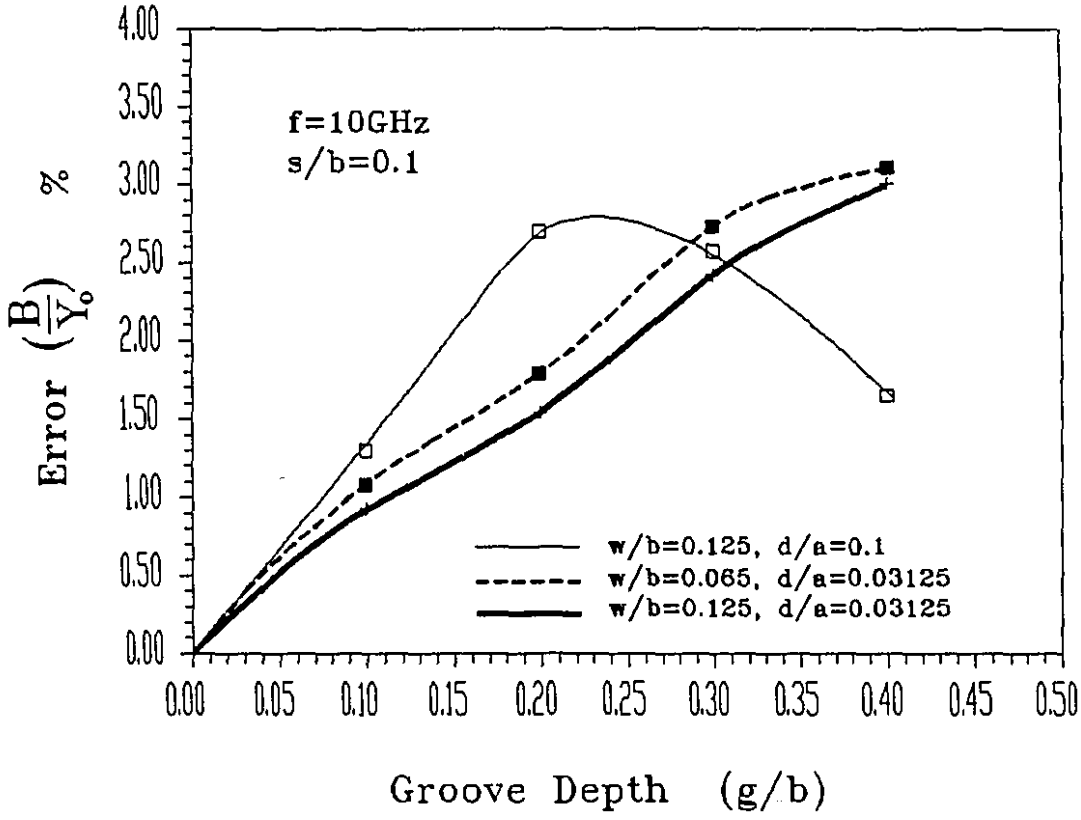

Figure 6-10

Effect of mounting groove on the normalized susceptance of inductive strip in unilateral finlines with different slot width and substrate thickness.

discontinuity parameters can go as high as 3%. If the groove depths are greater than 2/5 of the height of the waveguide housing, it is expected that a large portion of the single-mode operating bandwidth will be corrupted by higher order modes.

6.5 Effects of Metalization Thickness

A thin layer of conducting substance is deposited on the surface of the dielectric to form the desired circuit pattern. At lower microwave frequencies, the thickness of the metalization is relatively thin and negligible compared to the wavelength of the operating frequency. However, as the frequency approaches the millimeter-wave range, the thickness of the metalization of the circuit pattern becomes more and more visible to the electrical signal. Therefore, the effect of metalization thickness becomes stronger at the higher frequency range. The effect of the finite thickness of the fin is equivalent to capacitive loading in the guide. Fig. 6-11 shows the effect of susceptance of inductive strips versus the operating frequencies, for various slot widths, and different metalization thicknesses. Fig. 6-12 gives the corresponding error plot with respect to the metalization thickness. It is seen that the effect of the metalization loading is close to 2% for metalization thickness of less than 0.1% of the width of the waveguide housing, when a practical slot-width is considered. As indicated in Fig. 6-12, when the fin thickness of the unilateral finlines rises to 0.3% of the width of the waveguide housing, the error can go as high as nearly 7%. From these results, it is also quite evident that the thickness of the fin affects the discontinuity parameters most severely when the slot width of the finline is small. To keep the effect of metalization loading below 3%, the thickness of the fin must be kept below 0.2%. Evidently, this condition is not a problem for most microwave applications; however, it is a factor to be taken into consideration for applications in the millimeter-wave range.

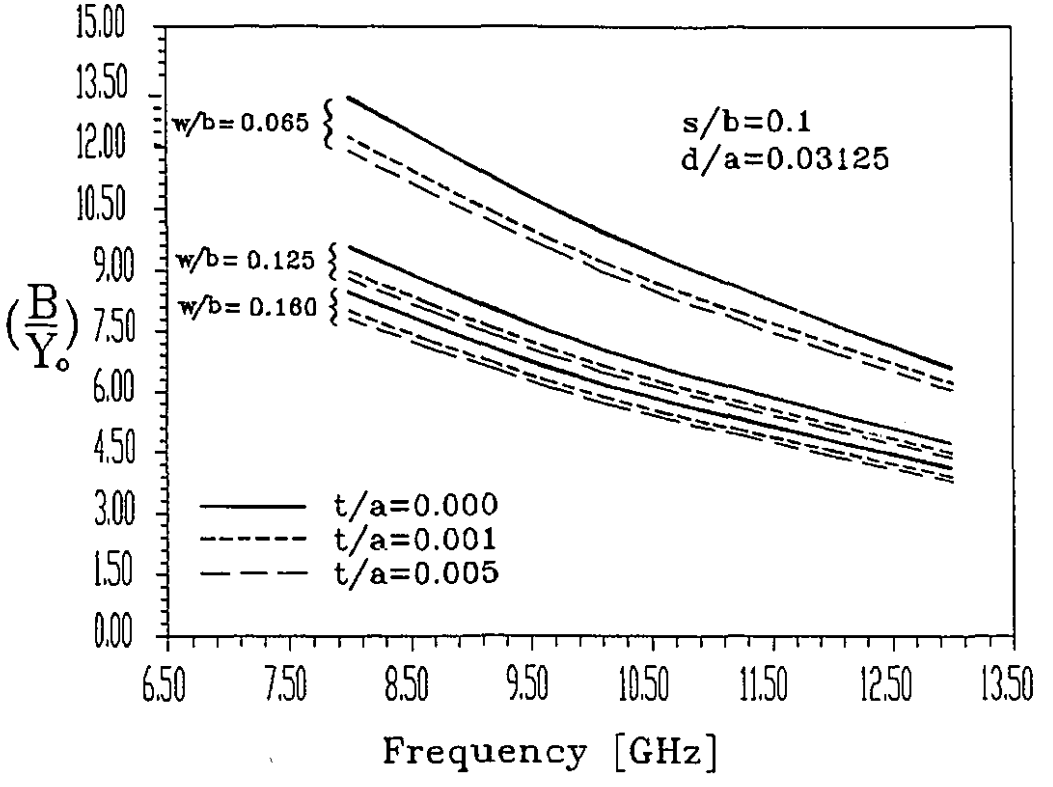

Figure 6-11
Normalized susceptance of inductive strips in unilateral finlines of different metalization thickness

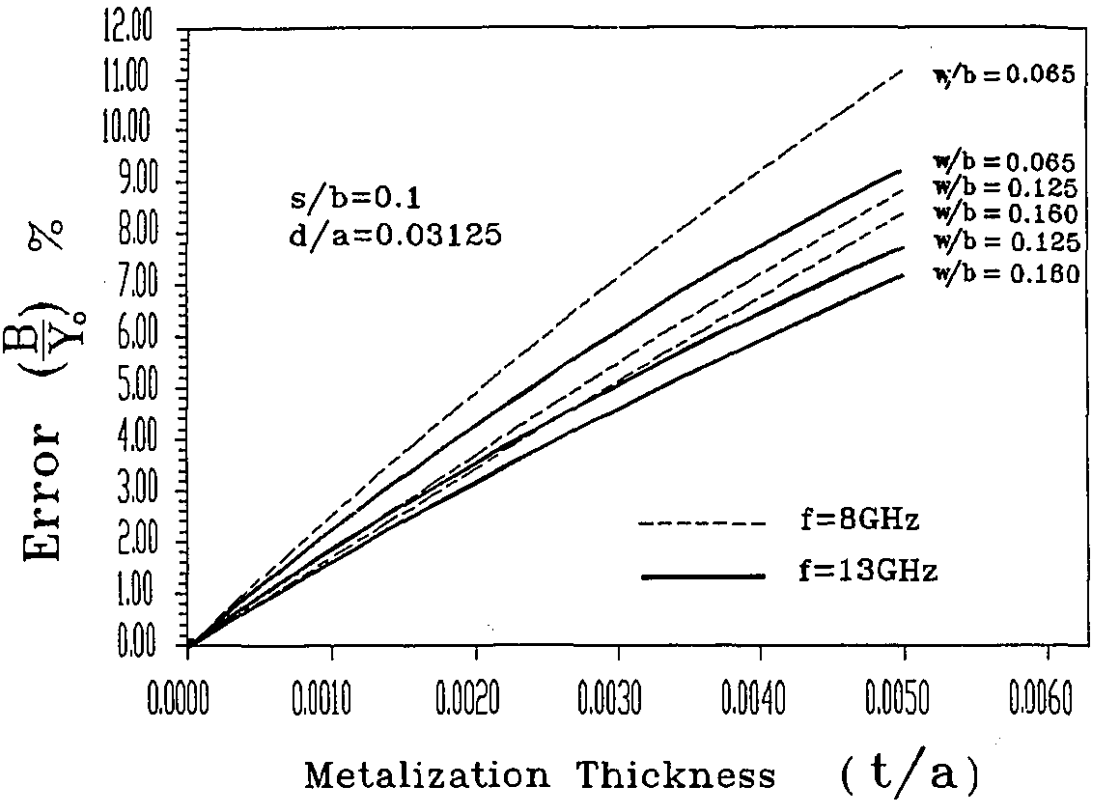

Figure 6-12

Effect of Metalization thickness on the normalized susceptance of inductive strips in idealized unilateral finlines

6.6 Effects of Substrate Bending

For very high frequency applications, above E- or F-band operating frequencies, the thickness of the dielectric substrate that the circuit pattern is printed on becomes extremely thin, in the range of hundreds of microns (less than 1 millimeter). In such cases, the substrate itself can be bended. The substrate bending can be a result of the mechanical fitting, or a result of the thermal expansion when the finline component is subject to an extreme thermal environment. Furthermore, for some applications, a soft dielectric substrate is preferred. In these cases, the substrate including the circuit pattern can be bent easily, especially in millimeter-wave applications. Fig. 6-13 gives the susceptance of the inductive strip for different values of deflection at different frequencies, with the slot-width of w/b=0.125. The susceptance of the inductive strip is also ploted in percentage error compared to the idealized model in Fig. 6-14. It is seen that substrate deformation can cause a significant amount of deviation in the discontinuity parameter. The effect of the substrate bending can go as high as $4\% - 5\%$ when the substrate is deformed by a distance of about 4% from the straight position, compared to the width of the metallic enclosure.

6.7 Conclusions

Three-dimensional finite elements in conjunction with the boundary-marching algorithm are used to examine inductive strips in unilateral finlines, including all the effects resulting from the limitations of manufacturing processes. By using mixed-order finite elements, no spurious-mode problem is encountered in the solutions. The boundary-marching algorithm is used to generate matrix representations of the uniform finline sections. By using the matrix representation of the uniform finline to interrelate

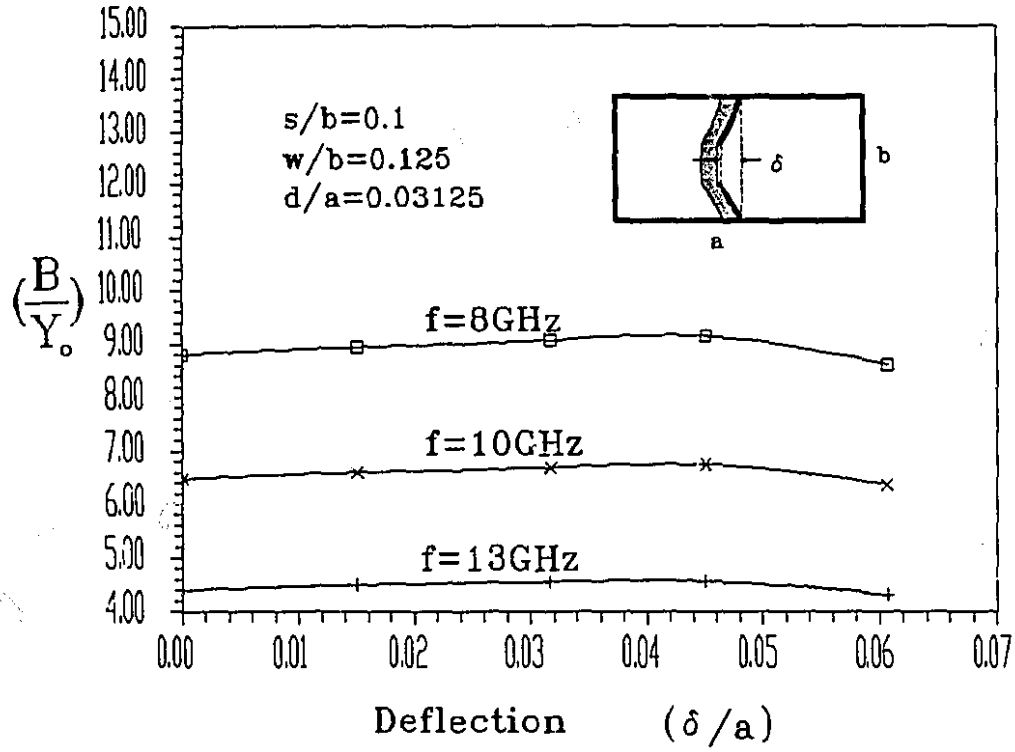

Figure 6-13

Normalized susceptance of inductive strips in unilateral finlines of varying degree of substrate bending

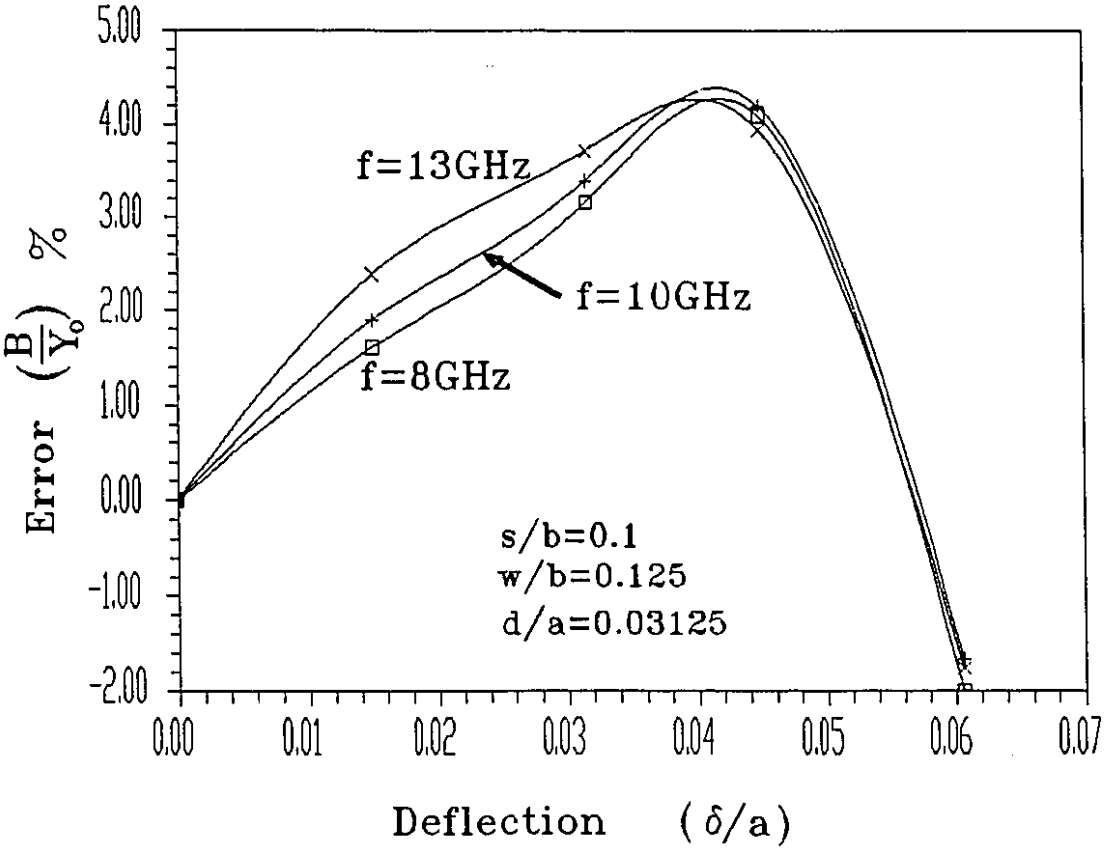

Figure 6-14

Effect of substrate bending on the normalized susceptance of inductive strips in idealized unilateral finlines

the electric field at the discontinuity to the propagation field on the far-field plane, one may truncate the finite element mesh at a proximity very close to the discontinuity. As a result, the system of equations of the three-dimensional problem is reduced to a relatively small matrix size, in the order of a few thousands. The results obtained by using the present method agree with the results computed with the hybrid-mode spectral domain method to within 2%, with only 98 elements used in the discontinuity region. The effects of manufacturing processes, including the mounting grooves, metalization thickness, and the substrate bending, on the finline discontinuity are examined with the finite element method. Various plots are provided for estimating such effects.

Chapter 7

Conclusions

7.1 Summary

This thesis describes the development of a finite element scheme for analyzing three dimensional scattering problems in inhomogeneous-dielectric-loaded waveguide structures. The algorithm is, in general, applicable to any arbitrarily-shaped waveguiding structure. Two major techniques used and developed in this thesis are: the ballooning method proposed by Silvester in 1977 [2], and the mixed-order curvilinear finite element method proposed by Crowley in 1988 [6].

The following are the major contributions of this thesis.

(i) **Boundary-marching algorithm for waveguides.**

This algorithm is based on the previous work of Silvester [2] developed for static problems with open boundaries. In this thesis, the ballooning algorithm is extended to the wave equation, especially tailored for waveguide applications. It is shown that the boundary-marching algorithm is a simple yet accurate technique to generate the necessary auxiliary matrix for interrelating the field distribution in the near-field region to the field distribution in the far-field region. In this thesis, the boundary-

marching algorithm is first used to generate the far-field solution in a given waveguide structure. The far-field solution is, in turn, used to terminate the waveguide.

(ii) **Three dimensional scattering problems in waveguides.**

For many scattering problems, the scattering object under investigation is of relatively large dimension compared to the operating frequency. For such cases, the three dimensional finite element method requires very large storage and memory. By using the static condensation technique, it is shown in this thesis that the problem can be solved by subdividing the geometry into several subsections and therefore reduces the storage and memory requirements. This approach not only improves the speed of numerical computation by taking the advantage of the possibility of parallel processing; most importantly, it eliminates the limitation previously set by the length of the scattering object.

(iii) **Characteristics of finline discontinuities.**

The transmission/reflection characteristics of inductive strips in unilateral finline are studied by using the three-dimensional finite element scheme. It is shown that results with satisfactory accuracy can be obtained by using the proposed approach with relatively small number of elements. For the first time, the effects of the circuit manufacturing processes, including the effect of mounting grooves, influence of the finite metalization thickness of the fin, and the effect of substrate deflection on the finline discontinuities are studied in detail.

Appendix I

Mixed-order curvilinear finite elements

1. Variational Formulation in Curvilinear Coordinates

The functional to be considered here is,

$$\mathcal{F}(\mathbf{E}) = \frac{1}{2}\int_{\Omega}\left\{-\frac{1}{\mu_r}(\nabla\times\mathbf{E})\cdot(\nabla\times\mathbf{E}) + k_0^2\epsilon_r\mathbf{E}\cdot\mathbf{E}\right\}d\Omega, \tag{A-1}$$

where $\mathbf{E}$ is the electric field vector, μ_r is the relative permeability of the medium, ϵ_r is the relative permitivity of the medium and $k_0 = \omega^2(\epsilon_o\mu_o)$ is the free-space wave constant. The orthospectral (mixed-order hexahedral) finite elements, cast in terms of the projection components [6], are used for the discretization. Within each element, the electric field vector $\mathbf{E}$ is written

$$\mathbf{E} = 1^{\xi}E_{\xi} + 1^{\eta}E_{\eta} + 1^{\nu}E_{\nu}, \tag{A-2}$$

where 1^{ξ}, 1^{η}, 1^{ν} are reciprocal unitaries of the local curvilinear coordinates, and E_{ξ}, E_{η}, E_{ν} are the covariant projection components of $\mathbf{E}$. The reciprocal unitaries can be

written in terms of unitary vectors 1_ξ, 1_η, 1_ν of the curvilinear coordinate system as follows,

$$1^\xi = \frac{1}{V}\cdot(1_\eta \times 1_\nu), \tag{A-3}$$

$$1^\eta = \frac{1}{V}\cdot(1_\nu \times 1_\xi), \tag{A-4}$$

$$1^\nu = \frac{1}{V}\cdot(1_\xi \times 1_\eta), \tag{A-5}$$

where V is the volume of the parallelepiped formed by the three unitaries,

$$V = 1_\xi\cdot(1_\eta \times 1_\nu) = 1_\eta\cdot(1_\nu \times 1_\xi) = 1_\nu\cdot(1_\xi \times 1_\eta). \tag{A-6}$$

The geometrical properties of space with respect to any curvilinear system of coordinates can be completely characterized by a set of coefficients called the *metrical coefficients*. In this case, one can express the differential volume in terms of the metrical coefficients as follows,

$$d\Omega = V \cdot d\xi\, d\eta\, d\nu\,, \tag{A-7}$$

where

$$V^2 = g = \begin{vmatrix} g_{11} & g_{12} & g_{13} \\ g_{21} & g_{22} & g_{23} \\ g_{31} & g_{32} & g_{33} \end{vmatrix}, \tag{A-8}$$

and

$$g_{11} = l_\xi \cdot l_\xi = \frac{dx}{d\xi}\cdot\frac{dx}{d\xi} + \frac{dy}{d\xi}\cdot\frac{dy}{d\xi} + \frac{dz}{d\xi}\cdot\frac{dz}{d\xi}, \quad \text{(A-9)}$$

$$g_{12} = l_\xi \cdot l_\eta = \frac{dx}{d\xi}\cdot\frac{dx}{d\eta} + \frac{dy}{d\xi}\cdot\frac{dy}{d\eta} + \frac{dz}{d\xi}\cdot\frac{dz}{d\eta}, \quad \text{(A-10)}$$

$$g_{13} = l_\xi \cdot l_\nu = \frac{dx}{d\xi}\cdot\frac{dx}{d\nu} + \frac{dy}{d\xi}\cdot\frac{dy}{d\nu} + \frac{dz}{d\xi}\cdot\frac{dz}{d\nu}, \quad \text{(A-11)}$$

$$g_{21} = l_\eta \cdot l_\xi = \frac{dx}{d\eta}\cdot\frac{dx}{d\xi} + \frac{dy}{d\eta}\cdot\frac{dy}{d\xi} + \frac{dz}{d\eta}\cdot\frac{dz}{d\xi}, \quad \text{(A-12)}$$

$$g_{22} = l_\eta \cdot l_\eta = \frac{dx}{d\eta}\cdot\frac{dx}{d\eta} + \frac{dy}{d\eta}\cdot\frac{dy}{d\eta} + \frac{dz}{d\eta}\cdot\frac{dz}{d\eta}, \quad \text{(A-13)}$$

$$g_{23} = l_\eta \cdot l_\nu = \frac{dx}{d\eta}\cdot\frac{dx}{d\nu} + \frac{dy}{d\eta}\cdot\frac{dy}{d\nu} + \frac{dz}{d\eta}\cdot\frac{dz}{d\nu}, \quad \text{(A-14)}$$

$$g_{31} = l_\nu \cdot l_\xi = \frac{dx}{d\nu}\cdot\frac{dx}{d\xi} + \frac{dy}{d\nu}\cdot\frac{dy}{d\xi} + \frac{dz}{d\nu}\cdot\frac{dz}{d\xi}, \quad \text{(A-15)}$$

$$g_{32} = l_\nu \cdot l_\eta = \frac{dx}{d\nu}\cdot\frac{dx}{d\eta} + \frac{dy}{d\nu}\cdot\frac{dy}{d\eta} + \frac{dz}{d\nu}\cdot\frac{dz}{d\eta}, \quad \text{(A-16)}$$

$$g_{33} = l_\nu \cdot l_\nu = \frac{dx}{d\nu}\cdot\frac{dx}{d\nu} + \frac{dy}{d\nu}\cdot\frac{dy}{d\nu} + \frac{dz}{d\nu}\cdot\frac{dz}{d\nu}. \quad \text{(A-17)}$$

Substituting eqns. (A-6) and (A-7) into eqn. (A-1), one obtains the functional for the problem in terms of the covariant projection components of E as

$$\mathcal{F}(\mathbf{E}) = \frac{1}{2}\int_\Omega \left\{ -\frac{1}{\mu_r}(\nabla\times\mathbf{E})\cdot(\nabla\times\mathbf{E}) + k_0^2\epsilon_r\mathbf{E}\cdot\mathbf{E}\right\} \sqrt{g}\ \cdot\ \mathrm{d}\xi\ \mathrm{d}\eta\ \mathrm{d}\nu\ . \quad \text{(A-18)}$$

2. Geometric Interpolation Functions

The geometry of each curvilinear element can be fully described by 27 geometric nodes interpolated by smooth functions. The metrical coefficients of the element can then be evaluated in terms of these geometric nodes and the interpolation functions. Fig. A-1 shows the numbering scheme of the geometric nodes. The Cartesian coordinates are approximated by three geometric interpolation functions, $\beta_k(\xi, \eta, \nu)$, as follows :

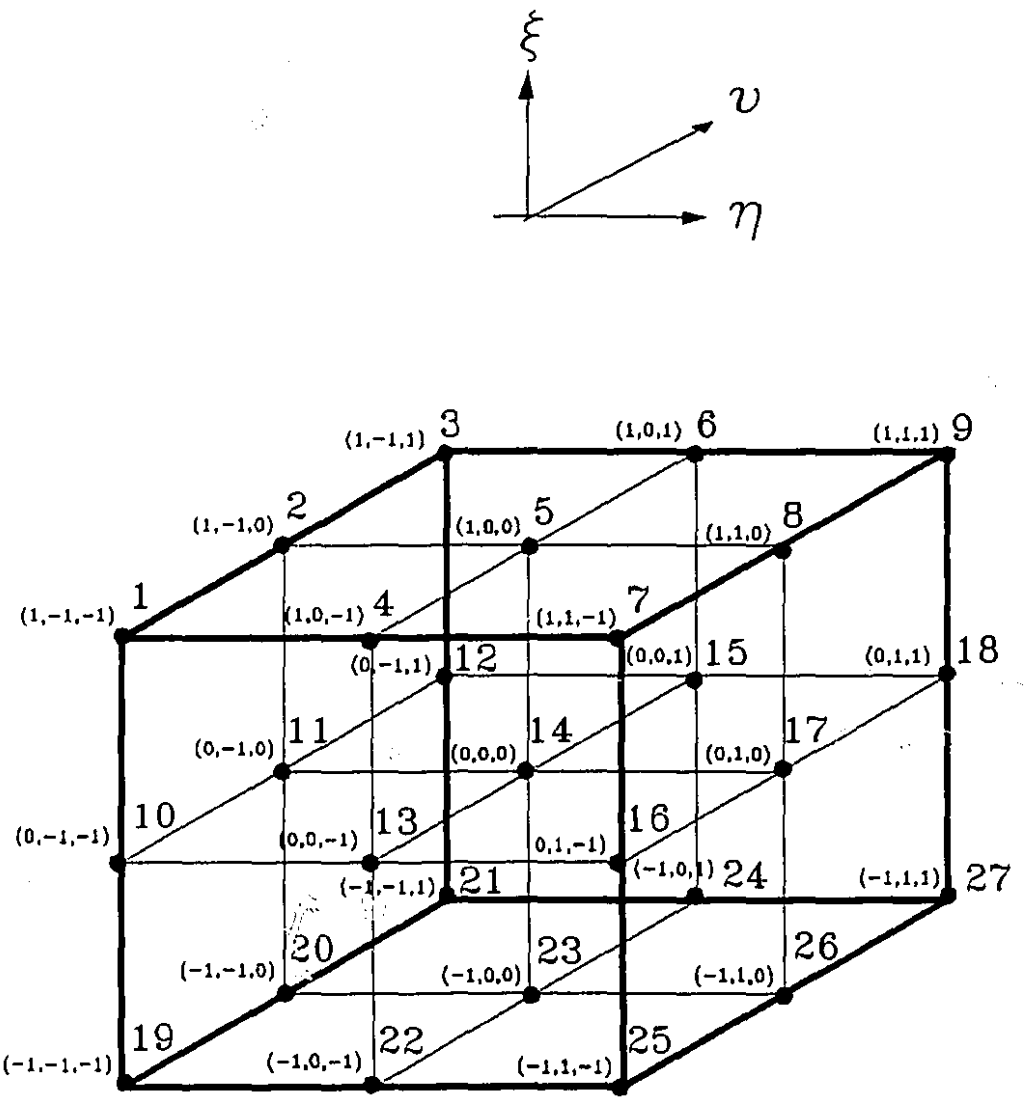

Figure A-1

Numbering sheme of geometric nodes

$$x = \sum_{k=1}^{27} x_k \, \beta_k(\xi, \eta, \nu), \tag{A-19}$$

$$y = \sum_{k=1}^{27} y_k \, \beta_k(\xi, \eta, \nu), \tag{A-20}$$

$$z = \sum_{k=1}^{27} z_k \, \beta_k(\xi, \eta, \nu), \tag{A-21}$$

where the interpolation function satisfy the following criteria,

$$\beta_k(\xi, \eta, \nu) = \delta_{kj} = \begin{cases} +1, & \text{if } k=j, \\ 0, & \text{else .} \end{cases} \tag{A-22}$$

Notice that the coordinate system is such that the origin (0,0,0) of the element is at the center of the element and, $-1<\xi<1$, $-1<\eta<1$, $-1<\nu<1$. The geometric interpolation functions are given explicitly in the following table:

Geometric Node	Local Coordinate	Geometric Interpolation Functions $\beta_k\ (\xi, \eta, \nu)$
1	(1,-1,-1)	$\frac{1}{8}\,\xi(\xi+1)\eta(\eta-1)\nu(\nu-1)$
2	(1,-1, 0)	$\frac{1}{8}\,\xi(\xi+1)\eta(\eta-1)\,(1-\nu^2)$
3	(1,-1, 1)	$\frac{1}{8}\,\xi(\xi+1)\eta(\eta-1)\nu(\nu+1)$
4	(1, 0,-1)	$\frac{1}{8}\,\xi(\xi+1)\,(1-\eta^2)\nu(\nu-1)$
5	(1, 0, 0)	$\frac{1}{8}\,\xi(\xi+1)\,(1-\eta^2)\,(1-\nu^2)$
6	(1, 0, 1)	$\frac{1}{8}\,\xi(\xi+1)\,(1-\eta^2)\nu(\nu+1)$
7	(1, 1,-1)	$\frac{1}{8}\,\xi(\xi+1)\eta(\eta+1)\nu(\nu-1)$
8	(1, 1, 0)	$\frac{1}{8}\,\xi(\xi+1)\eta(\eta+1)\,(1-\nu^2)$
9	(1, 1, 1)	$\frac{1}{8}\,\xi(\xi+1)\eta(\eta+1)\nu(\nu+1)$
10	(0,-1,-1)	$\frac{1}{8}\,(1-\xi^2)\eta(\eta-1)\nu(\nu-1)$
11	(0,-1, 0)	$\frac{1}{8}\,(1-\xi^2)\eta(\eta-1)\,(1-\nu^2)$
12	(0,-1, 1)	$\frac{1}{8}\,(1-\xi^2)\eta(\eta-1)\nu(\nu+1)$
13	(0, 0,-1)	$\frac{1}{8}\,(1-\xi^2)\,(1-\eta^2)\nu(\nu-1)$
14	(0, 0, 0)	$\frac{1}{8}\,(1-\xi^2)\,(1-\eta^2)\,(1-\nu^2)$
15	(0, 0, 1)	$\frac{1}{8}\,(1-\xi^2)\,(1-\eta^2)\nu(\nu+1)$
16	(0, 1,-1)	$\frac{1}{8}\,(1-\xi^2)\eta(\eta+1)\nu(\nu-1)$
17	(0, 1, 0)	$\frac{1}{8}\,(1-\xi^2)\eta(\eta+1)\,(1-\nu^2)$
18	(0, 1, 1)	$\frac{1}{8}\,(1-\xi^2)\eta(\eta+1)\nu(\nu+1)$
19	(-1,-1,-1)	$\frac{1}{8}\,\xi(\xi-1)\eta(\eta-1)\nu(\nu-1)$
20	(1,-1, 0)	$\frac{1}{8}\,\xi(\xi-1)\eta(\eta-1)\,(1-\nu^2)$
21	(-1,-1, 1)	$\frac{1}{8}\,\xi(\xi-1)\eta(\eta-1)\nu(\nu+1)$
22	(-1, 0,-1)	$\frac{1}{8}\,\xi(\xi-1)\,(1-\eta^2)\nu(\nu-1)$
23	(-1, 0, 0)	$\frac{1}{8}\,\xi(\xi-1)\,(1-\eta^2)\,(1-\nu^2)$
24	(-1, 0, 1)	$\frac{1}{8}\,\xi(\xi-1)\,(1-\eta^2)\nu(\nu+1)$
25	(-1, 1,-1)	$\frac{1}{8}\,\xi(\xi-1)\eta(\eta+1)\nu(\nu-1)$
26	(-1, 1, 0)	$\frac{1}{8}\,\xi(\xi-1)\eta(\eta+1)\,(1-\nu^2)$
27	(-1, 1, 1)	$\frac{1}{8}\,\xi(\xi-1)\eta(\eta+1)\nu(\nu+1)$

The Jacobian matrix for the coordinate transformation between the cartesian coordinates and the curvilinear coordinates is given by

$$\begin{bmatrix} l_\xi \\ l_\eta \\ l_\nu \end{bmatrix} = \begin{bmatrix} \frac{dx}{d\xi} & \frac{dy}{d\xi} & \frac{dz}{d\xi} \\ \frac{dx}{d\eta} & \frac{dy}{d\eta} & \frac{dz}{d\eta} \\ \frac{dx}{d\nu} & \frac{dy}{d\nu} & \frac{dz}{d\nu} \end{bmatrix} \begin{bmatrix} \hat{x} \\ \hat{y} \\ \hat{z} \end{bmatrix}, \tag{A-23}$$

or,

$$\begin{bmatrix} \hat{x} \\ \hat{y} \\ \hat{z} \end{bmatrix} = \begin{bmatrix} \frac{d\xi}{dx} & \frac{d\eta}{dx} & \frac{d\nu}{dx} \\ \frac{d\xi}{dy} & \frac{d\eta}{dy} & \frac{d\nu}{dy} \\ \frac{d\xi}{dz} & \frac{d\eta}{dz} & \frac{d\nu}{dz} \end{bmatrix} \begin{bmatrix} l_\xi \\ l_\eta \\ l_\nu \end{bmatrix}. \tag{A-24}$$

3. Field Interpolation Functions

Each component of the electric field **E** in each element is approximated by element functions $\alpha_m^\xi(\xi,\eta,\nu)$, $\alpha_m^\eta(\xi,\eta,\nu)$, $\alpha_m^\nu(\xi,\eta,\nu)$:

$$E_\xi = \sum_{m=1}^{18} E_m^\xi \alpha_m^\xi(\xi,\eta,\nu), \tag{A-25}$$

$$E_\eta = \sum_{m=19}^{36} E_m^\eta \alpha_m^\eta(\xi,\eta,\nu), \tag{A-26}$$

$$E_\nu = \sum_{m=37}^{54} E_m^\nu \alpha_m^\nu(\xi,\eta,\nu), \tag{A-27}$$

where the element functions $\alpha_m^{\xi}(\xi,\eta,\nu)$, $\alpha_m^{\eta}(\xi,\eta,\nu)$, $\alpha_m^{\nu}(\xi,\eta,\nu)$ are the first/second-order polynomials of the local coordinates ξ,η,ν. The numbering scheme for the field nodes of of the first/second-order hexahedral element is shown in Fig. A-2 to Fig. A-4. Unlike the conventional tetrahedron element, the three element functions are not the same polynomial:

$\alpha_m^{\xi}(\xi,\eta,\nu)$ — Quadratic in η, ν ; Linear in ξ,

$\alpha_m^{\eta}(\xi,\eta,\nu)$ — Quadratic in ξ, ν ; Linear in η,

$\alpha_m^{\nu}(\xi,\eta,\nu)$ — Quadratic in ξ, η ; Linear in ν.

The element functions are chosen according to the following criteria:

1. ξ - component, $\alpha_m^{\xi}(\xi_j,\eta_j,\nu_j) = \begin{cases} +1, & \text{if m=j and } 1 \le m \le 9 \\ -1, & \text{if m=j and } 10 \le m \le 18 \\ 0, & \text{if } m \ne j \end{cases}$

2. η - component, $\alpha_m^{\eta}(\xi_j,\eta_j,\nu_j) = \begin{cases} +1, & \text{if m=j and } 19 \le m \le 27 \\ -1, & \text{if m=j and } 28 \le m \le 36 \\ 0, & \text{if } m \ne j \end{cases}$

3. ν - component, $\alpha_m^{\nu}(\xi_j,\eta_j,\nu_j) = \begin{cases} +1, & \text{if m=j and } 37 \le m \le 45 \\ -1, & \text{if m=j and } 46 \le m \le 54 \\ 0, & \text{if } m \ne j \end{cases}$

Notice that the element functions are chosen such that all the unitaries are pointed outward from the element.

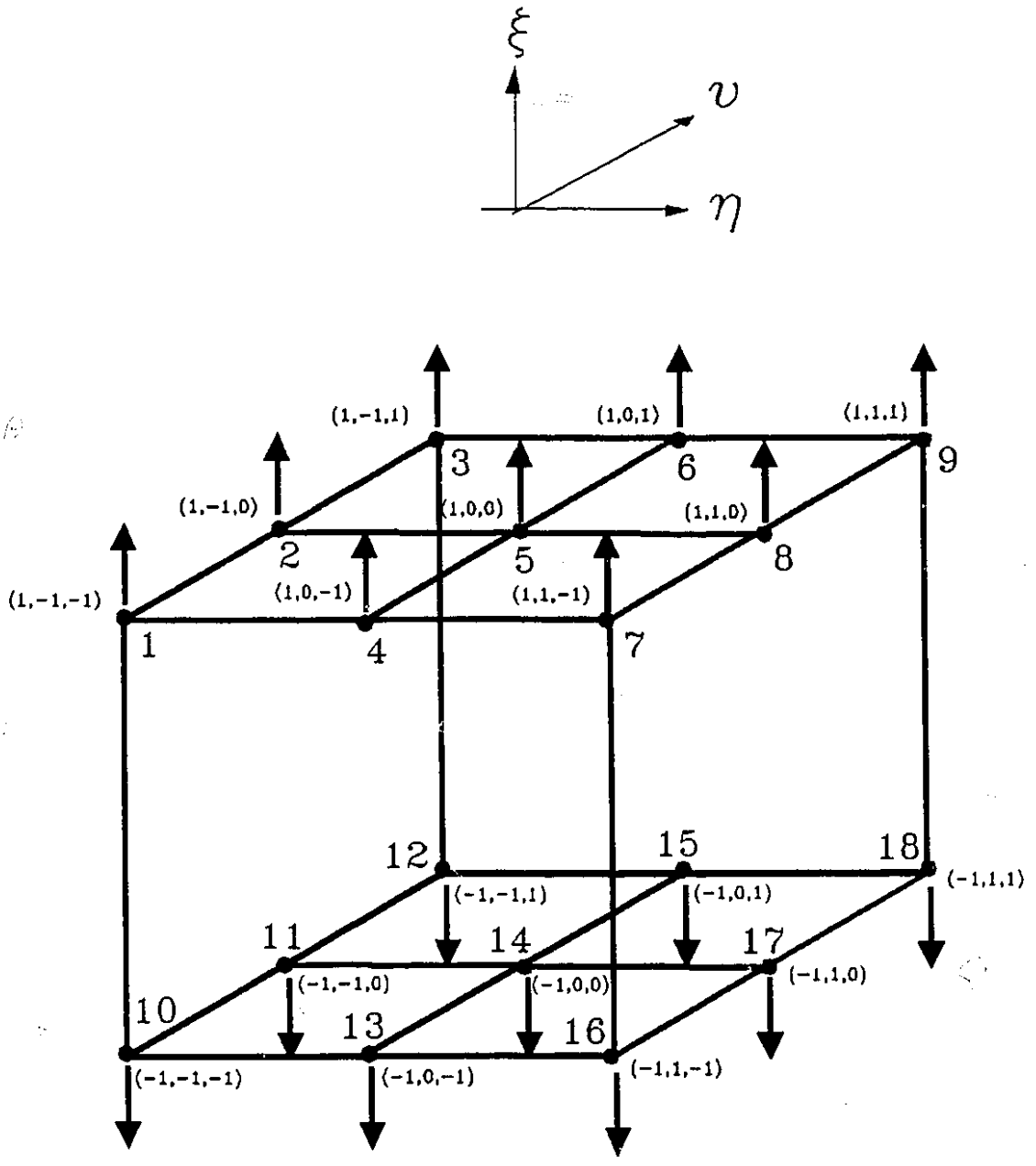

Figure A-2
Numbering scheme of field component - ξ component

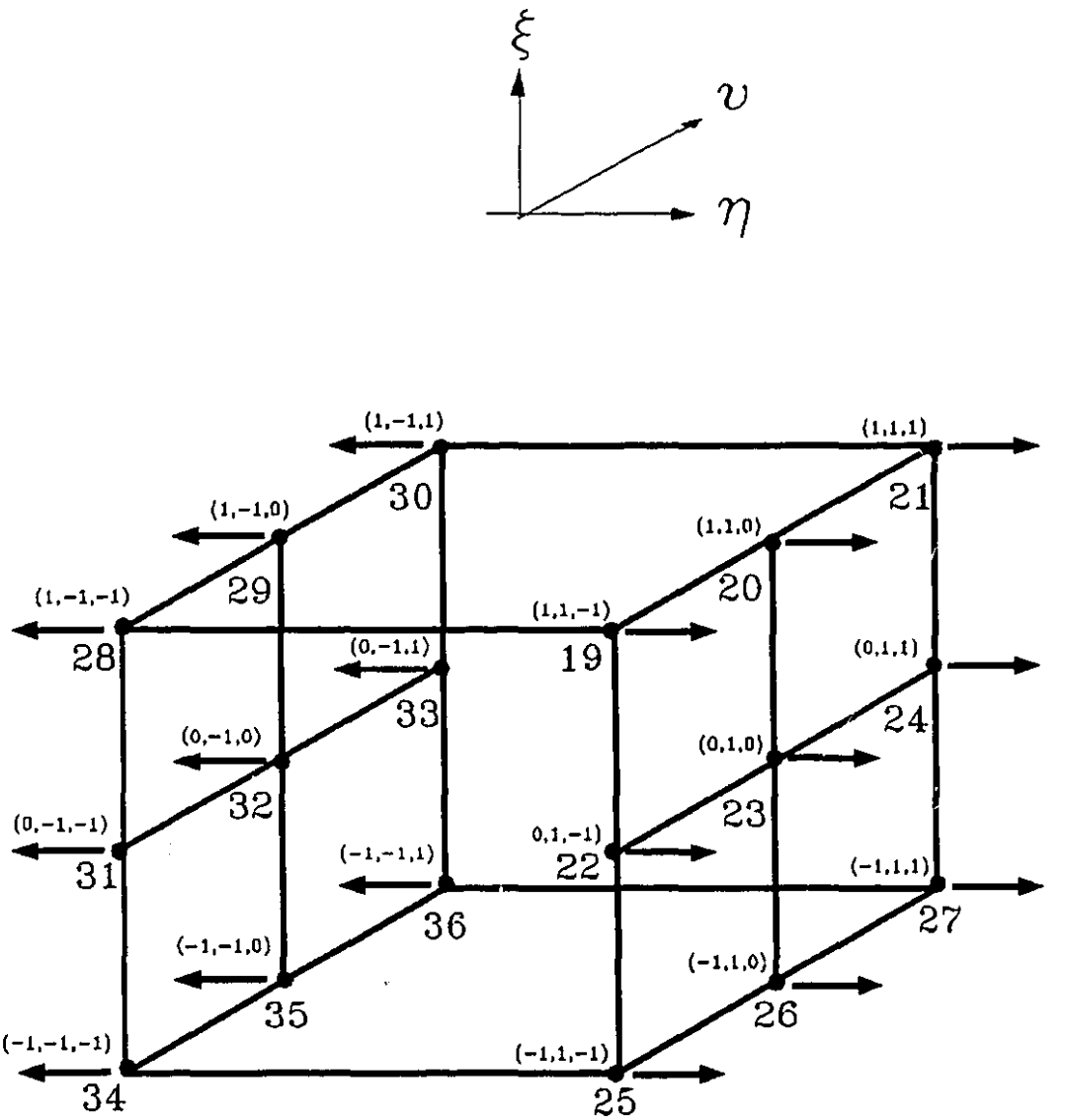

Figure A-3
Numbering scheme of field component - η component

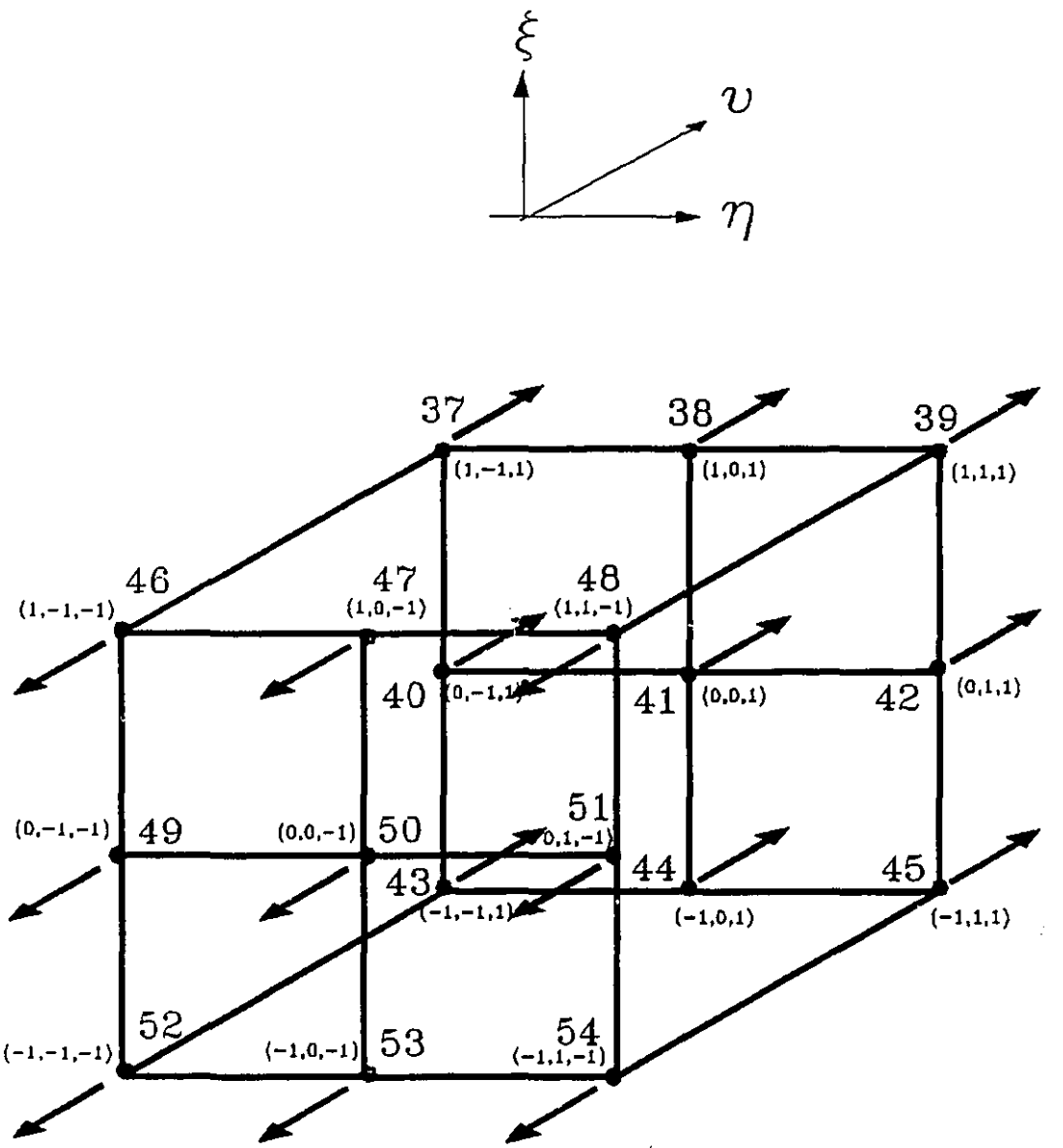

Figure A-4
Numbering scheme of field nodes - υ component

The element functions in their explicit forms are given in the following tables:

I. Interpolation functions for the ξ component.

Field Node Number	Local Coordinate	Interpolation Function $\alpha_m^{\xi}(\xi_j, \eta_j, \nu_j)$
1	(1,-1,-1)	$\frac{1}{8}(\xi+1)\eta(\eta-1)\nu(\nu-1)$
2	(1,-1, 0)	$\frac{1}{8}(\xi+1)\eta(\eta-1)(1-\nu^2)$
3	(1,-1, 1)	$\frac{1}{8}(\xi+1)\eta(\eta-1)\nu(\nu+1)$
4	(1, 0,-1)	$\frac{1}{8}(\xi+1)(1-\eta^2)\nu(\nu-1)$
5	(1, 0, 0)	$\frac{1}{8}(\xi+1)(1-\eta^2)(1-\nu^2)$
6	(1, 0, 1)	$\frac{1}{8}(\xi+1)(1-\eta^2)\nu(\nu+1)$
7	(1, 1,-1)	$\frac{1}{8}(\xi+1)\eta(\eta+1)\nu(\nu-1)$
8	(1, 1, 0)	$\frac{1}{8}(\xi+1)\eta(\eta+1)(1-\nu^2)$
9	(1, 1, 1)	$\frac{1}{8}(\xi+1)\eta(\eta+1)\nu(\nu+1)$
10	(-1,-1,-1)	$\frac{1}{8}(\xi-1)\eta(\eta-1)\nu(\nu-1)$
11	(-1,-1, 0)	$\frac{1}{8}(\xi-1)\eta(\eta-1)(1-\nu^2)$
12	(-1,-1, 1)	$\frac{1}{8}(\xi-1)\eta(\eta-1)\nu(\nu+1)$
13	(-1, 0,-1)	$\frac{1}{8}(\xi-1)(1-\eta^2)\nu(\nu-1)$
14	(-1, 0, 0)	$\frac{1}{8}(\xi-1)(1-\eta^2)(1-\nu^2)$
15	(-1, 0, 1)	$\frac{1}{8}(\xi-1)(1-\eta^2)\nu(\nu+1)$
16	(-1, 1,-1)	$\frac{1}{8}(\xi-1)\eta(\eta+1)\nu(\nu-1)$
17	(-1, 1, 0)	$\frac{1}{8}(\xi-1)\eta(\eta+1)(1-\nu^2)$
18	(-1, 1, 1)	$\frac{1}{8}(\xi-1)\eta(\eta+1)\nu(\nu+1)$

II. Interpolation functions for the η component.

Field Node Number	Local Coordinate	Interpolation Function $\alpha_m^{\eta}(\xi_j, \eta_j, \nu_j)$
1	(1, 1,-1)	$\frac{1}{8}\,\xi(\xi+1)(\eta+1)\nu(\nu-1)$
2	(1, 1, 0)	$\frac{1}{8}\,\xi(\xi+1)(\eta+1)(\,1-\nu^2)$
3	(1, 1, 1)	$\frac{1}{8}\,\xi(\xi+1)(\eta+1)\nu(\nu+1)$
4	(0, 1,-1)	$\frac{1}{8}\,(1-\xi^2)(\eta+1)\nu(\nu-1)$
5	(0, 1, 0)	$\frac{1}{8}\,(1-\xi^2)(\eta+1)(\,1-\nu^2)$
6	(0, 1, 1)	$\frac{1}{8}\,(1-\xi^2)(\eta+1)\nu(\nu+1)$
7	(-1, 1,-1)	$\frac{1}{8}\,\xi(\xi-1)(\eta+1)\nu(\nu-1)$
8	(-1, 1, 0)	$\frac{1}{8}\,\xi(\xi-1)(\eta+1)(\,1-\nu^2)$
9	(-1, 1, 1)	$\frac{1}{8}\,\xi(\xi-1)(\eta+1)\nu(\nu+1)$
10	(1,-1,-1)	$\frac{1}{8}\,\xi(\xi+1)(\eta-1)\nu(\nu-1)$
11	(1,-1, 0)	$\frac{1}{8}\,\xi(\xi+1)(\eta-1)(\,1-\nu^2)$
12	(1,-1, 1)	$\frac{1}{8}\,\xi(\xi+1)(\eta-1)\nu(\nu+1)$
13	(0,-1,-1)	$\frac{1}{8}\,(1-\xi^2)(\eta-1)\nu(\nu-1)$
14	(0,-1, 0)	$\frac{1}{8}\,(1-\xi^2)(\eta-1)(\,1-\nu^2)$
15	(0,-1, 1)	$\frac{1}{8}\,(1-\xi^2)(\eta-1)\nu(\nu+1)$
16	(-1,-1,-1)	$\frac{1}{8}\,\xi(\xi-1)(\eta-1)\nu(\nu-1)$
17	(-1,-1, 0)	$\frac{1}{8}\,\xi(\xi-1)(\eta-1)(\,1-\nu^2)$
18	(-1,-1, 1)	$\frac{1}{8}\,\xi(\xi-1)(\eta-1)\nu(\nu+1)$

III. Interpolation functions for the ν component.

Field Node Number	Local Coordinate	Interpolation Function $\alpha_m^{\nu}(\xi_j, \eta_j, \nu_j)$
1	(1,-1, 1)	$\frac{1}{8}\,\xi(\xi+1)\eta(\eta-1)(\nu+1)$
2	(1, 0, 1)	$\frac{1}{8}\,\xi(\xi+1)(1-\eta^2)(\nu+1)$
3	(1, 1, 1)	$\frac{1}{8}\,\xi(\xi+1)\eta(\eta+1)(\nu+1)$
4	(0,-1, 1)	$\frac{1}{8}\,(1-\xi^2)\eta(\eta-1)(\nu+1)$
5	(0, 0, 1)	$\frac{1}{8}\,(1-\xi^2)(1-\eta^2)(\nu+1)$
6	(0, 1, 1)	$\frac{1}{8}\,(1-\xi^2)\eta(\eta+1)(\nu+1)$
7	(-1,-1, 1)	$\frac{1}{8}\,\xi(\xi-1)\eta(\eta-1)(\nu+1)$
8	(-1, 0, 1)	$\frac{1}{8}\,\xi(\xi-1)(1-\eta^2)(\nu+1)$
9	(-1, 1, 1)	$\frac{1}{8}\,\xi(\xi-1)\eta(\eta+1)(\nu+1)$
10	(1,-1,-1)	$\frac{1}{8}\,\xi(\xi+1)\eta(\eta-1)(\nu-1)$
11	(1, 0,-1)	$\frac{1}{8}\,\xi(\xi+1)(1-\eta^2)(\nu-1)$
12	(1, 1,-1)	$\frac{1}{8}\,\xi(\xi+1)\eta(\eta+1)(\nu-1)$
13	(0,-1,-1)	$\frac{1}{8}\,(1-\xi^2)\eta(\eta-1)(\nu-1)$
14	(0, 0,-1)	$\frac{1}{8}\,(1-\xi^2)(1-\eta^2)(\nu-1)$
15	(0, 1,-1)	$\frac{1}{8}\,(1-\xi^2)\eta(\eta+1)(\nu-1)$
16	(-1,-1,-1)	$\frac{1}{8}\,\xi(\xi-1)\eta(\eta-1)(\nu-1)$
17	(-1, 0,-1)	$\frac{1}{8}\,\xi(\xi-1)(1-\eta^2)(\nu-1)$
18	(-1, 1,-1)	$\frac{1}{8}\,\xi(\xi-1)\eta(\eta+1)(\nu-1)$

4. Functional in Matrix Form

The functional consists of two terms: the curl-curl term and the dot product term. To find the matrix representation of the functional, we need to determine the matrices for the curl-curl of the corresponding vector and the dot product of the vector in terms of the covariant projection components.

$(\nabla \times A) \cdot (\nabla \times A)$ TERM

The curl of a vector **A** referred to a system of curvilinear coordinates can be expressed in terms of the covariant projection components, A_ξ, A_η, A_ν, and the unitary vectors, $\mathbf{1}_\xi$, $\mathbf{1}_\eta$, $\mathbf{1}_\nu$, as follows

$$\nabla \times \mathbf{A} = \frac{1}{\sqrt{g}} \left[\left(\frac{\partial A_\nu}{\partial \eta} - \frac{\partial A_\eta}{\partial \nu} \right) \mathbf{1}_\xi + \left(\frac{\partial A_\xi}{\partial \nu} - \frac{\partial A_\nu}{\partial \xi} \right) \mathbf{1}_\eta + \left(\frac{\partial A_\eta}{\partial \xi} - \frac{\partial A_\xi}{\partial \eta} \right) \mathbf{1}_\nu \right]. \tag{A-28}$$

Therefore, the product of the curl of a vector **A** and the curl of a vector **B** is

$$(\nabla \times \mathbf{A}) \cdot (\nabla \times \mathbf{B}) = \tag{A-29}$$

$$\begin{aligned}
&\left(\frac{1}{g}\right) \Big[\left(\frac{\partial A_\nu}{\partial \eta} - \frac{\partial A_\eta}{\partial \nu}\right)\left(\frac{\partial B_\nu}{\partial \eta} - \frac{\partial B_\eta}{\partial \nu}\right) \mathbf{1}_\xi \cdot \mathbf{1}_\xi + \left(\frac{\partial A_\nu}{\partial \eta} - \frac{\partial A_\eta}{\partial \nu}\right)\left(\frac{\partial B_\xi}{\partial \nu} - \frac{\partial B_\nu}{\partial \xi}\right) \mathbf{1}_\xi \cdot \mathbf{1}_\eta + \left(\frac{\partial A_\nu}{\partial \eta} - \frac{\partial A_\eta}{\partial \nu}\right)\left(\frac{\partial B_\eta}{\partial \xi} - \frac{\partial B_\xi}{\partial \eta}\right) \mathbf{1}_\xi \cdot \mathbf{1}_\nu \\
&+ \left(\frac{\partial A_\xi}{\partial \nu} - \frac{\partial A_\nu}{\partial \xi}\right)\left(\frac{\partial B_\nu}{\partial \eta} - \frac{\partial B_\eta}{\partial \nu}\right) \mathbf{1}_\eta \cdot \mathbf{1}_\xi + \left(\frac{\partial A_\xi}{\partial \nu} - \frac{\partial A_\nu}{\partial \xi}\right)\left(\frac{\partial B_\xi}{\partial \nu} - \frac{\partial B_\nu}{\partial \xi}\right) \mathbf{1}_\eta \cdot \mathbf{1}_\eta + \left(\frac{\partial A_\xi}{\partial \nu} - \frac{\partial A_\nu}{\partial \xi}\right)\left(\frac{\partial B_\eta}{\partial \xi} - \frac{\partial B_\xi}{\partial \eta}\right) \mathbf{1}_\eta \cdot \mathbf{1}_\nu \\
&+ \left(\frac{\partial A_\eta}{\partial \xi} - \frac{\partial A_\xi}{\partial \eta}\right)\left(\frac{\partial B_\nu}{\partial \eta} - \frac{\partial B_\eta}{\partial \nu}\right) \mathbf{1}_\nu \cdot \mathbf{1}_\xi + \left(\frac{\partial A_\eta}{\partial \xi} - \frac{\partial A_\xi}{\partial \eta}\right)\left(\frac{\partial B_\xi}{\partial \nu} - \frac{\partial B_\nu}{\partial \xi}\right) \mathbf{1}_\nu \cdot \mathbf{1}_\eta + \left(\frac{\partial A_\eta}{\partial \xi} - \frac{\partial A_\xi}{\partial \eta}\right)\left(\frac{\partial B_\eta}{\partial \xi} - \frac{\partial B_\xi}{\partial \eta}\right) \mathbf{1}_\nu \cdot \mathbf{1}_\nu \Big].
\end{aligned}$$

Approximate the vectors **A** and **B** with the element functions described above:

$$A_\xi = \sum_{m=1}^{18} A_m^\xi \alpha_m^\xi(\xi,\eta,\nu), \qquad B_\xi = \sum_{m=1}^{18} B_m^\xi \alpha_m^\xi(\xi,\eta,\nu), \tag{A-30}$$

$$A_\eta = \sum_{m=19}^{36} A_m^\eta \alpha_m^\eta(\xi,\eta,\nu), \qquad B_\eta = \sum_{m=19}^{36} B_m^\eta \alpha_m^\eta(\xi,\eta,\nu), \tag{A-31}$$

$$A_\nu = \sum_{m=37}^{54} A_m^\nu \alpha_m^\nu(\xi,\eta,\nu), \qquad B_\nu = \sum_{m=37}^{54} B_m^\nu \alpha_m^\nu(\xi,\eta,\nu). \tag{A-32}$$

Substituting eqn. (A-30) to eqn. (A-32), into eqn. (A-29), yields the matrix representation of the product of the curl of **A** and the curl of **B** as follows

$$\sum_{m=1}^{54}\sum_{n=1}^{54} [A_m^\xi, A_m^\eta, A_m^\nu] \begin{bmatrix} K_{mn}^{\xi\xi} & K_{mn}^{\xi\eta} & K_{mn}^{\xi\nu} \\ K_{mn}^{\eta\xi} & K_{mn}^{\eta\eta} & K_{mn}^{\eta\nu} \\ K_{mn}^{\nu\xi} & K_{mn}^{\nu\eta} & K_{mn}^{\nu\nu} \end{bmatrix} \begin{bmatrix} B_n^\xi \\ B_n^\eta \\ B_n^\nu \end{bmatrix}, \tag{A-33}$$

where,

$$K_{mn}^{\xi\xi} = \frac{1}{g}\left[g_{22}\left(\frac{\partial\alpha_m^\xi}{\partial\nu}\cdot\frac{\partial\alpha_n^\xi}{\partial\nu}\right) - g_{23}\left(\frac{\partial\alpha_m^\xi}{\partial\nu}\cdot\frac{\partial\alpha_n^\xi}{\partial\eta}\right) - g_{32}\left(\frac{\partial\alpha_m^\xi}{\partial\eta}\cdot\frac{\partial\alpha_n^\xi}{\partial\nu}\right) + g_{33}\left(\frac{\partial\alpha_m^\xi}{\partial\eta}\cdot\frac{\partial\alpha_n^\xi}{\partial\eta}\right)\right],$$

$$K_{mn}^{\xi\eta} = -\frac{1}{g}\left[g_{21}\left(\frac{\partial\alpha_m^\xi}{\partial\nu}\cdot\frac{\partial\alpha_n^\eta}{\partial\nu}\right) - g_{23}\left(\frac{\partial\alpha_m^\xi}{\partial\nu}\cdot\frac{\partial\alpha_n^\eta}{\partial\xi}\right) - g_{31}\left(\frac{\partial\alpha_m^\xi}{\partial\eta}\cdot\frac{\partial\alpha_n^\eta}{\partial\nu}\right) + g_{33}\left(\frac{\partial\alpha_m^\xi}{\partial\eta}\cdot\frac{\partial\alpha_n^\eta}{\partial\xi}\right)\right],$$

$$K_{mn}^{\xi\nu} = \frac{1}{g}\left[g_{21}\left(\frac{\partial\alpha_m^\xi}{\partial\nu}\cdot\frac{\partial\alpha_n^\nu}{\partial\eta}\right) - g_{22}\left(\frac{\partial\alpha_m^\xi}{\partial\nu}\cdot\frac{\partial\alpha_n^\nu}{\partial\xi}\right) - g_{31}\left(\frac{\partial\alpha_m^\xi}{\partial\eta}\cdot\frac{\partial\alpha_n^\nu}{\partial\eta}\right) + g_{32}\left(\frac{\partial\alpha_m^\xi}{\partial\eta}\cdot\frac{\partial\alpha_n^\nu}{\partial\xi}\right)\right],$$

$$K_{mn}^{\eta\xi} = -\frac{1}{g}\left[g_{12}\left(\frac{\partial\alpha_m^\eta}{\partial\nu}\cdot\frac{\partial\alpha_n^\xi}{\partial\nu}\right) - g_{13}\left(\frac{\partial\alpha_m^\eta}{\partial\nu}\cdot\frac{\partial\alpha_n^\xi}{\partial\eta}\right) - g_{32}\left(\frac{\partial\alpha_m^\eta}{\partial\xi}\cdot\frac{\partial\alpha_n^\xi}{\partial\nu}\right) + g_{33}\left(\frac{\partial\alpha_m^\eta}{\partial\xi}\cdot\frac{\partial\alpha_n^\xi}{\partial\eta}\right)\right],$$

$$K^{\eta\eta}_{mn} = \frac{1}{g}\left[g_{11}\left(\frac{\partial\alpha^{\eta}_{m}}{\partial\nu}\cdot\frac{\partial\alpha^{\eta}_{n}}{\partial\nu}\right) - g_{13}\left(\frac{\partial\alpha^{\eta}_{m}}{\partial\nu}\cdot\frac{\partial\alpha^{\eta}_{n}}{\partial\xi}\right) - g_{31}\left(\frac{\partial\alpha^{\eta}_{m}}{\partial\xi}\cdot\frac{\partial\alpha^{\eta}_{n}}{\partial\nu}\right) + g_{33}\left(\frac{\partial\alpha^{\eta}_{m}}{\partial\xi}\cdot\frac{\partial\alpha^{\eta}_{n}}{\partial\xi}\right)\right],$$

$$K^{\eta\nu}_{mn} = -\frac{1}{g}\left[g_{11}\left(\frac{\partial\alpha^{\eta}_{m}}{\partial\nu}\cdot\frac{\partial\alpha^{\nu}_{n}}{\partial\eta}\right) - g_{12}\left(\frac{\partial\alpha^{\eta}_{m}}{\partial\nu}\cdot\frac{\partial\alpha^{\nu}_{n}}{\partial\xi}\right) - g_{31}\left(\frac{\partial\alpha^{\eta}_{m}}{\partial\xi}\cdot\frac{\partial\alpha^{\nu}_{n}}{\partial\eta}\right) + g_{32}\left(\frac{\partial\alpha^{\eta}_{m}}{\partial\xi}\cdot\frac{\partial\alpha^{\nu}_{n}}{\partial\xi}\right)\right],$$

$$K^{\nu\xi}_{mn} = \frac{1}{g}\left[g_{12}\left(\frac{\partial\alpha^{\nu}_{m}}{\partial\eta}\cdot\frac{\partial\alpha^{\xi}_{n}}{\partial\nu}\right) - g_{13}\left(\frac{\partial\alpha^{\nu}_{m}}{\partial\eta}\cdot\frac{\partial\alpha^{\xi}_{n}}{\partial\eta}\right) - g_{22}\left(\frac{\partial\alpha^{\nu}_{m}}{\partial\xi}\cdot\frac{\partial\alpha^{\xi}_{n}}{\partial\nu}\right) + g_{23}\left(\frac{\partial\alpha^{\nu}_{m}}{\partial\xi}\cdot\frac{\partial\alpha^{\xi}_{n}}{\partial\eta}\right)\right],$$

$$K^{\nu\eta}_{mn} = -\frac{1}{g}\left[g_{11}\left(\frac{\partial\alpha^{\nu}_{m}}{\partial\eta}\cdot\frac{\partial\alpha^{\eta}_{n}}{\partial\nu}\right) - g_{13}\left(\frac{\partial\alpha^{\nu}_{m}}{\partial\eta}\cdot\frac{\partial\alpha^{\eta}_{n}}{\partial\xi}\right) - g_{21}\left(\frac{\partial\alpha^{\nu}_{m}}{\partial\xi}\cdot\frac{\partial\alpha^{\eta}_{n}}{\partial\nu}\right) + g_{23}\left(\frac{\partial\alpha^{\nu}_{m}}{\partial\xi}\cdot\frac{\partial\alpha^{\eta}_{n}}{\partial\xi}\right)\right],$$

$$K^{\nu\nu}_{mn} = \frac{1}{g}\left[g_{11}\left(\frac{\partial\alpha^{\nu}_{m}}{\partial\eta}\cdot\frac{\partial\alpha^{\nu}_{n}}{\partial\eta}\right) - g_{12}\left(\frac{\partial\alpha^{\nu}_{m}}{\partial\eta}\cdot\frac{\partial\alpha^{\nu}_{n}}{\partial\xi}\right) - g_{21}\left(\frac{\partial\alpha^{\nu}_{m}}{\partial\xi}\cdot\frac{\partial\alpha^{\nu}_{n}}{\partial\eta}\right) + g_{22}\left(\frac{\partial\alpha^{\nu}_{m}}{\partial\xi}\cdot\frac{\partial\alpha^{\nu}_{n}}{\partial\xi}\right)\right].$$

DOT PRODUCT TERM

A vector **A** can be resolved into covariant projection components with respect to the reciprocal unitaries of the local coordinate system,

$$\mathbf{A} = A_{\xi}\,1^{\xi} + A_{\eta}\,1^{\eta} + A_{\nu}\,1^{\nu},$$

where A_{ξ}, A_{η}, A_{ν} are the covariant projection components of **A**, and 1^{ξ}, 1^{η}, 1^{ν}, are the reciprocal unitaries of the local coordinate system. The product of two such vectors can therefore be written as,

$$\begin{aligned}\mathbf{A}\cdot\mathbf{B} = {} & A_{\xi}B_{\xi}\,1^{\xi}\cdot 1^{\xi} + A_{\xi}B_{\eta}\,1^{\xi}\cdot 1^{\eta} + A_{\xi}B_{\nu}\,1^{\xi}\cdot 1^{\nu} \\ & + A_{\eta}B_{\xi}\,1^{\eta}\cdot 1^{\xi} + A_{\eta}B_{\eta}\,1^{\eta}\cdot 1^{\eta} + A_{\eta}B_{\nu}\,1^{\eta}\cdot 1^{\nu} \\ & + A_{\nu}B_{\xi}\,1^{\nu}\cdot 1^{\xi} + A_{\nu}B_{\eta}\,1^{\nu}\cdot 1^{\eta} + A_{\nu}B_{\nu}\,1^{\nu}\cdot 1^{\nu}\,.\end{aligned} \qquad \text{(A-34)}$$

Substituting eqn. (A-30) to eqn. (A-32) into eqn. (A-34), the matrix form of the dot product follows

$$\sum_{m=1}^{54}\sum_{n=1}^{54}[A_m^{\xi}, A_m^{\eta}, A_m^{\nu}]\begin{bmatrix} L_{mn}^{\xi\xi} & L_{mn}^{\xi\eta} & L_{mn}^{\xi\nu} \\ L_{mn}^{\eta\xi} & L_{mn}^{\eta\eta} & L_{mn}^{\eta\nu} \\ L_{mn}^{\nu\xi} & L_{mn}^{\nu\eta} & L_{mn}^{\nu\nu} \end{bmatrix}\begin{bmatrix} B_n^{\xi} \\ B_n^{\eta} \\ B_n^{\nu} \end{bmatrix}, \tag{A-35}$$

where,

$$\begin{aligned}
L_{mn}^{\xi\xi} &= g^{11}\,\alpha_m^{\xi}\,\alpha_m^{\xi}\,, \\
L_{mn}^{\xi\eta} &= g^{12}\,\alpha_m^{\xi}\,\alpha_m^{\eta}\,, \\
L_{mn}^{\xi\nu} &= g^{13}\,\alpha_m^{\xi}\,\alpha_m^{\nu}\,, \\
L_{mn}^{\eta\xi} &= g^{21}\,\alpha_m^{\eta}\,\alpha_m^{\xi}\,, \\
L_{mn}^{\eta\eta} &= g^{22}\,\alpha_m^{\eta}\,\alpha_m^{\eta}\,, \\
L_{mn}^{\eta\nu} &= g^{23}\,\alpha_m^{\eta}\,\alpha_m^{\nu}\,, \\
L_{mn}^{\nu\xi} &= g^{31}\,\alpha_m^{\nu}\,\alpha_m^{\xi}\,, \\
L_{mn}^{\nu\eta} &= g^{32}\,\alpha_m^{\nu}\,\alpha_m^{\eta}\,, \\
L_{mn}^{\nu\nu} &= g^{33}\,\alpha_m^{\nu}\,\alpha_m^{\nu}\,.
\end{aligned}$$

The reciprocal metrical coefficients can be determined using the relationship between the unitary vectors and the reciprocal unitary vectors given by eqn.(A-3) to eqn.(A-5). They can be explicitly expressed in terms of the metrical coefficients as follows:

$$
\begin{aligned}
g^{11} &= \mathbf{1}^{\xi}.\mathbf{1}^{\xi} &&= \tfrac{1}{g}\,[\, g_{22}\, g_{33} - g_{23}\, g_{32}\,],\\
g^{12} &= \mathbf{1}^{\xi}.\mathbf{1}^{\eta} &&= \tfrac{1}{g}\,[\, g_{23}\, g_{31} - g_{21}\, g_{33}\,],\\
g^{13} &= \mathbf{1}^{\xi}.\mathbf{1}^{\nu} &&= \tfrac{1}{g}\,[\, g_{21}\, g_{32} - g_{22}\, g_{31}\,],\\
g^{21} &= \mathbf{1}^{\eta}.\mathbf{1}^{\xi} &&= \tfrac{1}{g}\,[\, g_{32}\, g_{13} - g_{33}\, g_{12}\,],\\
g^{22} &= \mathbf{1}^{\eta}.\mathbf{1}^{\eta} &&= \tfrac{1}{g}\,[\, g_{33}\, g_{11} - g_{31}\, g_{13}\,],\\
g^{23} &= \mathbf{1}^{\eta}.\mathbf{1}^{\nu} &&= \tfrac{1}{g}\,[\, g_{31}\, g_{12} - g_{32}\, g_{11}\,],\\
g^{31} &= \mathbf{1}^{\nu}.\mathbf{1}^{\xi} &&= \tfrac{1}{g}\,[\, g_{12}\, g_{23} - g_{13}\, g_{22}\,],\\
g^{32} &= \mathbf{1}^{\nu}.\mathbf{1}^{\eta} &&= \tfrac{1}{g}\,[\, g_{13}\, g_{21} - g_{11}\, g_{23}\,],\\
g^{33} &= \mathbf{1}^{\nu}.\mathbf{1}^{\nu} &&= \tfrac{1}{g}\,[\, g_{11}\, g_{22} - g_{12}\, g_{21}\,].
\end{aligned}
$$

Now, define a column matrix, [E], representing the nodal electric field; a square matrix [S] representing the curl-curl term in the functional; a [T] representing the dot-product term in the functional, as follows

$$
[\mathbf{E}] = \begin{bmatrix} E_m^{\xi} \\ E_m^{\eta} \\ E_m^{\nu} \end{bmatrix}, \qquad [S] = \begin{bmatrix} S_{mn}^{\xi\xi} & S_{mn}^{\xi\eta} & S_{mn}^{\xi\nu} \\ S_{mn}^{\eta\xi} & S_{mn}^{\eta\eta} & S_{mn}^{\eta\nu} \\ S_{mn}^{\nu\xi} & S_{mn}^{\nu\eta} & S_{mn}^{\nu\nu} \end{bmatrix}, \qquad [T] = \begin{bmatrix} T_{mn}^{\xi\xi} & T_{mn}^{\xi\eta} & T_{mn}^{\xi\nu} \\ T_{mn}^{\eta\xi} & T_{mn}^{\eta\eta} & T_{mn}^{\eta\nu} \\ T_{mn}^{\nu\xi} & T_{mn}^{\nu\eta} & T_{mn}^{\nu\nu} \end{bmatrix},
$$

where,

$$
S_{mn}^{\tau\kappa} = \int_{\Omega} K_{mn}^{\tau\kappa}\, d\Omega\,; \qquad \tau, \kappa = \xi, \eta, \nu,
$$

$$
T_{mn}^{\tau\kappa} = \int_{\Omega} L_{mn}^{\tau\kappa}\, d\Omega\,; \qquad \tau, \kappa = \xi, \eta, \nu.
$$

The integrations can be carried out numerically by using the Gauss-Legendre quadrature method given in Appendix II.

By using the above definitions, one can establish the following relationships

$$\int_{\Omega} (\nabla \times \mathbf{E}) \cdot (\nabla \times \mathbf{E}) \, d\Omega \;=\; [\mathbf{E}]^c[\mathrm{S}]\,[\mathbf{E}], \tag{A-36}$$

$$\int_{\Omega} \mathbf{E} \cdot \mathbf{E} \; d\Omega \;=\; [\mathbf{E}]^c[\mathrm{T}]\,[\mathbf{E}]\,. \tag{A-37}$$

Substituting eqn. (A-36) and eqn. (A-37) into eqn. (A-1), the functional $\mathcal{F}$ is expressed in the matrix form in terms of the [S] and [T] matrix as follow:

$$\begin{aligned} \mathcal{F}(\mathbf{E}) \;&=\; \tfrac{1}{2}\int_{\Omega}\Big\{ -\tfrac{1}{\mu_r}(\nabla \times \mathbf{E}) \cdot (\nabla \times \mathbf{E}) + k_0^2 \epsilon_r \mathbf{E} \cdot \mathbf{E}\Big\} d\Omega \\ &=\; -\tfrac{1}{2}\,\tfrac{1}{\mu_r}\,[\mathbf{E}]^c[\mathrm{S}]\,[\mathbf{E}] \;+\; \tfrac{1}{2}\,k_0^2\epsilon_r[\mathbf{E}]^c[\mathrm{T}]\,[\mathbf{E}] \\ &=\; -\tfrac{1}{2}\,[\mathbf{E}]^c\Big\{\,\tfrac{1}{\mu_r}\,[\mathrm{S}] \;+\; k_0^2\epsilon_r[\mathrm{T}]\,\Big\}[\mathbf{E}]. \end{aligned} \tag{A-38}$$

Applying the standard finite element minimization procedure to eqn. (A-38) gives the following system of equations:

$$\{\, -\tfrac{1}{\mu_r}[S] + k_0^2\epsilon_r[T]\,\}\;[\mathrm{E}] = [0]. \tag{A-39}$$

Appendix II

Gauss-Legendre quadrature

Evaluations of the [S] and [T] matrices of Appendix I involve integrations of the following form:

$$I = \int_{-1}^{1}\int_{-1}^{1}\int_{-1}^{1} f(\xi, \eta, \nu)\ d\xi\, d\eta\, d\nu\ .$$

To evaluate such integral, the Gauss-Legendre quadrature is used here. Gauss-Legendre quadrature provides twice the degree of precision compared to equally-spaced integration methods. It has varying weighting coefficients as well as node locations. As a result, one can achieve Gaussian quadrature formulas whose order is almost twice that of a Newton-Cotes formula with the same number of function evaluations.

The numerical integration of the integral can be expressed as follows

$$I = \sum_{k=1}^{3}\sum_{j=1}^{3}\sum_{i=1}^{3} H_i\, H_j\, H_k\, f(\xi_i, \eta_j, \nu_k)\ .$$

With the Gauss-Legendre quadrature, the coefficients H_i, H_j, H_k and the locations of integrations ξ_i, η_j, ν_k must be chosen according to the following table:

	Location of Integrations	Weighting Coefficients
$i/j/k$	$\xi_i/\eta_j/\nu_k$	$H_i/H_j/H_k$
1	$\sqrt{\frac{3}{5}} = 0.774596669241483$	$\frac{5.0}{9.0} = 0.555555555555556$
2	0.000000000000000	$\frac{8.0}{9.0} = 0.888888888888889$
3	$-\sqrt{\frac{3}{5}} = -0.774596669241483$	$\frac{5.0}{9.0} = 0.555555555555556$

Appendix III

Determining S-parameters with finite element method

A description of circuit components can follow with equivalent voltage and current waves. This description, and the derived equivalent resistance, lead to a representation through distinct equivalent-circuit diagrams with concentrated circuit components. However, representation of microwave networks by impedance or admittance matrices is not very convenient since voltages, currents and impedances cannot be measured in a direct manner at microwave frequencies. In microwave engineering, a description of microwave circuits called scattering (S) parameters is preferred. This is because the S-parameters are defined in terms of the quantities that are directly measurable, both in amplitude and phase. These quantities are the incident or reflected waves, or the reflection coefficient and the transmission coefficient. These form the basis of the scattering matrix formulation.

Fig. A-5 shows the configuration of a discontinuity problem in a general two-port waveguide. A scattering matrix represents the relationship between the parameters a_n

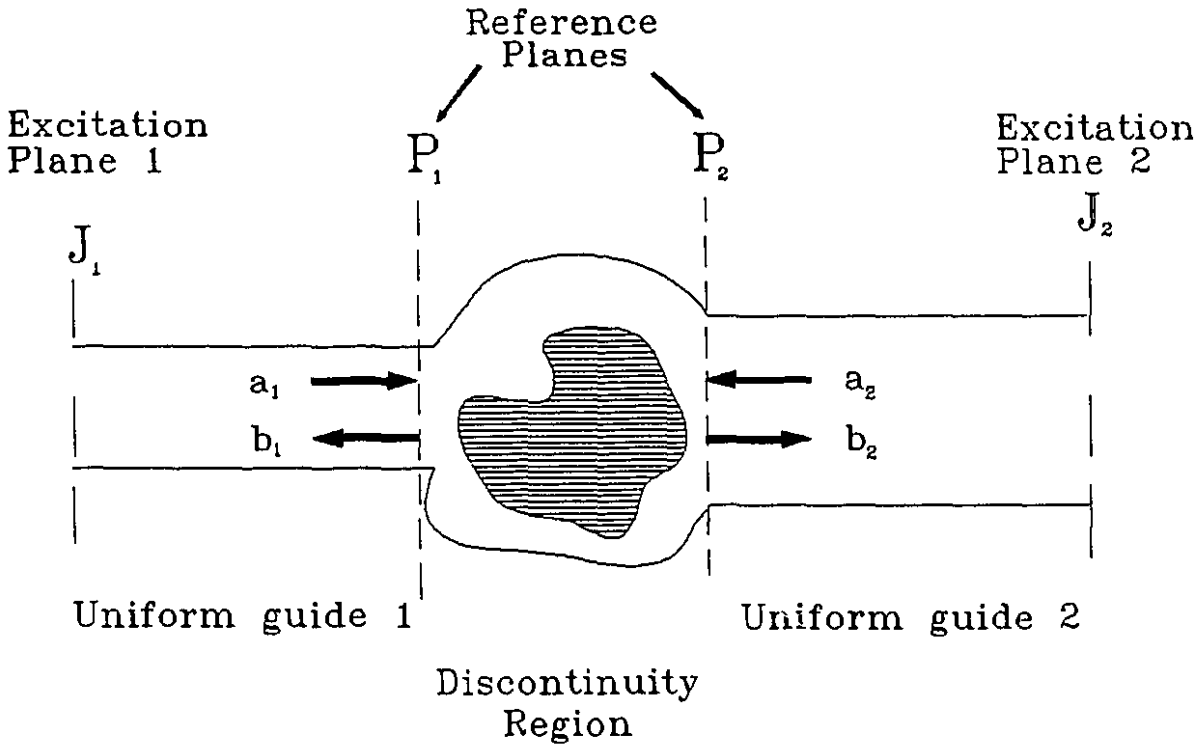

Figure A-5
A general two-port waveguide discontinuity

proportional to the incident wave at port n, and the parameters b_n proportional to the outgoing waves at port n. The final objective is to determine the amplitudes and phases of the S-parameters which fully describe the discontinuity region, with respect to the two reference planes P_1 and P_2. In matrix notation, the system of equations of the circuit can be written as

$$\begin{bmatrix} b_1 \\ b_2 \end{bmatrix} = \begin{bmatrix} S_{11} & S_{12} \\ S_{21} & S_{22} \end{bmatrix} \begin{bmatrix} a_1 \\ a_2 \end{bmatrix}, \tag{A-1}$$

where

$$S_{11} = \frac{b_1}{a_1}\Big|_{a_2=0} = \text{Reflectivity at port 1 with port 2 terminated,}$$

$$S_{21} = \frac{b_2}{a_1}\Big|_{a_2=0} = \text{Forward transmission from port 1 to port 2 with port 2 terminated,}$$

$$S_{12} = \frac{b_1}{a_2}\Big|_{a_1=0} = \text{Reverse transmission from port 2 to port 1 with port 1 terminated,}$$

$$S_{22} = \frac{b_2}{a_2}\Big|_{a_1=0} = \text{Reflectivity at port 2 with port 1 terminated.}$$

These parameters are defined under the assumption that only the dominant mode can propagate inside the waveguide. For multimode operation, a more general description, called the general S-parameter method, must be used. Since the S-parameters measure the transmission and reflection coefficients of a given wave pattern, they must be calculated with respect to a known field distribution. This field distribution is

introduced into the system by using the two far-field planes, J_1 and J_2. Since the far-field planes are placed at a distance sufficiently far away from the discontinuity for all evanescent modes to have decayed, the field pattern on these planes is purely determined by the eigenvector of the dominant mode. The total tangential field on the two far-field planes can be expressed in terms of the incident and reflected waves as follows

$$\begin{cases} \mathbf{E}_t^i = V_i \, e_i \, , \\ \\ \mathbf{H}_t^i = I_i \, h_i \, , \end{cases} \tag{A-2}$$

where e_i and h_i are the tangential field distributions of the dominant mode of the given guide, and the voltage and current at port i are defined as

$$\begin{cases} V_i = a_i + b_i \, , \\ \\ I_i = a_i - b_i \, . \end{cases} \tag{A-3}$$

A general admittance matrix [Y] can be defined for the two-port network as

$$\begin{bmatrix} I_1 \\ I_2 \end{bmatrix} = \begin{bmatrix} Y_{11} Y_{12} \\ Y_{21} Y_{22} \end{bmatrix} \begin{bmatrix} V_1 \\ V_2 \end{bmatrix} \, ,$$

where

$$Y_{11} = \frac{I_1}{V_1}\Big|_{v_2=0} = \text{Short-circuit input admittance at port 1,}$$

$$Y_{21} = \frac{I_2}{V_1}\Big|_{v_2=0} = \text{Short-circuit forward transfer admittance,}$$

$$Y_{12} = \frac{I_1}{V_2}\Big|_{v_1=0} = \text{Short-circuit reverse transfer admittance,}$$

$$Y_{22} = \frac{I_2}{V_2}\Big|_{v_1=0} = \text{Short-circuit admittance at port 2.}$$

It has been shown [8,16] that the Y-parameters can be expressed in terms of the functional of the problem as follows

$$\mathbf{Y}_{ij} = j\,(\tfrac{1}{\omega\mu_o})(\tfrac{1}{P_i V_i})\cdot F(\mathbf{E}^i,\ \mathbf{E}^j), \tag{A-4}$$

where

$\mathbf{E}^i$ = FEM solution when plane J_i excited with $V_i e_i$, and else shorted,

$\mathbf{E}^j$ = FEM solution when plane J_j excited with $V_j e_j$, and else shorted,

$P_i = \int_\Omega (e_i \times h_i)\cdot n \ d\Omega,$

$F(\mathbf{E}^i, \mathbf{E}^j)$ = Value of the functional with column matrices $[E^i]$ and $[E^j]$

= $[E^i]^c[W][E^j]$; [W] is the system matrix of the problem.

To characterize a two-port circuit, one needs to solve the problem with finite element method twice: once for the $[E^1]$, exciting port 1 with dominant mode field with port 2

shorted, and once for the $[E^2]$, exciting port 2 with dominant mode field with port 1 shorted. When $[E^1]$ and $[E^2]$ are known, the Y-parameters of the two-port circuit can be determined by using eqn.(A-4). The Y-parameters can then be converted to the desired S-parameters, using the following expressions:

$$S_{11} = \frac{(Y_o - Y_{11})(Y_o + Y_{22}) + Y_{12}Y_{21}}{(Y_o + Y_{11})(Y_o + Y_{22}) - Y_{12}Y_{21}}, \tag{A-5}$$

$$S_{12} = \frac{-Y_{12}Y_0}{(Y_o + Y_{11})(Y_o + Y_{22}) - Y_{12}Y_{21}}, \tag{A-6}$$

$$S_{21} = \frac{-Y_{21}Y_0}{(Y_o + Y_{11})(Y_o + Y_{22}) - Y_{12}Y_{21}}, \tag{A-7}$$

$$S_{22} = \frac{(Y_o + Y_{11})(Y_o - Y_{22}) + Y_{12}Y_{21}}{(Y_o + Y_{11})(Y_o + Y_{22}) - Y_{12}Y_{21}}. \tag{A-8}$$

So far, the procedure provides a set of S-parameters with the phase uncalibrated to any specific plane of reference. The discontinuity is not fully characterized until the phase is properly calibrated to a selected plane. To calibrate the phase, it is necessary to repeat the procedure with the discontinuity section replaced by a uniform guide section of any desired length. The length of this uniform guide section will determine the plane of reference where the phase is calibrated to. If the length of the uniform section is the same as that of the discontinuity itself, then the phase will be calibrated to the center of the discontinuity. The Y-parameters of the two-port network with the discontinuity region replaced by a uniform guide section are determined with eqn. (A-4). The calibration factors are determined by setting the magnitude of the forward transmission coefficient of the S-parameters to unity and the phase to 0 degrees. Then the scattering

parameters of the structure including the discontinuity are computed by replacing the calibration segment with the discontinuity. The calibrated S-parameters of the discontinuity can then be obtained by subtracting the phase offset determined by the calibration procedure. The calibration also eliminates any potential errors which may arise from signal loss in the two uniform waveguides.

Bibliography

Finite Element References

[1] Kisak, E., Silvester, P., Telford, W.M.: 'A recursive method in the E-polarization of magnetotelluric modeling by high-order finite elements'. *Acta Geodaetica, Geophysica et Montanistica Acad. Sci. Hungaricae*, vol. **12**, pp. 255-266, 1977.

[2] Silvester, P.P, Lowther D.A., Carpenter C.J., Wyatt, E.A.: 'Exterior finite elements for 2-dimensional field problems with open boundaries'. *Proc. IEE*, vol. **124**, pp. 1267–1270, Dec. 1977.

[3] Crowley, C.W., Pinchuk, A.R., Silvester, P.P.: 'Spurious solutions to vector diffusion and wave field problems'. *IEEE Transactions on Magnetics*, vol. **MAG-24**, no.1, pp. 158-61, Jan 1988.

[4] Ise, K., Inoue, K., Koshiba, M.: 'Three-dimensional finite-element solution of dielectric scattering obstacles in a rectangular waveguide'. *IEEE Trans. on Microwave Theory and Techniques*, vol. **MTT-38**, no. 9, pp. 1352-1359, Sep. 1990.

[5] Foo, S.L., Silvester, P.P. : 'Boundary-marching method for discontinuity analysis in waveguides of arbitrary cross section'. Submitted to IEEE MTT in 1991.

[6] Crowley, C.W., Silvester, P.P., Hurwitz, H., Jr.: 'Covariant projection elements for 3-D vector field problems'. *IEEE Transactions on Magnetics*, vol. **MAG-24**, no. 1, pp. 397-400, Jan 1988.

[7] Pinchuk, A.R., Crowley, C.W., Silvester, P.P.: 'Spectrally correct finite element operators for electromagnetic field problems'. *J. Appl. Phys. (USA),* Vol. 63, no. 8, pt. 2A, pp. 3025-7, April 1987.

[8] Webb, J.P., Maile, G.L., Ferrari, R.L. : 'Finite-element solution of three-dimensional electromagnetic problems'. *IEE Proc.*, Vol 130, Pt. H, no. 2, March 1983, pp. 153-159.

[9] Koshiba, M., Hayata, K., Suzuki, M. : 'Improved finite-element formulation in terms of the magnetic field vector for dielectric waveguide'. *IEEE Trans. on Microwave Theory and Techniques*, Vol. **MTT-33**, no. 3, pp. 227-233, March 1985.

[10]Svedin, J.A.M. : 'A numerically efficient finite-element formulation for the general waveguide problem without spurious modes'. *IEEE Trans. on Microwave Theory and Techniques,* Vol. **MTT-37**, no. 11, November 1989, pp. 1708-1715.

[11]Angkaew, T., Matsuhara, M., Kumagai, N. : 'Finite-element analysis of waveguide modes : A novel approach that eliminates spurious modes'. *IEEE Trans. on Microwave Theory and Techniques*, vol. **MTT-35**, no. 2, February 1987, pp. 117-123.

[12]Rahman, B.M.A., Davies, J.B. : 'Penalty function improvement of waveguide solution by finite elements'. *IEEE Trans. on Microwave Theory and Techniques*, vol. **MTT-32**, no. 8, August 1984, pp. 922-928.

[13]Hayata, K., Koshiba, M., Suzuki, M. : 'Vectorial finite-element method without any spurious solutions for dielectric waveguiding problems using transverse magnetic-field component'. *IEEE Trans. on Microwave Theory and Techniques,* vol. **MTT-34**, no. 11, November 1986, pp. 1120-1124.

[14]English, W.J., Young, F.J. : 'An $\boldsymbol{E}$ vector variational formulation of the Maxwell equations for cylindrical waveguide problems'. *IEEE Trans. on Microwave Theory and Techniques*, vol. **MTT-19**, no. 1, January 1970, pp. 40-46.

[15]Hayata, K., Eguchi, M., Koshiba, M. : 'Finite element formulation for guided-wave problems using transverse electric field component'. *IEEE Trans. on Microwave Theory and Techniques*, vol. **MTT-37**, no. 1, January 1988, pp. 256-258.

[16]Webb, J.P., Parihar, S. : 'Finite element analysis of H-plane rectangular waveguide problems'. *IEE Proc.*, vol. 133, Pt. H, no. 2, April 1986, pp. 91-94.

[17]Koshiba, M., Sato, M., Suzuki, M. : 'Application of finite-element method to E-plane waveguide discontinuities'. *The Transactions of the IECE of Japan*, vol. **E66**, no. 7, July 1983, pp. 457-458.

[18]Koshiba, M., Sato, M., Suzuki, M. : 'Finite-element analysis of arbitrarily shaped H-plane waveguide discontinuities'. *The Transactions of the IECE of Japan*, vol. **E66**, no. 2, February 1983, pp. 82-87.

[19]Webb, J.P. : 'The finite-element method for finding modes of dielectric-loaded cavities'. *IEEE Trans. on Microwave Theory and Techniques*, vol. **MTT-33**, no. 7, July 1985, pp. 635-639.

[20]Hano, M. : 'Finite-element analysis of dielectric-loaded waveguides'. *IEEE Trans. on Microwave Theory and Techniques*, vol. **MTT-32**, no. 10, October 1984, pp. 1275-1279.

[21]Kanellopoulos, V.N., Webb, J.P. : 'A complete E-plane analysis of waveguide junctions using the finite element method'. *IEEE Trans. on Microwave Theory and Techniques*, vol. **MTT-38**, no. 3, March 1990, pp. 295.

[22]Hara, M., Wada, T., Fukasawa, T., Kikuchi, F. : 'A three dimensional analysis of RF electromagnetic fields by the finite element method'. *IEEE Trans. on Magnetics*, vol. **MAG-19**, no. 6, November 1983, pp. 2417-2424.

[23]Konrad, A. : 'Vector variational formulation of electromagnetic fields in anisotropic media'. *IEEE Trans. on Microwave Theory and Techniques*, vol. **MTT-24**, no. 9, September 1976, pp. 553-559.

[24]Konrad, A. : 'A direct three-dimensional finite element method for the solution of electromagnetic fields in cavities'. *IEEE Trans. on Magnetics,* vol. **MAG-21**, no. 6, November 1985, pp. 2276-2279.

[25]Thomas, D.T. : 'Functional approximations for solving boundary value problems by computer'. *IEEE Trans. on Microwave Theory and Techniques,* vol. **MTT-17** ,no. 8, August 1969, pp. 447-454.

[26]English W.J. : 'Vector variational solutions of inhomogeneously loaded cylindrical waveguide structures'. *IEEE Trans. on Microwave Theory and Techniques,* vol. **MTT-19**, no. 1, January 1971, pp. 9-18.

[27]Picon, O., Hanna, V.F., Citerne, J. : 'Three dimensional finite-element formulation for finline dicontinuity problems'. *IEEE MTT-S Digest 1986,* pp. 789-792.

Finline References

[28]Jansen, R.H., Koster, N.H.L. : 'Some New Results on the Equivalent Circuit Parameters of the Inductive Strip Discontinuity in Unilateral Fin Lines'. *AEU 35 [1981],* pp. 497-499.

[29]Biswas, A., Bhat B. : 'Accurate characteriazation of an inductive strip in finline'. *IEEE Trans. on Microwave Theory and Techniques,* vol. **MTT-36,** no. 8, August 1988, pp. 1233-1238.

[30]Eswarappa, Costache, G.I., Hoefer, W.J.R. : 'Finlines in rectangular and circular waveguide housings including substrate mounting and bending effects — Finite element analysis'. *IEEE Trans. on Microwave Theory and Techniques,* vol. **MTT-37,** no. 2, pp. 299-305, Feb. 1989.

[31]Pramanick, P., Mansour, R.R., MacPhie, R.H. : 'Computer-aided design models for unilateral finlines with finite metalization thickness and arbitrarily located slot widths'. *IEEE MTT-S Digest,* 1987, pp. 703-704.

[32]Knorr, J.B., Deal, J.C. : 'Scattering coefficients of an inductive strip in a finline : Theory and experiment'. *IEEE Trans. on Microwave Theory and Techniques*, vol. **MTT-33**, no. 10, October 1985, pp. 1011-1017.

[33]Saad, A.M.K., Schunemann K. : 'Design and performance of fin-line bandpass filters'. *9th Eur. Microwave Conf. Digest*, Sept. 1979, pp. 397-401.

[34]Bornemann, J., Vahldieck, R., Arndt, F. : 'Optimized low-insertion-loss millimetre-wave fin-line and metal insert filters'. *The Radio and Electronic Engineer*, vol. 52, no. 11/12, pp. 513-521, November/December 1982.

[35]Shih., Y.C., Itoh, T., Bui, L.Q. : 'Computer-aided design of millimeter-wave E-plane filters'. *IEEE Trans. on Microwave Theory and Techniques*, vol. **MTT-31**, no. 2, February 1983, pp. 135-142.

[36]Vahldieck, R., Hoefer, W.J.R. : 'The influence of metalization thickness and mounting grooves on he characterizatics of finlines'. *IEEE MTT-S Digest, 1985*, pp. 143-144.

[37]Kitazawa, T., Mittra, R. : 'Analysis of finline with finite metalization thickness'. *IEEE Trans. on Microwave Theory and Techniques*, vol. **MTT-32**, no. 11, November 1984, pp. 1484-1487.

[38]Vahldieck, R. : 'Accurate hybrid-mode analysis of various finline configurations including multilayered dielectrics, finite metalization thickness, and substrate holding grooves'. *IEEE Trans. on Microwave Theory and Techniques*, vol. **MTT-32**, no. 11, November 1984, pp. 1454-1460.

[39]Rozzi, C.A., Rycroft, C.M.D. : 'An approximate variational solution to the step discontinuity in finline'. *IEEE Trans. on Microwave Theory and Techniques*, vol. **MTT-37**, no. 6, June 1989, pp. 977-983.

[40]Eswarappa, Costache, G., Hoefer, W.J.R. : 'Numerical modeling of generalized millimeter-wave transmission media with finite element and transmission line matrix methods'. *International Journal of Infrared and Millimeter Waves*, vol. 10, no. 1, 1989, pp. 21-31.

[41]Mansour, R., Macphie R.H. : 'A unified hybrid-mode analysis for planar transmission lines with multilayer isotropic/anisotropic substrates'. *IEEE Trans. on Microwave Theory and Techniques*, vol. **MTT-35**, no. 12, December 1987, pp. 1382-1391.

[42]Meier, P.J. : 'Integrated fin-line millimeter components'. *IEEE Trans. on Microwave Theory and Techniques*, vol. **MTT-22**, no. 12, December 1974, pp. 1209-1215.

[43]Saad, A.M.K., Schunemann, K. : 'A rectangular equivalent for bilateral and unilateral fin-lines'. *AEU., Band 35, 1981,* Heft 7/8. pp. 287-292.

[44]Hennawy, H.E., Schunemann, K. : 'Analysis of fin-line discontinuities'. *9th Eur. Microwave Conf. Proc.*, 1979, pp. 448-452.

[45]Webb, K.J., Mittra, R. : 'Solution of the finline step-discontinuity problem using the generalized variational technique'. *IEEE Trans. on Microwave Theory and Techniques*, vol. **MTT-33**, no. 10, October 1985, pp. 1004-1010.

[46]Sorrentino, R., Itoh, T. : 'Transverse resonance analysis of finline discontinuities'. *IEEE Trans. on Microwave Theory and Techniques*, vol. **MTT-32**, no. 12, December 1984, pp. 1633-1638.

[47]Hennawy, H.E., Schunemann : 'Impedance transformation in fin lines'. *IEE Proc.*, vol. 129, Pt. H, no. 6, December 1982, pp. 342-350.

[48]Schmidt, L.P., Itoh, T. : 'Spectral domain analysis of dominant and higher order modes in fin-lines'. *IEEE Trans. on Microwave Theory and Techniques,* vol. **MTT-28**, no. 9, September 1980, pp. 981-985.

[49]Zhang, Q., Itoh, T. : 'Spectral-domain analysis of scattering from E-plane circuit elements'. *IEEE Trans. on Microwave Theory and Techniques,* vol. **MTT-35**, no. 2, February 1986, pp. 138-149.

[50]Worm, S.B., Pregla, R. : 'Hybrid-mode analysis of arbitrarily shaped planar microwave structures by the method of lines'. *IEEE Trans. on Microwave Theory and Techniques,* vol. **MTT-32**, no. 2, February 1984, pp. 191-196.

[51]Helard, M., Citerne, J., Picon, O., Hanna, V.F. : 'Theoretical and experimental investigation of finline dicontinuities'. *IEEE Trans. on Microwave Theory and Techniques,* vol. **MTT-33**, no. 10, October 1985, pp. 994-1003.

[52]Jansen, R.H. : 'Hybrid mode analysis of end effects of planar microwave and millimeterwave transmission lines'. *IEE Proc.,* vol. 128, no. 2, April 1981, pp. 77-86.

[53]Olley, C.A., Rozzi, T.E. : 'Systematic characterization of the spectrum of unilateral finline'. *IEEE Trans. on Microwave Theory and Techniques,* vol. **MTT-34**, no. 11, November 1986, pp. 1147-1155.

[54]Meier, P.J. : 'Equivalent relative permittivity and Unloaded Q-factor of integrated fin-line'. *Electron. Lett.*, vol. 9, no. 7, pp. 162-163, April 1973.

[55]Cohn, S.B. : 'Slot-line on a dielectric substrate'. *IEEE Trans. on Microwave Theory and Techniques,* vol. **MTT-17**, Oct. 1969, pp. 768-778.

[56]Sharma, A.K., Hoefer, W.J.R. : 'Emprical expressions for finline design'. *IEEE Trans. on Microwave Theory and Techniques,* vol. **MTT-31**, April. 1983, pp. 350-356.

[57]Itoh, T., Mittra, R. : 'A technique for computing dispersion characteristics of shielded microstrip lines'. *IEEE Trans. on Microwave Theory and Techniques,* vol. **MTT-22**, Oct. 1974, pp. 896-898.

[58]Wexler, A. : 'Solution of Waveguide discontinuities by modal analysis'. *IEEE Trans. on Microwave Theory and Techniques*, vol. **MTT-15**, Sept. 1967, pp. 508-517.

[59]Picon, O., Hanna, V.F., Citerne J. : 'Three dimensional finite-element formulation for finline discontinuity problems'. *IEEE MTT-S Digest 1986*, pp. 789-792.

Textbooks

[60]Marcuvitz, N.: *Waveguide handbook.* London: Peter Peregrinus, 1986.

[61]Silvester, P.P., Ferrari, R.L. : *Finite elements for electrical engineers*, 2nd ed. Cambridge: Cambridge University Press, 1990.

[62]Hughes, T.J.R. : *The finite element method: linear static and dynamic finite element analysis.* Englewood Cliffs, N.J.: Prentice-Hall, 1987.

[63]Bhat, B., Koul, S.K. : *Analysis design and applications of fin lines.* Norwood, MA. : Artech House Inc., 1987.

[64]Stratton, J.A. : *Electromagnetic Theory.* New York : McGraw-Hill, 1941.

[65]Collin, R.E. : *Field Theory of Guided Waves.* New York : McGraw-Hill, 1960.

[66]Pyle, I.C. : *The Ada Programming Language.* 1981

[67]Wallace, R.H. : *Practitioner's Guide to Ada.* 1986

[68]Luker, P.A. : *Good Programming Practice in Ada.* 1987.

[69]Skansholm, J. : *Ada from the Beginning* : Addison-Wesley Publishing Co., 1988.

[70]Habermann, A.N., Perry D.E. : *Ada for Experienced Programmers* : Addison-Wesley Publishing Co., 1983.

[71]Gonzalez, D.W. : *Ada Programmer's Handbook and Language Reference Manual LRM* : The Benjamen/Cummings Publishing Co., 1991.